AB-INITIO INSIGHT INTO THE ORGANIC PHOTOCHEMICAL DIVERSITY: NON-RADIATIVE DECAY IN URACIL AND DERIVATIVES AND INTRAMOLECULAR CHARGE TRANSFER MECHANISMS IN THE BENZONITRILE FAMILY

Yannick Mercier

Dipòsit Legal: T-1371-2011

Yannick Mercier

Ab-initio insight into the organic photochemical diversity: Non-radiative decay in uracil and derivatives and intramolecular charge transfer mechanisms in the benzonitrile family

Doctoral Thesis

under the direction of Dr. Mar Reguero

departament de Química Física i Inorgànica

Universitat Rovira i Virgili

Tarragona

2011

UNIVERSITAT ROVIRA I VIRGILI
AB-INITIO INSIGHT INTO THE ORGANIC PHOTOCHEMICAL DIVERSITY: NON-RADIATIVE DECAY IN URACIL AND DERIVATIVES AND INTRAMOLECULAR CHARGE TRANSFER MECHANISMS IN THE BENZONITRILE FAMILY
Yannick Mercier
DL:T. 1371-2011

UNIVERSITAT ROVIRA I VIRGILI

Maria del Mar Reguero de la Poza, titular de universitat de Química Física, del departament de Química Física i Inorgànica de la universitat Rovira i Virgili,

Fem constar que la present memòria, que porta per títol:

Ab-initio insight into the organic photochemical diversity: Non-radiative decay in uracil and derivatives and intramolecular charge transfer mechanisms in the benzonitrile family

ha estat realitzada sota la meva direcció al departament de Química Física i Inorgànica de la universitat Rovira i Virgili per Yannick Mercier per a obtenir el grau de doctor en Química.

Tarragona, maig de 2011

UNIVERSITAT ROVIRA I VIRGILI
AB-INITIO INSIGHT INTO THE ORGANIC PHOTOCHEMICAL DIVERSITY: NON-RADIATIVE DECAY IN URACIL AND DERIVATIVES AND INTRAMOLECULAR CHARGE TRANSFER MECHANISMS IN THE BENZONITRILE FAMILY
Yannick Mercier
DL:T. 1371-2011

Acknowledgments

I would first like to sincerely thank my PhD tutor, Dr. Mar Reguero for everything. She opened the doors of photochemistry to me and I will never be able to thank her enough for that. She has been always helpful every time needed, she (almost) never complained about my (numerous) bad habits, like my personal sense of organization (which might be called lack of organization, truth is...) or of timing. Thanks for keeping your smile all this time, it made working with you always pleasant. I am really glad to have done this journey with such a nice boss. Thanks as well to Isa, who explained me with an incredible patience the arcanes of Gaussian and Molcas at the start. Everything seemed logical, almost easy, when you explained it !

Sens dubte, estic completament agraït a la gent del grup de Química Física. Hi ha molta per nombrar-los a tots, entre els professors, doctors i estudiants de doctorat, tots han estat encantadors i de molta ajuda de diferents maneres. M'han ajudat presentant bones xerrades, en la feina, a les classes que he tingut que impartir o senzillament en les xerrades informals a l'hora del café. De tota manera, ha estat un plaer, gràcies a tots ells. I degut a que valoro molt la importancia del serveis informàtics per als químics computacionals, voldria agrair explicitament a José, Elisenda i Moises per el seu treball. Gracias en particular a todos los que trabajaron en nuestro despacho, sin duda ninguna, fue el mejor despacho del departamento ! Mentirosos los que digan lo contrario!

I would like to thank Professor Roberto Improta for the collaboration we did and for the always clear as crystal e-mail discussions we had during this time. It has been a real pleasure to work with you. Thanks of course to the other people who has been part of this collaboration.

Thanks to everybody I knew in Tarragona, the french connection and the others that supported our language switches without complaining (but without trying to learn neither, wich is more shameful !! Just kidding.), they are of course one of the

reasons I spent such a nice time here.

Merci à ma famille, mes parents, qui quelque part sont les premiers coupables de mes exactions dans la chimie, mes freres.

Et merci à Marie-Mad, sans qui cette aventure n'aurait sans doute pas commencée.

Contents

UNIVERSITAT ROVIRA I VIRGILI
AB-INITIO INSIGHT INTO THE ORGANIC PHOTOCHEMICAL DIVERSITY: NON-RADIATIVE DECAY IN URACIL AND DERIVATIVES AND INTRAMOLECULAR CHARGE TRANSFER MECHANISMS IN THE BENZONITRILE FAMILY
Yannick Mercier
DL:T. 1371-2011

Chapter 1

Introduction

More than one hundred years ago, on June the 8^{th} of 1908, one of the pioneers of photochemistry, Giacomo Cimician, presented a comprehensive account of his work. This talk addressed to the French Chemical Society has been not only of primary importance due to the large number of photochemical reactions characterized in collaboration with Paul Silber that were presented, but as well for the great vision of photochemistry as a 'better' chemistry. In his talk, Cimician went directly to the key point and started by this sentence: "To the great successes of modern organic chemistry, it has been often reproached of having being reached with too big a show of strength. And, to be correct, one has to acknowledge that such objection is not groundless. The use of an aggressive reagent and a high temperature can not be avoided when making organic synthesis in the lab. *Per se*, using a strong energy would not be humiliating for modern organic chemistry, were it not that the organic world give the wonderful example of greats results obtained by using the last mean." "Besides enzymes", he added, "there is another agent that is all important, at least for green plants, and the influence of which on organic processes deserves an in-depth examination, and this is light. For plants light is the source of energy.[...] It may thus happen that exploiting solar energy may become interesting also in a different way: when all of the coal will have been burned in our prodigal industries, it my be necessary, also for the economy of the society, to exploit solar energy. Photochemistry studies the conversion of the energy of radiation into chemical energy and chemical phenomena related to such problems". [1, 2]

In this few sentences, professor Cimician gave not only a basic definition of photochemistry but as well one of the great advantages that photochemistry might have on classic organic chemistry: now that the problem of energy resources is even more pressing, with oil sources known to end within this century almost certainly, the ne-

cessity to exploit solar energy is more than never a key point from an economic and social point of view. However, after a rich period in terms of development of photochemistry, with the works of other pioneers as Paterno or Stobbe, photochemistry progressed only slowly for the following decades. It will not be before the decade of the 50's, when the concept of electronically-excited states was theoretically understood, that development of molecular photochemistry began again.

Nowadays, the interest in photochemistry has raised impressively, both in terms of fields that are investigated and of potential applications. Photochemistry opens new paths different from those of classic chemistry, as it allows to reach unstable species that would be impossible to get by a thermal reaction. Specific electronic excited states might be obtained using the adequate wave length, that can turn into species with new properties. In this way, photochemistry is now a "must" tool in synthesis. Photoactive ligands are used in catalysis with good results. Photochemical phenomena are very common in biological processes. Its possibilities in terms of material science are interesting as well. Some molecules show photomagnetic, photochromic or photomechanic properties. Even if applications are on a long-term future, some electronic features like charge transfer reactions might lead to the design of molecular switches, logical gates and wires on a nanoscale, which would be a giant step compared to the physical limit of the current electronic industry based on silicon material. Due to the reversibility of some reactions and the possibility of controlling them by a fine tuning of the initial excitation, molecular motors are now designed with good prospects. The photochemistry field is now widely open and will attract more attention in the next years with the further development of technics. From the experimental point of view, new apparatus allows to investigate specific characteristics with better accuracy, as lifetime or quantum yield that were difficult to evaluate before. The same occurs in the theoretical approach, where both methods and computational capacities are adapted to this kind of studies, in spite that the peculiar nature of the field makes necessary a good knowledge in physics and chemistry for a good understanding. If photochemistry has been lately developed very fast, it is still without a doubt one of the most promising fields in the chemistry world.

Our work in this field focuses on the computational study, by the mean of *ab-initio* methods, of the mechanism of some photochemical processes. The theoretical methods chosen to develop this study allow a good description of the electronic states and potential energy surfaces involved in the reactions. The peculiarities of photochemistry make necessary the use of specific methods able to describe with the same precision the ground state and the excited ones to be able to reproduce the experimental data. The theoretical procedure used in this work fulfill these characteristics, as will be shown in

the studies developed in this thesis.

One of the processes studied is the non-radiative decay of photochemical system. Uracil shows an ultrafast nonradiative decay of primary biological importance, as this is the main mechanism of defence for DNA and RNA against damage by the solar light. This quick decay without emission nor a new final product preserves the genetic information. The path for this decay has been searched for in order to explain the different lifetime of the decays of uracil and uracil derivatives and the influence of substitution on the photochemical and photophysical properties. 5-fluorouracil, 5-aminouracil and 6 aminouracil, that show some differences with the parent system, allow us to check the influence of both the electronic effect and the position of the substituents on the general mechanism.

On a different work, we studied systems with donor-acceptor π groups. These molecules show charge transfer reactions that in turn lead to interesting features on their fluorescence. They can show two different types of fluorescence, called normal and anomalous fluorescence. The reaction mechanism has been investigated as well as the species responsible for the different emissions. For the same reasons than for the study or uracil, electronic and sterical substitution have been studied through different derivatives of the parent system 4-(N,N-dimethylamino)-benzonitrile: more or less rigid bicycles (5-cyanoindoline, 6-cyano-1,2,3,4-tetrahydroquinoline, 1-methyl-6-cyano-1,2,3,4-tetrahydroquinoline, 1-methyl-7-cyano-2,3,4,5-tetrahydro-1H-1-benzazepine, 7-cyano-2,3,4,5-tetrahydro-1H-1-benzazepine and 1-ter-butyl-6-cyano-1,2,3,4-tetrahydroquinoline), bulky substituents with the (di-tert-butylamino)benzonitrile isomers and finally the 2,3,5,6-tetrafluoro-4-(dimethylamino)benzonitrile to check influence of the fluoro-substitution.

This report has the following structure. Chapter two includes a brief presentation of the basics of photochemistry needed to understand this work, before a presentation in chapter three of the computational methods that have been used. Chapter four is devoted to the study of the photochemistry of Uracil and some derivatives. Systems showing charge transfer reaction are the subject of the chapter five. In the last chapter, the conclusion extracted from the different studies are summarized.

Bibliography

[1] Albini, A. and Dichiarante, V. *Photochemical & Photobiological Sciences* **8**(2), 248 (2009).

[2] Albini, A. and Fagnoni, M. *Green Chemistry* **6**(1), 1 (2004).

UNIVERSITAT ROVIRA I VIRGILI
AB-INITIO INSIGHT INTO THE ORGANIC PHOTOCHEMICAL DIVERSITY: NON-RADIATIVE DECAY IN URACIL AND DERIVATIVES AND INTRAMOLECULAR CHARGE TRANSFER MECHANISMS IN THE BENZONITRILE FAMILY
Yannick Mercier
DL:T. 1371-2011

Chapter 2

Photochemistry

2.1 Molecular photochemistry

Molecular photochemistry is a science concerned with description of physical and chemical processes induced by the absorption of photons, in terms of a concrete mechanistic model based on molecular structures and their implied properties.[1, 2, 3]

The "photo" part of molecular photochemistry might be seen as a too restrictive prefix but is the historic one. Indeed, although photons are the most convenient means of initiating photochemical reactions, light is not required to produce electronically excited states. Thermal pathways may produce excited states as well and can therefore cause photoreactions to occur "in the dark". The "molecular" part emphasizes the use of the molecule as a crucial and unifying intellectual unit, which is used to parametrize, systemize and visualize photochemical processes at the microscopic level from their very start to their termination, id est from the absorption of a photon to the isolation of products.

Photochemical reactions have a wide range of characteristics. They can occur in all phases, including solid state, at very low temperature and can be triggered with different light radiations, even if the most common ones are UV radiations (200-380 nm) and visible light (380-700 nm). The process can be extremely fast, even faster than some photophysical processes as it will be seen later in this chapter. Moreover, photochemical reactions might be regioselective, as different cromophores absorb the excitation light at different wavelenghts. In that way, the position and type of chromophores influence the results of a given reaction, as well as the wavelenght used to initiate the reaction.

2.2 Potential energy surfaces

The theoretical treatment of photophysical and photochemical processes within the framework of the Born-Oppenheimer (B.O.) [4] approximation requires some knowledge of the Potential Energy Surfaces (PES) [5] of the ground state and of one or more excited states. The B.O. approximation simplifies the general molecular problem by separating nuclear and electronic motions. Due to their higher masses, nuclei move slower than electrons, so that it could be considered that electrons react essentially instantaneously to changes in nuclear positions. Within the framework of this approximation, a molecule formed by N atoms will have 3N-6 degrees of freedom. Indeed, a N atoms molecule will have 3N coordinates, of which three will describe the overall translation of the molecule and others three the overall rotation with respect to the three axes. In the case of a linear molecule, only two coordinates are necessary for describing rotation so that it leaves 3N-5 degrees of freedom. The electronic energy of the molecule will so be function of this internal coordinates, giving an hypersurface that connect the energy with the molecular structure. This PES forms the basis for a detailed description of the reaction process. But as a two-dimensional energy curve is more readily visualized than an energy surface, it is often used, plotting energy along one internal coordinate. Each point on a potential energy curve represents a specific nuclear geometry (horizontal axis) and a specific energy (vertical axis). Replacing the concept of a group of nuclei with the notion of a center of mass, a representative point that moves with the same characteristics as a single particle, allows us to visualize in a simple way an energy trajectory of a complex system of particles executing complicated motions.

Figure 2.1 shows two potential energy curves that maps the possible pathways of a photochemical reaction.

Figure 2.1: Scheme of a photochemical reaction using potential energy curves.

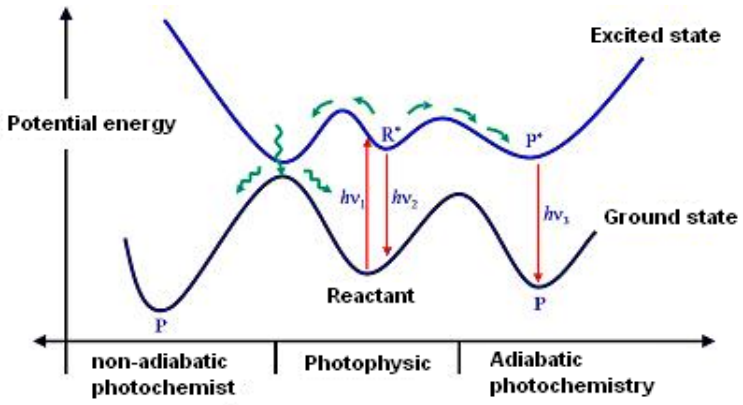

After radiation's absorption, the reactants go to an excited state R*. Once excited,

there are three possible pathways:

- an adiabatic process, which corresponds to the right part of the scheme. In that case, the molecule will move adiabatically on the excited surface to a local minimum and then go back to the ground state with radiation emission.
- a non adiabatic reaction, on the left of the scheme, where a non-radiative process occurs trough what is called a funnel or hole. On that point, energies of both states are so close that a radiationless jump is allowed. The process will then go on along the ground-state surface, to the initial reactant or a different product depending on the topology.
- a photophysical reaction, with the excited state going back to the ground state and losing the excitation energy by an emission of light.

Knowing that, we can make some important generalizations:

- Absorption and emission of light tends to occur at nuclear geometries that corresponds to minima in both the ground and the excited surface.
- radiationless jumps are most facile for geometries for which two surfaces come close together in energy, and the efficiency of these jumps will be the key point for non-adiabatic photochemical processes.
- the location and heights of energy barriers on both the excited and ground state surfaces may determine the specific pathway of a photoreaction.
- the course of a photoreaction depends on competing photophysical as well as photochemical processes. Especially, the quantum yield of the reaction will be determined by that competition.

2.3 Radiative and non-radiative mecanisms

As said before, these two processes compete and determine some of the characteristics of a photochemical reaction. Basically, the main difference between both mechanisms is that a photophysical process lead to alternative states of the same species such that at the end the chemical identity of the molecule is preserved, while a photochemical process converts the molecule into another chemical species.

In every case, reactions start with the absorption of a photon. When a molecule is irradiated, both electric fields, the molecule's one and the radiation's one, interact.

The molecule is said to become polarized by the electric field, and a Transition Dipole Moment (TDM) is induced. The direction of this induced dipole is always parallel to the direction of the external field. If its energy corresponds to the difference in energy between two stationary states of the molecule, a photon can be absorbed, transferring its energy to the molecule what causes a change in the electronic structure.

This TDM can be calculated with the following relation:

$$\text{TDM}_{n\rightarrow m} = \sum_{\alpha=x,y,z} < \Phi_n|\hat{U}_\alpha|\Phi_m >$$

where Φ_n and Φ_m are the wave functions of the initial and final states of the transition and $\hat{U_\alpha}$ the dipole moment operator of the radiation. The oscillator strenght is often used as a measure of the spectral intensity, where the following equation allows to bridge the classical concept of oscillator strength with the quantum mechanical concept of TDM:

$$\text{f}_{n\rightarrow m} = 2/3 \ \triangle \text{E}_{nm}|\text{TDM}_{n\rightarrow m}|^2$$

which is a general approximation of the complete equation:

$$\text{f}_{n\rightarrow m} = \frac{m_e c^2}{e^2}.\tilde{\nu}_{nm}. \ \frac{8\pi}{3h}|\text{TDM}_{n\rightarrow m}|^2$$

So that the oscillator strength of a transition is directly proportional to the square of the dipole moment associated to the energy difference between the two states involved in the transition. This value will give a good idea of which state mainly absorbs the radiation, as forbidden transitions give an oscillador strength close to zero when allowed ones give an oscillador strength closer to one.

Since electronic motions are much faster than nuclear motion, electronic transitions occur most favourably when the nuclear structure of the initial and final state are similar. This is called the Franck-Condon principle, and by analogy with the potential energy curves, we will talk of vertical transitions to describe theses radiative transitions. Once that the molecule absorbs the photon, it will have an excess of energy. This excess can be dissipated either by photophysical processes or photochemical ones that will compete. The relative importance of these various processes depends on the molecular structure, the electronic state as well as on the surroundings of the molecule. All these processes can be seen on the Jablonski diagram below (Figure 2.2) and can be classified in three main categories:

- Photophysical radiative processes, which imply an emission from the excited sate to the electronic ground state.

- Radiationless mecanisms, which can be photophysical or photochemical.
- Quenching processes, or bimolecular processes, where the energy transfer will be done from one molecule to another.

Figure 2.2: Jablonski diagram.

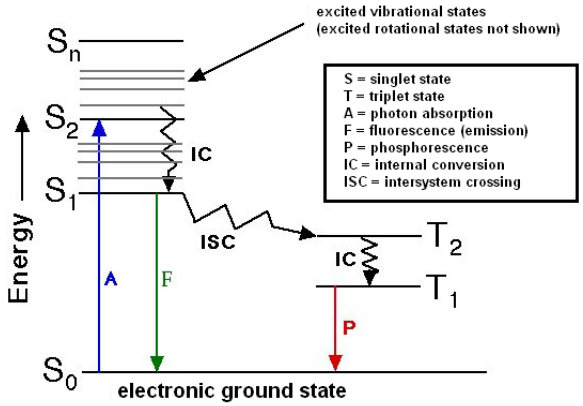

As it can be seen on the diagram, there are two kinds of radiative transitions: fluorescence and phosphorescence. In both cases, the emission usually takes place from the lowest excited states, due to the so-called Kasha rules.[?] Fluorescence is a process that take place between two states with the same spin state, so that it will be usually $S_1 \rightarrow S_0$ transition, a transition from the first excited singlet state and the ground state. On the other hand, if the two states have different spin, phosphorescence will happen. For example, the lowest excited triplet state may be populated from the lowest singlet state trough an intersystem crossing (ISC), and then it emits phosphorescence due to the $T_1 \rightarrow S_0$ transition. Phosphorescence's lifetimes are usually longer than fluorescence's lifetimes, which can produce emission in the range of picoseconds or nanoseconds.

About non-radiative processes, we will talk only of the intramolecular mechanism. Indeed, as said before, quenching processes are non radiative, but take place between two molecules. If absorption or emission might be called "vertical" transition, non-radiative mechanisms would be considered as horizontal transitions, as they occur between states almost degenerated in energy. In the same way that for radiative mechanisms, we can separate non-radiative transitions in two different processes, depending on the spin multiplicity of the implicated states. We will talk of Internal Conversion (IC) in the case of a transition between two states with the same spin multiplicity, and of Intersystem crossing (ISC), when the two states show a different spin multiplicity. As well as for radiative transitions, IC are spin-allowed transition and ISC are spin-forbidden, which in fact means it will be slightly permitted.

2.4 Adiabatic and non-adiabatic photochemistry.

Within the Born-Oppenheimer approximation, we talk about adiabatic photochemistry when a reaction occurs along only one potential energy surface. But we can make the following statement about photochemical reaction: every molecule, independently from the geometric changes it can undergo, will eventually return to the ground state. A process that starts from an electronic excited state and ends up in the potential energy surface of another electronic state trough a non-radiative transition, is called non-adiabatic.

If the Born-Oppenheimer approximation is valid in the case of adiabatic pathway, this is not the case for non-adiabatic mechanisms. In the vicinity of surface crossings, non-adiabatic coupling effects need to be taken into account to correctly describe the evolution of the molecular system. This is done, for instance, when one needs to describe a jump between two different, energetically close, PES. As spin-orbit coupling is not taken into account in the case of the Born-Oppenheimer approximation, that one is not valid anymore.

The importance of the non-radiative decay trough CI was first point out by Teller [7] before than Zimmerman [8] and Michl [9] suggested that this intersection between surface might be the origin of some products of photochemical reaction. The name "Conical Intersection" comes directly from the form that take the crossing as a double cone, when representing the energy of both states of the crossings along some specific coordinates as explained below. The term funnel was as well used by both scientists.

Two characteristics are necessary for the presence of such a crossing:

1. Both states should have the same energy.
2. They should not interact.

This two conditions mean, in the context of a multistates treatment, that the effective Hamiltonian should verify:

$$H_{11} = H_{22} \text{ and } H_{12} = H_{21} = 0$$

Due to this conditions, the number of degrees of freedom of the system is shortened and the dimensionality of the subspace in which the energies of the two touching states are equal, that is the intersection coordinate subspace, is n-2 where n value is 3N-6 (3N-5 for a linear molecule) as seen before. The remaining two dimensions are labelled x_1 and x_2 and define the so-called branching space. At the cones touching point, the

two states are degenerate, and as ones moves away from the apex of the cone by an infinitesimal amount along the x_1, x_2 axes, the degeneracy is lifted. Vector x_1 is defined as the gradient difference and vector x_2 as the derivative coupling. This n-2 dimensional space, called as well "intersection space", is a hyperline consisting of an infinite number of conical intersection points.

Figure 2.3: Scheme of a conical intersection.

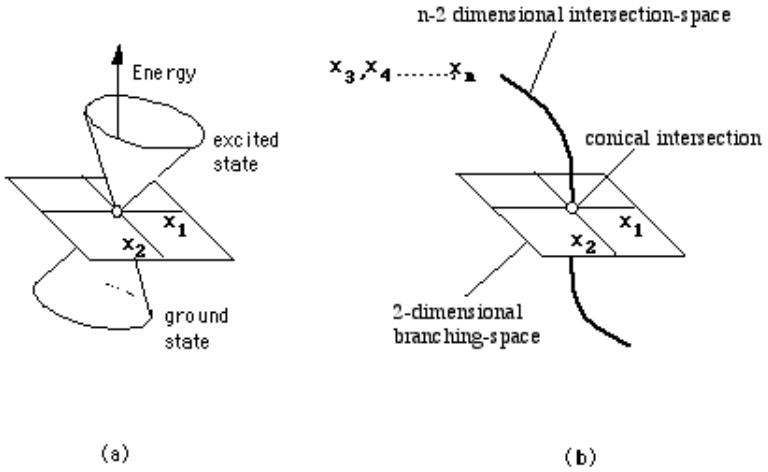

On figure 2.3, scheme (a) shows the conical representation of a crossing. On scheme (b) it is represented the hyperline of conical intersections, which can be called as well the seam of the conical intersection. Along that line, the structure can be modified along one of the coordinates of the intersection space, that is all coordinates but x_1 and x_2, without lifting the degeneracy. Energies of both states would have changed, but they will stay degenerated.

In general, the evolution of the excited reactant depends on the topology of the excited state potential energy surface and on the topology of the funnel. The non-radiative decay can occur in different points of the conical intersection, but of course, there is some minima in energies that would be more interesting, as internal conversion as well as intersystem crossing would be more probable trough these points. This is why the topology of the potential energy surface is so important in the vicinity of a crossing, as it will control the process of photoproduct formation.

From the theoretical point of view, a non-adiabatic transition between states of the same symmetry occurs through a topological feature called conical intersection. To understand the relationship between surface crossing and photochemical reactivity, it is useful to draw a parallel between the role of a transition state in thermal reactivity and that of a conical intersection in photochemical reactivity (see figure 2.4. In thermal reactivity, the Transition State (TS) forms a bottleneck that separate reactants from products. The same occurs with an accessible Conical Intersection that separates two

branches, with different excited states, on the same pathway.[6] The only difference is that while a TS connects two points on a unique pathway, intersection act as a spike and may connect the excited state reactant to two or more products of the ground state, trough a branching into several ground state relaxation channels.

Figure 2.4: Schematic representation of a) TS b) CI

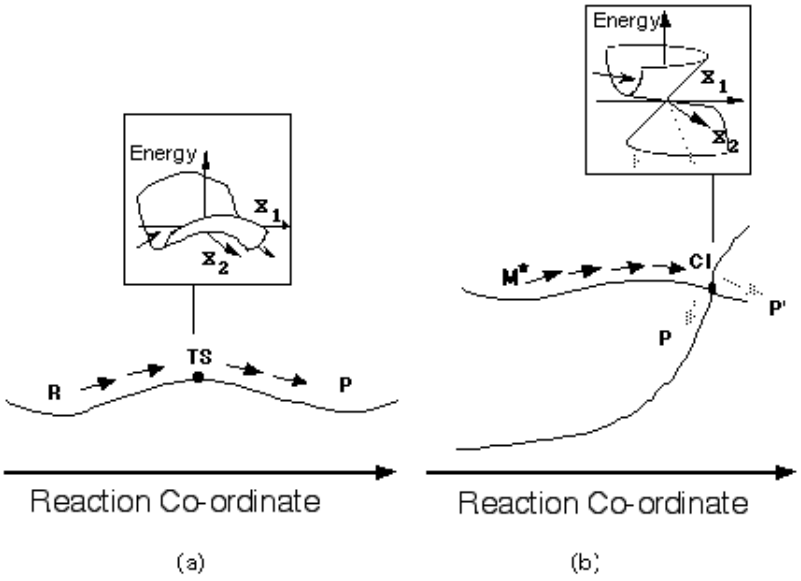

2.5 Conical Intersection's Topology

There are three basic types of conical intersection as seen in the following figure (Figure 2.5), called here following the terminology introduced by Rudenberg.[10]

The first conical intersection labelled a) is a peaked CI. In that case, the minimum of the conical intersection is a minimum on excited state surface and a maximum on the ground state one. From the gradient of the two curve on the bidimensional representation, which are opposite, we can affirm that both electronic states will have a minimum on the lower surface. For the last conical intersection c), called sloped one, one of the electronic state will have a minimum on the excited state surface, since the minimum in energy of the crossing is upper than a local minimum on the excited state surface. The last case b) is considered intermediate between the two first.

But the evolution of the reaction not only depends on the topology of the funnel but as well on the topology of the excited state surface before the intersection and then on the topology of the ground state surface after the CI. So that the three cases seen can be subdivided as shown on figure 2.6.

Using the classification of Rudenberg, cases (a), (b), (d) and (f) are peaked conical

Figure 2.5: Tridimentional and bidimentional scheme of peaked (a), intermediate (b) and sloped (c) conical intersections.

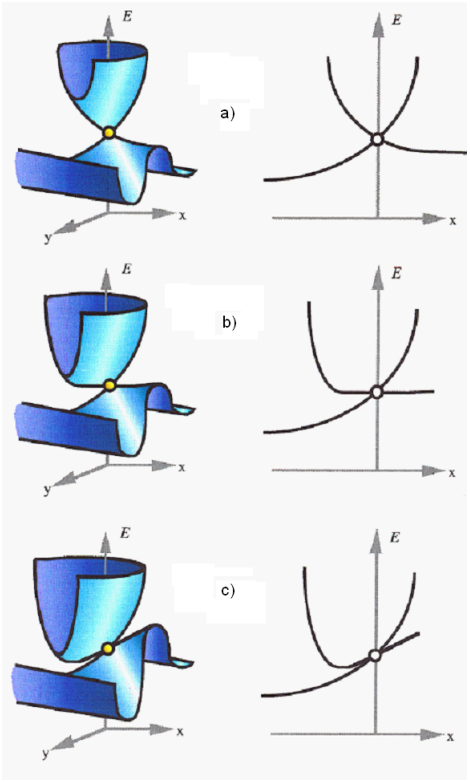

intersection and cases (c) and (e) sloped ones. We can make a few considerations about the different cases shown here.[11] If there is no barrier in the reaction coordinate on the excited state surface (Figure 2.6 (b), (d), and (f)) then the reaction may be ultrafast. On the other hand, the presence of a barrier on S1 (Figure 2.6 (a)) gives an activated excited state process and one may observe temperature or wavelength dependent photochemistry. One particular case is the one of the sloped conical intersection (figure 2.6 (c) and (e)), which is not really an activated process as that in scheme (a). Even if there is sufficient energy to access the surface crossing, the system may oscillate between excited and ground states in the crossing region for some considerable time before decay to the ground state occurs. The rate of the reaction may thus be slower than that predicted on the basis of the energy barrier. With a peaked conical intersection, once reached the crossing, decay to the ground state takes place on a time scale of less than a vibration.

As well as the type of conical intersection, the position of the funnel along the reaction coordinate and the number and orientation of the ground state relaxation paths departing near the funnel will affect the process of the photoproduct formation. These paths define ground state valleys that originate at the CI and end at a different photoproduct energy minima, as can be seen on figure 2.6 (a) and (b) where there are

Figure 2.6: Schematic representation of the reaction path topology and position of the photochemical funnel (a conical intersection) along the reaction coordinate: (a) Transition state (TS) before a peaked conical intersection; (b) barrierless path with a peaked conical intersection; (c) path with a sloped conical intersection; (d) like a or b but with an intersection on the product side of the reaction co-ordinate, (e) like c but with an intersection on the product side of the reaction co-ordinate; (f) like a or b but with multiple competitive ground state relaxation paths.

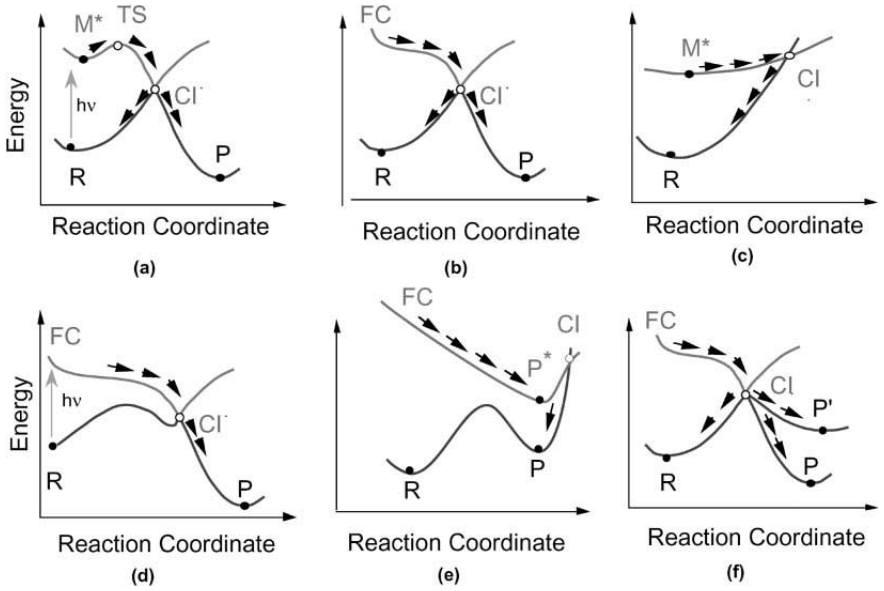

two paths leading either back to the reactant or to the product. The case of figure (f) shows multiple ground state relaxation paths departing from the same peaked CI which leads to different photoproducts. Moreover, if the crossing occurs in the photoproduct side of the reaction coordinate, as in figure (d) and (e), one has an excited state adiabatic reaction which can be substantially completed before the non-adiabatic event occurs returning the system to the gournd state of the product. If there is a substantial thermal barrier to the thermal back reaction to the reactant, then the product yield would be enhanced.

In the vicinity of a conical intersection, the condition on the hamiltonian H_{12}= H_{21}= 0 is not anymore fulfilled. Indeed, the structure is slightly modified along the axis $x_1$and x_2. Even if the energies of both states are equal without taking into account the interaction between them, that is H_{11}= H_{22}, the energy of the interacting states changes:

$$E_{1,2}= \frac{1}{2}\left\{H_{11}+H_{22} \pm \left[(H_{11}-H_{22})^2+4H_{12}^2\right]^{1/2}\right\}$$

We have what is called an avoided crossing, as shown on figure 2.7, where ϕ_i and ϕ_j are the dominant electronic configuration of the two states.

Figure 2.7: Schematic representation of an avoided crossing: (a) weakly avoided (b) strongly avoided. Dotted lines represent the diabatic surfaces and full lines the adiabatic surfaces.

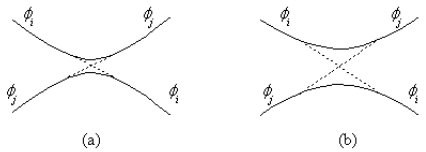

When the diagonal elements of the hamiltonian are small, case (a) of the figure 2.7, this is a weakly avoided crossing. The energy difference between the adiabatic and the diabatic surfaces is small, and the configuration change of the electronic configuration ($\phi_i \rightleftharpoons \phi_j$) would occur in a small range of molecular geometries. The "jump" would then be quick. On the other hand, in the case (b) of a strongly avoided crossing, the change of configuration will be slower and will start far from the crossing point of the diabatic surfaces, as it can occur along a large range of molecular geometries. We can see that in an avoided crossing, the lower adiabatic surface has a transition state and the upper one a minimum. As we will see in the next chapter, these points are usually hard to find for technical reason, but are of high importance. Indeed, if a conical intersection is located, then it can be assumed that there will exist at least one transition state of an adiabatic surface that will be lower in energy than the conical intersection.

All these possible features of a photochemical reaction make it more difficult to study it from a technical point of view than a "classic" thermal reaction. But different tools have been developed by theoricians to study theses phenomena, thanks as well to the development of computational science. That will be the subject of the next chapter.

Bibliography

[1] Klessinger, M. and Michl, J. *Excited States and Photochemistry of Organic Molecules.* VCH Publishers, New York, (1994).

[2] Michl, J. and Bonacic-Koutecky, V. *Electronic Aspects of Organic Photochemistry.* Wiley, New York, (1990).

[3] Turro, J. N. *Modern Molecular Photochemistry.* University Science Books, Californie, (1991).

[4] Born, M. and Oppenheimer, J. R. *Ann. Physik.* **84**, 457 (1927).

[5] Dewar, M. J. S. and Dougherty, R. *The PMO Theory of Organic Chemistry.* Plenum, New York, (1975).

[6] Bernardi, F., Olivucci, M., and Robb, M. A. *Chem. Soc. Rev.* , 321–328 (1996).

[7] Teller, E. J. *J. Phys. Chem* **41**, 109 (1937).

[8] Zimmerman, H. E. J. *J. Am. Chem. Soc.* **88**, 1566 (1966).

[9] Michl, J. *J. Mol. Photochem.* , 243 (1972).

[10] Atchity, G. J., Xantheas, S. S., and Ruedenberg, K. *J. Chem. Phys.* **95**, 1862 (1991).

[11] Robb, M. A. and Olivucci, M. *J. Photochem. Photobiol. A: Chem.* , 1 (2001).

UNIVERSITAT ROVIRA I VIRGILI
AB-INITIO INSIGHT INTO THE ORGANIC PHOTOCHEMICAL DIVERSITY: NON-RADIATIVE DECAY IN URACIL AND DERIVATIVES AND INTRAMOLECULAR CHARGE TRANSFER MECHANISMS IN THE BENZONITRILE FAMILY
Yannick Mercier
DL:T. 1371-2011

UNIVERSITAT ROVIRA I VIRGILI
AB-INITIO INSIGHT INTO THE ORGANIC PHOTOCHEMICAL DIVERSITY: NON-RADIATIVE DECAY IN URACIL AND DERIVATIVES AND INTRAMOLECULAR CHARGE TRANSFER MECHANISMS IN THE BENZONITRILE FAMILY
Yannick Mercier
DL:T. 1371-2011

Optimism is a strategy for making a better future. Because unless you believe that the future can be better, it's unlikely you will step up and take responsibility for making it so. If you assume that there's no hope, you guarantee that there will be no hope. If you assume that there is an instinct for freedom, there are opportunities to change things, there's a chance you may contribute to making a better world. The choice is yours.

Noam CHOMSKY

UNIVERSITAT ROVIRA I VIRGILI
AB-INITIO INSIGHT INTO THE ORGANIC PHOTOCHEMICAL DIVERSITY: NON-RADIATIVE DECAY IN URACIL AND DERIVATIVES AND INTRAMOLECULAR CHARGE TRANSFER MECHANISMS IN THE BENZONITRILE FAMILY
Yannick Mercier
DL:T. 1371-2011

Chapter 3

Computational methods

As seen before, the general approach used to follow the course of a photochemical reaction involves looking for the so-called "photochemical reaction path". Such a path will usually originate at the Franck Condon geometry, will evolve along an excited state potential energy surface and will eventually end up on the ground state. The final molecule might be a new product or the initial ground state reactant that will be reached trough a deactivation channel. So, while a thermal reaction is governed by the topography of a single energy surfaces, a photochemical reaction involves at least two potential energy surface. For that reason, the development of ab-initio quantum mechanical methods for theoretical photochemistry has been slower than for the investigation of the reactivity of molecules in their electronic ground state.

Indeed, if a single electronic configuration usually describes correctly most systems in the ground state at areas close to their equilibrium geometry, this is not the case for the description of geometries corresponding to electronically excited states, which might have several configurations equally relevant. Theoretical photochemistry request, then, methods using the multiconfigurationnal approach.[1]

In this chapter we present an overview of the multiconfigurational methods used in the studies collected here. All of these methods are implemented in one or the other computational packages used to develop our work, i.e. Gaussian [2] and Molcas [3, 4, 5]

3.1 Multiconfigurational approach: the CASSCF method

The Complete Active Space Self consistent Field (CASSCF) [6] method is nowadays widely used. The idea behind the CAS model is to generalize the HF model, based on the orbital concept, to make it able to handle situations where a single configuration is not enough to describe the electronic distribution. In that way, CASSCF is more complex as it is based on a multiconfiguration wavefunction, but keeps the technical and conceptual simplicity of HF method. The building blocks are the molecular orbitals like in the HF method but they are now classified in different categories: Inactive orbitals, active orbitals and virtual orbitals. Inactive orbitals include orbitals that do not participate in the reaction. They are considered always as strictly doubly occupied in all the configurations, which means that inactive electrons will be twice the number of inactive orbitals. Active orbitals are the ones that might participate from the chemical point of view to the reaction, that means which occupation can change. This category include bonding orbitals, usually occupied by valence electrons, and by anti-bonding orbitals. These active orbitals have an occupation number between zero and two and the number of electrons in the active space is the total number of electrons of the molecule less the inactive electrons. The virtual orbitals represent the anti-bonding orbitals that are not relevant from the chemical point of view, that is that will not be populated during the reaction. Their occupation is always zero and the size of the virtual space will depend on the one-electron basis set employed. The wavefunction is then formed by a linear combination of all possible configurations of the active electrons in the active orbitals. The optimisation of the orbital set corresponds to a full-CI in the active space while inactive orbitals will be treated as in the restricted HF function. It allows the use of a high level calculation restricted to a small number of orbitals and electrons, as full-CI is cost-prohibitive apart from the case of very small systems. The active space used is represented in the CASSCF method by CAS(n,m) where n is the number of active electrons and m the number of active orbitals that formed the active space.

That said, it becomes clear that the key-point when using the CASSCF method is the choice of the active space. The active orbitals should be carefully chosen or it may give meaningless results from the chemical point of view. It is necesary to assume in advance some hypothesis about the nature of the excited states and the orbitals involved in the photochemical process, like bond breaking or weakening. Typically, in the study of reactions of small organic molecules as is our case, a good active space will include the valence orbitals, like the π and π^* ones, the HOMOs and LUMOs, that

might be known from previous low-level calculations. Some specific orbitals others than the previous ones that might participate in relevant excitations during the reaction should be as well included. Of course, the active space must not change along the reaction path, which means that the selection should be adequate for the whole range of geometries and states of interest for the reaction studied. In the end, intuition as well as calibration calculations would allow a good election of this active space. Anyway, there is a limitation on this election, that prohibits to take simply all orbitals involved, i.e. the computational cost. The major technical difficulty lies in the size of the complete CI expansion in the active orbital subspace, that might quickly becomes unmanageably large when the number of active orbitals is increased.

In such cases, a restricted form of the CASSCF wavefunction might be used, the RASSCF method (for Restricted *Active Space Self-Consistent Field*).[7, 8, 9] In this method, the former active space is divided again in three subspaces, called RAS1, RAS2 and RAS3:

- RAS1 space will include all orbitals that are doubly occupied, but where we would allow a limited number of excitations.
- RAS2 will remain like the active space of the CASSCF method. It is composed of the orbitals for which occupation between zero and two is allowed.
- RAS3 will include orbitals that have an occupation number of zero, with a limited number of allowed excited electrons.

So that the new nomenclature will be of the type CAS (n, $m^{I} + m^{II} + m^{III}$) [h,e], where n indicates the number of electrons in the active space as before, m^{I}, m^{II} and $m^{III}$the number of active orbitals in the three subspaces and h and e the number of holes permitted in the RAS1 space and electrons in the RAS3 space respectively.

This RASSCF method allows to enlarge the active space, that the current computational facilities limit to around 12-14 electrons in the same number of active orbitals for the CASSCF method.

It must be as well pointed out another specificity of the CASSCF method. If in principle it is possible to make calculations on higher roots optimizing just one root, experience shows that in most cases, it is almost impossible for roots higher than the second one. In that case, State-Average (SA) CASSCF calculations might be used, where the orbitals are obtained from a density matrix averaged.

Last but not least, a photochemical reaction usually starts with absorption and might ends with emission of a radiation. Therefore, it is necessary to know trans-

ition probabilities. This information can be given by the transition dipole moment, proportional to the transition probabilities. Malmqvist introduced the *CAS State Interaction* (CASSI) [10, 11] to compute transition density matrices between CASSCF wave functions with their own sets of optimized orbitals. This method makes possible to compute effciently first and second order transition density matrices. Transition dipole moments are then accessible, but these density matrices are also useful in other cases, for example to use localized orbitals as in studies of charge transfer reactions.

3.2 Adding the dynamical correlation: the CASPT2 method

The CASSCF method is widely used in photochemistry because it is regarded as one of the most efficient methods. Indeed it can describe completely the ground state but also map out full energy surfaces. In spite of this, it suffers from one disadvantage, which is that it does not take into account full electron correlation. Only the long-range effects related to the static correlation effect (or non-dynamic correlation effect) are included together with the dynamic electron correlation due to the electrons in the active space. Therefore, CASSCF is usually used in combination with some other method to take into account the remaining correlation effect associated with the instantaneous short-range electron-electron interaction. Variational methods like multi-reference CI (MRCI) [12, 13] are quite accurate but they are computationally expensive. Instead, the last decade has seen the development of the multiconfigurational second order perturbation theory (CASPT2) [14, 15], which has shown to be an efficient alternative with a good ratio between quality of the results and computational cost.

The development of this approach was inspired by the success of the Moller-Plesset second order pertubation theory (MP2), used to treat the electron correlation of the ground state. In the CASPT2 method, the CASSCF wave function is used as the reference function (zeroth-order wave function).

It sometimes happens that the zeroth-order wave function, that is the reference wavefunction, has a weight too low, due to some intruders states in the second-order calculation. That means that the CASPT2 wavefunction includes some participation of orbitals from outside the active space, i.e. that the description is not complete enough. This is a common problem in the case of small organic molecules where the active space does not include the full π orbital valence system. In the same way, the weight of the reference configuration of an excited state may be too low compared to the ground state one due to a large number of minor contributions higher in energy.

Usually, enlarging the active space might overcome this problem, but once again, that would be at the price of a higher computational cost. That is why it is usually used a level-shift that removes weak intruder states by the addition of a shift parameter. This shift has to be the lowest possible and should be of course the same for all the calculations for a given reaction.

It is sometimes needed to have more than one reference state in the perturbation treatment. This is the case of avoiding crossings for example, where two different electronic states are really closed in energy and can be mixed. The multi-state CASPT2 (MS-CASPT2) [16, 17] procedure might then be used. It represents an extension of the CASPT2 method for cases that cannot be fully accounted for by just a single-reference perturbation treatment. In the MS-CASPT2 method, an effective hamiltonian matrix is constructed with the CASPT2 energies on the diagonal and the off-diagonal elements representing the coupling up to second order of the dynamic correlation energy of the two electronic states. It will finally give the MS-CASPT2 wavefunctions and energies. When using the MS-CASPT2 method, it should be checked that the off-diagonal elements of the effective hamiltonian matrix, i.e. the coupling between both states, are small and the matrix symmetrical otherwise it could lead to meaningless results on energies.

CASPT2 geometry optimizations are now available in the Molcas package, but they are still very expensive computationally and so reserved to small size systems. They were consequently only used sparely as proof calculations and usually only on the ground state.

3.3 ONIOM method

As we have seen before, one of the major drawback of the previous methods is their computational cost. This cost prohibits the studies of bigger systems, leaving sometimes the work on models as the unique solution. Of course, the never-ending progress in the computational facilities make easier day by day calculations at the ab-initio level of bigger molecules. But to overcome this technical limitation at the time being, we can use hybrid methods.

Warshel and Levitt [18] implemented for the first time a quantum mechanical/molecular mechanical (QM/MM) method. The basic idea is to describe a relatively small region of a system at the quantum level while the remainder is described with a classical force field. The ONIOM method (Our own n-layered Integrated molecular Orbital Mechanic) that we have used has been developed by Morokuma and coworkers.

[19, 20, 21, 22, 23, 24, 25] In it it is possible to establish up to three different parts of the system to be studied at three different levels of theory. The aim is to describe the relevant part of the system from the reaction point of view at a high level of theory, usually using an ab-initio method, while the rest can be described at a lower level. The complete system is called the "real system" while what is called the "model system" is represented by a simplified molecule where some parts are substituted by hydrogen atoms. The high level calculation will be applied only to the model system while the low level of theory will be applied to both the real system and the model one. The final ONIOM energy would then simply be

$$E^{ONIOM} = (E_{model})^{CASSCF} + (E_{real})^{MM} - (E_{model})^{MM}$$

Once again, that kind of technique is not at all a black box. The model system should include the whole part of the molecule where the reaction takes place. In the case of photochemistry, the excitation must be described at the highest level of theory. It should be pointed that the use of MM to describe the real system prevents from taking into account most of the electronic effect of the part of the molecule not included in the model system, so that part will mainly contribute to the sterical level. To overcome this problem it is possible to work with two different quantum mechanic levels of theory, but neither in this case the electronic distribution of the model will be affected by the electronic distribution of the rest of the system. So in short, the choice of both theory levels as well as the design of the model should be carefully made and its advisability confirmed by calibration. If so, this method will allow the use of a high level of theory to study the reactivity in quite large systems with a relative cheap computational cost.

3.4 Modeling the solvent: the PCM method

It is well know that solvents can strongly affect the electronic properties of molecules. This is especially true when dealing with biological systems, which natural environment is mainly liquid phase, but not only. Experimental chemists work usually in solvent environments what affects sometimes measurements. For example, most of the spectrometric techniques show broadening of the absorption and fluorescence bands as well as the so-called solvatochromic shifts of the same bands. The interaction between solute and solvent molecules modify their ground and excited states, stabilizing preferentially one or the others depending on their chemical nature.

However, in theoretical chemistry, most of the reactions were studied in gas phase until the 90s. But continuum solvation models have become more and more developed

to be now widely used to study computationally solvent effects.[26] The range of molecular systems where this technique might be used go from the small organic molecules to the large biochemical systems such as proteins or enzymes. Especially, the last years have seen the development of a special class of solvation model, using an Apparent Surface Charge (ASC) as a descriptor of the solvent polarization. This is currently the preferential approach to take into account solvent effects in QM calculations. The Polarizable Continuum Model (PCM) [27] is nowadays the most commonly used method and the one that has been used in our studies.

This method is characterized by the use of a set of apparent charges representing the polarization of the dielectric medium to describe the solvent effect. There exist different methods to define the molecular cavities, that is the portion of space within the surrounding medium that is occupied by the solute molecule, and the surface of these cavities.

However, even if the PCM model gives often very good results, it is not adequate to represent specific interaction between the solvent and the solute. For example, a continuum model of the solvent will not account for hydrogen bonding. To correct this defect, the best way is to add some explicite molecules of the solvent around the molecule studied on top of the solvation model, in order to take into account these local interactions. If we take the case of water, it would be then possible to add a few molecules and disposing them around the solute molecule. As that will increases the size of the system that the QM method will have to take into account, this method increases the computational cost, so it should be carefully pondered. Moreover, as the aim is to describe some local interactions, the position of these molecules regarding the solute molecule is as important as their number.

Bibliography

[1] Olivucci, M. *Computational Chemistry, Theoretical and Computational Chemistry V.16.* (2005).

[2] M. J. Frisch, G. W. Trucks, H. B. Schlegel, G. E. Scuseria, M. A. Rob, J. R. Cheeseman, J. A. Montgomery Jr., T. Vreven, K. N. Kudin, J. C. Burant, J. M. Millam, S. S. Iyengar, J. Tomasi, V. Barone, B. Mennucci, M. Cossi, G. Scalmani, N. Rega, G. A. Peter and Pople, J. A. *Gaussian 03 (Gaussian, Inc., Wallingford, CT, 2003)* .

[3] Aquilante, F. and L. De Vico, N. Ferré, G. Ghigo, P.-ÅMalmqvist, P. Neogrády, T.B. Pedersen, M. Pitonak, M. Reiher, Björn. O. Roos, L. Serrano-Andrés, M. Urban, V. Veryazov, R. L. *J. Comp. Chem.* **31**, 224 (2010).

[4] Karlström, G. and R. Lindh, P.-Å. Malmqvist, Björn O. Roos, U. Ryde, V. Veryazov, P.-O. Widmark, M. Cossi, B. Schimmelpfennig, P. Neogrády, L. S. *Computational Material Science* **28**, 222 (2003).

[5] Veryazov, V. and P.-O. Widmark, L. Serrano-Andres, R. Lindh, B. R. *Int. J. Quantum Chem.* **100**, 626 (2004).

[6] Roos, B. O. *in Ab initio Methods in Quantum Chemistry - II, Lawlwy, K. P., Wiley* (1987).

[7] Malmqvist, P.-A., Rendell, A. P., and Roos, B. O. *J. Phys. Chem.* **90**, 5477 (1990).

[8] Olsen, J., Roos, B. O., Jorgesen, P., and Jensen, H. J. A. *J. Chem. Phys.* **89**, 2185 (1988).

[9] Boggio-Pasqua, M., Bearpark, M. J., Klene, M., and Robb, M. A. *J. Chem. Phys.* **120**, 7849 (2004).

[10] Malmqvist, P.-A. *Int. J. Quantum Chem.* **30**, 479 (1986).

[11] Malmqvist, P.-A. and Roos, B. O. *Chem. Phys. Letters* (155), 189 (1989).

[12] Roos, B. O. and Siegbahn, P. E. M. *Int. J. Quantum Chem.* (17), 485 (1980).

[13] Buenker, R. J., Hirsch, G., Li, Y., Gu, J.-P., Alekseyev, A. B., Liebermann, H.-P., and Kimura, M. *P. Jensen and P.R. Bunkers (eds), Wiley, chichester* (2000).

[14] Anderson, K., Malmqvist, P.-A., Roos, B. O., Sadlej, A. J., and Wolinski, K. *J. Phys. Chem* **94**, 5483 (1990).

[15] Andersson, K., Malmqvist, P.-A., Roos, B. O., and Serrano-Andrés, L. *Chem. Phys. Lett.* **228**, 299 (1998).

[16] Roos, B. O. *A Perturbation-Variation Treatment of the Multi-State Problem in CASPT2.* Lund University, (1996).

[17] Finley, J., Malmqvist, P.-A., Roos, B. O., and Serrano-Andrés, L. *Chem. Phys. Lett.* **228**, 299 (1998).

[18] Warshel, A. and Levitt, M. *J. Mol. Biol.* **103**, 227 (1976).

[19] Maseras, F. and Morokuma, K. *J. Comput. Chem.* **16**, 1170 (1995).

[20] Humbel, S., Sieber, S., and Morokuma, K. *J. Phys. Chem.* **105**, 1959 (1996).

[21] Svensson, M., Humbel, S., Froese, R. D. J., Matsubara, T., Sieber, S., and Morokuma, K. *J. Phys. Chem.* **100**, 19357 (1996).

[22] Svensson, M., Humbel, S., and Morokuma, K. *J. Phys. Chem.* **105**, 3654 (1996).

[23] Dapprich, S., Komaroni, I., Byun, K., Morokuma, K., and Frisch, M. J. *J. Theochem. J. Mol. Struct.* **462**, 1 (1999).

[24] Vreven, T. and Morokuma, K. *J. Comp. Chem.* **21**, 1419 (2000).

[25] Vreven, T., Mennucci, B., Da Silva, C. O., Morokuma, K., and Tomasi, J. *J. Phys. Chem.* **115**, 62 (2001).

[26] Mennucci, B. and Cammi, R. *Continuum Solvation models in Chemical Physics: Theory and Applications.* (2007).

[27] Tomasi, J., Mennucci, B., and Cammi, R. *Chem. Rev.* **105**, 2999 (2005).

The reasonable man adapts himself to the world; the unreasonable one persists in trying to adapt the world to himself. Therefore, all progress depends on the unreasonable man.

George Bernard SHAW

UNIVERSITAT ROVIRA I VIRGILI
AB-INITIO INSIGHT INTO THE ORGANIC PHOTOCHEMICAL DIVERSITY: NON-RADIATIVE DECAY IN URACIL AND DERIVATIVES AND INTRAMOLECULAR CHARGE TRANSFER MECHANISMS IN THE BENZONITRILE FAMILY
Yannick Mercier
DL:T. 1371-2011

Chapter 4

Uracil, DNA/RNA and light

4.1 DNA, RNA and solar light

Deoxyribonucleic acid (DNA) contains the genetic instructions used in the development and functioning of all known living organisms. It carries the genetic information to construct other cells as proteins, but it also has other purposes. The Ribonucleic acid (RNA) serves mainly as an intermediary between DNA and the proteins, but now it is also known to have catalytic properties. DNA and RNA are of vital importance for life on earth.

The solar radiation, as well essential on earth for living species, contains a significant amount of ultraviolet (UV) photons ($\lambda < 400$ nm). Both DNA and RNA show substantial absorption of the UV light, therefore this radiation constitutes a potential threat as excited states can be the beginning of a complex chain of events that might end in photodamage. In the case of DNA and RNA, nothing less than mutation, genomic instability or carcinogenesis may be the result of this absorption [1]. As the principle of *survival-of-the-fittest* prevails in nature, evolution must have found a way to prevent or correct any potential damage to the genetic material, otherwise the altered structure resulting from the photodegradation would interfere with the normal cellular processing of DNA.

To correct the damages there exist some repair mechanisms. In order not to overload the organism's repair machinery, there are also different pathways for the excess electronic energy coming for the absoprtion of the UV radiations to relax. That might be by photon emission or by nonradiative transitions. Anyway, the shorter the lifetime of the excited states, the lower the probability of reaction yielding inconvenient photoproducts. That makes highly efficient nonradiative decay the best answer of evolution to the problem of DNA and RNA photodamage.

4.1.1 DNA and RNA structure

DNA and RNA share most of their structural characteristics and differs on a few ones. Both nucleic acids are polymers, consisting of an alternating sugar/phosphate backbone with nucleobases attached to each sugar. A block of a nucleobase attached to a sugar/phosphate backbone is called a nucleotide. As can be seen on figure 4.1, the nucleobases are classified in two types, the purines that show a bicycle structure (adenine and guanine) and the pyrimidines (cytosine, thymine and uracil). Both DNA and RNA contain the two purines while only cytosine is present in both nucleoacids. Of the two other pyrimidines, thymine, that comes from the methylation of uracil, is used almost exclusively in DNA and is replaced by uracil in RNA. The other difference in the primary structure of the two polymers lies in the sugar that connect two phosphate groups. In the case of RNA, it is a ribose and in the case of DNA this is a deoxyribose as indicated by the names.

The major difference comes from the secondary structure. DNA is usually found in the well-know double helix form, where the nucleobases form hydrogen bonds with their complementary nucleobases: adenine forms two hydrogen bonds with thymine and guanine three with cytosine in the most common Watson-Crick pair systems. This double stranded form might take three different geometries, called A-form DNA, B-form DNA and Z-form DNA depending of environmental conditions like humidity or salt concentration. On the other hand, RNA is almost only found in a single stranded form, although it may locally form pairs, uracil combining in that case with adenine.

4.1.2 DNA/RNA and nucleobases photochemistry

Lots of work are currently done on DNA excited states by means of gas-phase spectroscopy as well as on modelisation of base pairs or even base multimers from the theoretical point of view. Regarding this last approach, although the use of models have limited biological realism, it is essential to fully understand the photodynamics of base monomers as a first step to reach the understanding of the photodynamics of these complex polymers. Indeed, the accessible decay mechanisms of DNA and RNA come from the photochemical properties of the nucleobases. Of course, the specific spatial organisation of the bases in DNA or RNA modifies the photophysical properties leading, among others things, to slightly different decay pathways with larger lifetimes. For example excitations in stacked bases are rapidly trapped to form long-lived excited states in high yields [2]. Anyway, the decay paths of nucleobases are still open in the DNA/RNA strand in all cases. Therefore, in this work we have focused our attention on the case of the monomers. Specifically, we have studied the case of uracil

Figure 4.1: Secondary structure and nucleobases of DNA and RNA

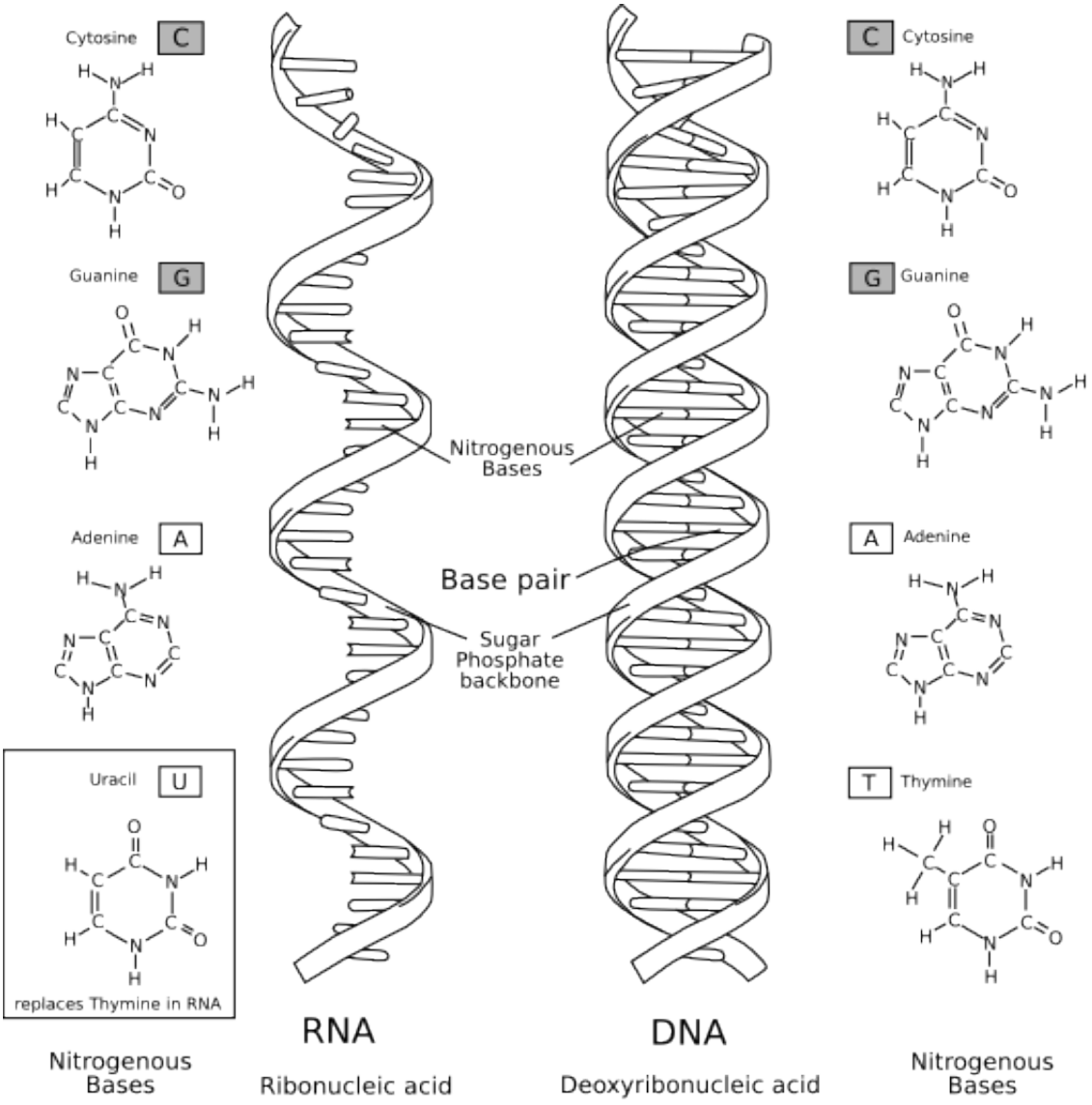

and some of its derivatives, to understand first what are the competitive mechanisms following an excitation, and then clarify the role of substitution in the molecule in these mechanisms.

The nucleobases have a number of structural isomers formed by permutation of the hydrogen atoms among the set of heteroatoms. These possible isomers are called tautomers and their existence complicate the interpretation of experimental results as they might lead to different electronic structures. Fortunately, most of the tautomers show significant higher energy than the minimum-energy tautomer, which allow to discard them in most of the cases. An exception is adenine which presents different tautomers close enough in energy to coexist in significant amounts [3, 4].

Different experimental and theoretical techniques have been used in the study of DNA/RNA and their building blocks like nucleobases. The ground state geometries were determined long ago by X-ray crystallographic and neutron diffraction techniques [5]. In the case of excited states, although experiments can give some information, a complete and precise geometry can not be determined. Absorption spectroscopy has been used for decades to give information about energy differences between the ground state and the excited states lying vertically above. In the same way, fluorescence and phosphorence spectra give information about singlet and triplet excited states respectively. Recent improvements of different spectroscopic techniques such as laser induced fluorescence (LIF) [6], resonance-enhanced multiphoton ionization (REMPI) [7, 8] or spectral hole burning (SHB) enhanced our knowledge about the physical and photochemical properties of the nucleic acid bases. And last but not least, femtosecond time-resolved [9, 10] or fluorescence up-conversion techniques [11] gives us now some primordial information about the lifetime of some of the excited states or the dynamics of nucleotides and isolated bases. From the theoretical point of view, different methods have been used, mainly multiconfigurational techniques for the reasons exposed in the chapter of methodology, and DFT and TD-DFT methods due to their good rate of accuracy versus computational cost [9].

It is well known that the absorption of UV radiations by DNA around 260 nm comes from the strongly allowed $^1(\pi\rightarrow\pi^*)$ transition on the nucleobases [12, 13]. There is now consensus about this fact, as both experimental techniques and theoretical calculations lead to this conclusion. The lone electron pairs of the various heteroatoms accounts for additional $^1(n\rightarrow\pi^*)$ excitations, but are experimentally poorly determined due to the forbidden character of these transitions. The electronic states diagram of the nucleobases is therefore quite complex as there might exist multiple $^1(\pi\rightarrow\pi^*)$ and $^1(n\rightarrow\pi^*)$ transitions in the low-energy region. On top of these singlet excited states, all nucleobases have triplet excited states of the same character ($^3(\pi\rightarrow\pi^*)$ and

$^3(n\rightarrow\pi^*)$ excited states) of low energy. The states are classified as bright or dark states according to whether they are reached by transitions from the ground state with large or small oscillator strength respectively. The dark states are difficult to characterize by traditional spectroscopic techniques even if some recent experiments have provided new insights about them. The phosphorence emission yield, which accounts for emission from a triplet excited state, is as well low in hydrogen-bonding solvents but higher in aprotic solvent.

A common feature of all the nucleobases is the very low yield of fluorescence produced after UV excitation. First measurements of the fluorescence quantum yield of nucleic acid bases dates back from 1971 and were confirmed later [15, 13]. This yield varies between 3×10^{-5} for Uracil and 2.6×10^{-4} for adenine. As the fluorescence lifetime, τ_f, is directly proportional to its fluorescence quantum yield, it means that these low fluorescence yields correspond to short excited-state lifetimes. These initial data have been confirmed by time-resolved emission measurements of excited electronic states, obtained with higher precisions due to the use of the newly developed femtosecond spectroscopic techniques. All the nucleobases show a lifetime of the initially populated excited state lower than 1 ps [9].

To resume, the different nucleobases all show a strong absorption band due to transition to the $^1(\pi\rightarrow\pi^*)$ excited state and short lifetime of this excited state. The question is then what is the mechanism of the ultrafast nonradiative decay, or in other words, what is the pathway of such decay from the bright state back to the ground state. On that point, there is an ongoing debate. Indeed, if there is now no doubt about the character of the excited state that absorbs the excitation, it is possible that other singlet excited states might be populated by internal conversion, or triplet excited states by intersystem crossing. On top of this, recent experimental studies have demonstrated that longer lifetimes, longer than the picosecond scale, coexist with the subpicosecond decay in water and other solvents [16, 17]. Two decay pathways on different timescale might then compete.

The controversy lies on two points:

- Does the ultrafast decay go back to the ground state through a single CI or indirectly trough two or more CIs involving an intermediate $^1(n\rightarrow\pi^*)$ state?
- What is the slower decay pathway and which excited states, singlet or triplet, are involved?

Resolving these two points has been the aim of our work on uracil and some of its derivatives, namely the 5-fluorouracil and 5- and 6-aminouracil, and the results are

exposed in the following part of this chapter, after a presentation of the computational details used for the calculations.

4.1.3 Natural monomers and derivatives

Going back to the idea of *survival-of-the-fittest*, it is interesting to wonder why these nucleobases were chosen to form genetic material and not one of their derivatives. Studies about the non-natural nucleobases tautomers or derivatives have shown that small modifications change sometimes greatly the photochemical and photophysical properties of the molecules [18, 9]. Experimental and theoretical studies demonstrate that the natural nucleobases have usually the shortest excited lifetime, which is coherent with the idea of a selection by the external conditions, i.e. potentially harmful UV light, that would have let only the most photostable molecules survive [19].

The study of derivatives contains another interest. It is possible to use them in medicine as a way to correct or alter some body misfunctions. One direct example of the potential use of these derivatives is in the post-operatory treatment of some cancers. For example, in the case of gastric cancer, chemotherapy is commonly used with other forms of treatment, usually surgery and/or radiotherapy [20, 21]. The understanding of the changes in photophysical and photochemical properties by some modifications of the natural monomers is then of vital importance to use them properly.

Finally, in order to answer the two controversial points pointed out above, it is as well interesting to explain how the substitutions modify the properties of the systems. Indeed, if we can explain from the theoretical point of view how a modification of the molecule leads to a change of properties, it will allow us to clarify the relative importance of the competitive mechanism.

4.1.4 Uracil and derivatives

As said before, we focused our work on the uracil molecule and some of its derivatives, that is the 5-fluorouracil (5-FU) and the 5- and 6-aminouracil (5-AU and 6-AU) depicted in figure 4.2. In this part, we will present the state of the art of the experimental results on the main photophysical properties of the molecules studied.

Uracil is one of the most studied nucleobases. All experimental results agree on the main photophysical data, that is about the absorption, emission and excited states' lifetimes. This information, together with the corresponding to 5-FU, is shown in the Table 4.1.

Figure 4.2: Scheme of uracil and its derivatives studied in this work.

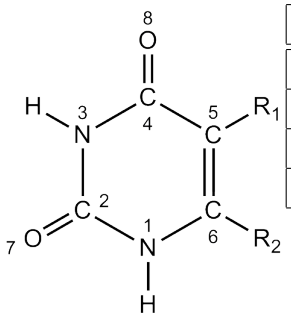

compound	R_1	R_2
uracil	H	H
5-fluorouracil	F	H
5-aminouracil	NH_2	H
6-aminouracil	H	NH_2

Table 4.1: Characteristic parameters of the first absorption and fluorescence bands of uracil and its fluoro derivative: peak wavelength, λ_{max}, fluorescence quantum yield, Φ_f.

	Absorption	emission	
compound	λ_{max}(nm)	λ_{max}(nm)	Φ_f(x10^4)
Uracil	259 [a]	312	0.35
	259.5 [b]	308 [f]	0.45 [f]
	259 [cd]		
	258.4 [e]		
	258 [fg]		
5-fluorouracil	266 [a]	335 [a]	2.21 [a]
	265.3 [e]		

[a] from reference [22] [b] from reference [12]
[c] from reference [23] [d] from reference [24]
[e] from reference [25] [f] from reference [15]
[g] from reference [26]

Uracil shows a maximum of absorption at a wavelenght between 258 and 259.5 nm and a fluorescence peak maximum between 308 and 312 nm [22, 12, 23, 24, 15, 26, 25]. The fluorescence quantum yield is low, $0.35{\cdot}10^{-4}$ for Gustavsson et al.[22] and $0.45{\cdot}10^{-4}$ for Daniels et al.[15]. 5-fluorouracil shows a red-shift both of the maximum absorption wavelength, of 1016 cm^{-1} to aproximatively 266 nm and of the fluorescence, of 2400 cm^{-1} to 335 nm [22, 25]. The quantum yield is higher, with a value of $2.21{\cdot}10^{-4}$ [22], which means that the emitting state must have different characteristics.

Figure 4.3 shows the spectra obtained for uracil and the amino-derivatives 5-AU and 6-AU by Gustavson et al. [27].

It is clear that the absorption spectrum of 5-AU is extremely different with respect to that of U. For the lowest energy absorption band it can be observed that the

Figure 4.3: Experimental absorption (left) and fluorescence (right) spectra U (solid), 5-AU (dashed) and 6-AU (dotted) in H_2O

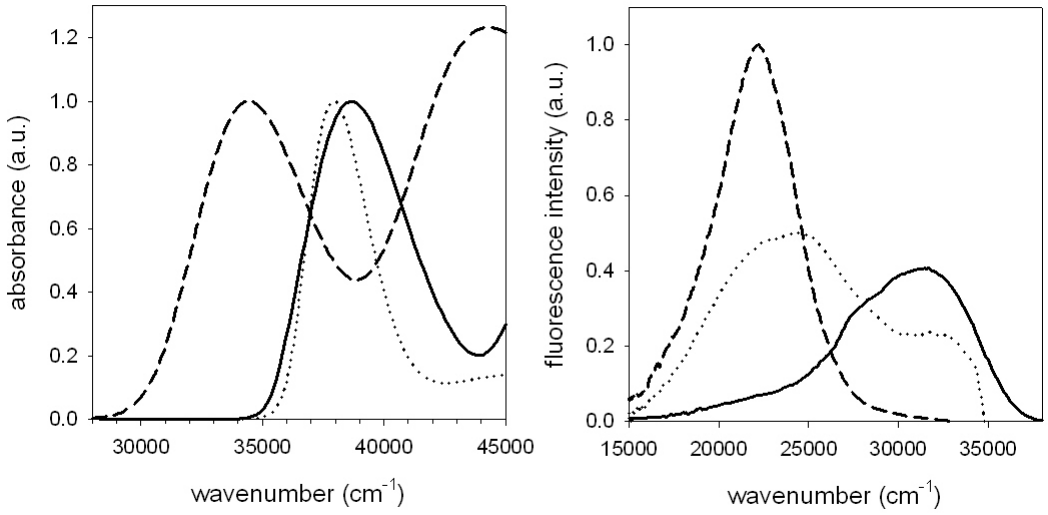

maximum is significantly red-shifted, by about 4030 cm^{-1} and it is much broader. Moreover, a higher transition, being more intense than the lowest energy one, can be observed at ca. 220 nm. On the other hand, the lowest energy absorption band of 6-AU is instead more similar to that of U, its maximum being red-shifted by only 645 cm^{-1}, but it is much sharper than that of U. A higher transition is also present at ca. 220 nm, but it is significantly less intense than the lowest energy one. Interestingly, taking uracil as reference, 5-AU and 6-AU exhibit the opposite behavior. This result confirms that the excited state behaviour of uracil derivatives is sensitive not only to the nature of the ring substituents but also on their position. Furthermore, substitution in positions 5 and 6 are confirmed to have a very different effect on uracil excited states as the double bond C_5-C_6 undergoes changes during the deactivation mechanism as it will be seen later. On the other hand, an amino substituent leads to more significant changes than a methyl substituent, also in position 6. The absorption spectrum of 6-methyluracil is extremely similar to that of U [27]. Inspection of the steady state fluorescence spectra confirms these considerations. In fact, the emission maxima of 6-AU and in particular 5-AU are remarkably red-shifted with respect to U. Consequently, the Stokes shift for both 5-AU and 6-AU are extremely high, ca. 12250 and 13700 cm^{-1} respectively, i.e more than twice as large as that of U (approx. 6000 cm^{-1} for Gustavsson et all [22]. Interestingly, the fluorescence spectrum of 5-AU is significantly sharper, and that of 6-AU much broader than that of U. It should be noted that the 6-AU emission spectrum exhibits a distinct band around 32000 cm^{-1}, close to the emission maximum of uracil.

The fluorescence lifetime of uracil and derivatives shows a two component decay.

In the case of uracil, the fast component is about 100 fs [22], while the slow one ranges from 1 to 4 ps depending of the experimental technique used. 5-FU has a larger decay time, about 700 fs for the fast component [22]. Indeed, 5-FU is the uracil derivative that show the slowest fluorescence decays.

There is only very few dynamic studies about the amino derivatives of uracil. A recent study about the dynamics of these derivatives shows interesting features [28]. While 6-AU shows an ultrafast fluoescence decay as most of the derivatives (about 0.14 ps), 5-AU exhibits major differences with the others derivatives: its fluorescence decay depends strongly of the excitation wavelength, which is not the case for the others systems. In the UV region, its decay is faster than for 5-FU, while in the visible domain, the opposite is true and the decay become dominated by the sub-picosecond component.

The results of our theoretical study should be able to explain not only the experimental features but also the differences observed between the uracil and its derivatives.

4.2 Computational details

In the study developed in this chapter, all geometries have been optimised using the Complete Active Space Self Consistent Field method (CASSCF), except in some particular cases where the optimization at the CASPT2 level seemed to be advisable for the reasons that will be explained in the next section. The nature of the stationary points located has been checked with their harmonic vibrational frequencies. Conical Intersections have been located at the CASSCF level using the method of Bearpark et al.[14] The energies of the stationary points were recalculated at the CASPT2 level, based on the CASSCF wave function, in the Single State and Multi-state approaches (as implemented in MOLCAS package), in order to integrate the effects of the dynamic correlation of the valence electrons. All geometry optimizations at the CASSCF level have been performed with valence double zeta basis set 6-31G(d), while for the computation of the energies at the CASPT2 level, two bases have been mainly used. We first used the 6-31G(d) basis set and switched then to an ANO basis set. Some benchmark calculations have been done as well to check the influence of the basis set on the energies with the cc-pVDZ basis set of Dunning. All CASPT2 calculations have been done with the standard zeroth-order Hamiltonian used in MOLCAS 7.0, that is the ionization potential-electronic afinity (IPEA) modified H_0 with a shift parameter of 0.25 by default, and state average of equal weights for each state. In the same way, the influence of the number of roots and their weight has been checked as it will

Figure 4.4: Atomic orbitals of the largest active space used

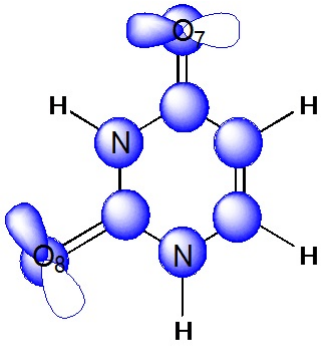

be shown in the result's section. The standard imaginary level-shift correction with a value of 0.2 was included in order to avoid the presence of intruder states. The oscillator strengths were calculated with MOLCAS using the CASCI method which uses the CASPT2 wave function.

Different active spaces were used, depending on the system and on the character of the excited state of the PES. For uracil as well as for 5-fluorouracil, the largest active space, of (14,10) (Figure 4.4), was used for the optimisation of the minima of ground state and of the two first excited states at the CASSCF level. This CAS includes all valence orbitals: the eight p orbitals of the C, N and O atoms and the n orbitals of the oxygen atoms that host their lone pairs. Given that the n_{O7}-π^* excitation is higher in energy than the excited states of interest, the n_{O7} orbital has been taken out of the active space for the CASPT2 single point calculations, where a (12,9) active space was used. For some particular points like some CIs, an active space of (10,8) has been used, where the n_{O8} orbital has been also excluded from the active space to make the calculations affordable. For aminouracil derivatives, the lone pair of the amino's nitrogen was also included in the active space. In this way, the largest active space, used for geometry optimization at the CASSCF level, was a (16,11) one. Like in the case of uracil and fluorouracil, this space has been reduced to a (14,10) for the single point CASPT2 calculations by taking out the n_{O7} orbital.

Geometry optimizations at CASSCF level were conducted with the Gaussian 03 package [?], while CASPT2 single point calculations were done with the MOLCAS package.[?, ?, ?] Paths have been calculated with the linearly interpolated internal-coordinate (LIIC) method, which is defined as the straight line in the multidimensional internal-coordinate space connecting a given initial structure with a given final one. The geometries of the points of these paths have been obtained with the Gaussian package and single-point energy calculations were done at CASPT2 level on each

geometry of the path.

As the natural environment of the nucleobases is not gas, to analyse the effect of the environment we did a study of uracil in aqueous media. We modelized the solvent as a surrounding field using the PCM model, which uses cavities of general shape, modelled on the actual solute molecule. The reaction field is then expressed in terms of a collection of apparent charges (solvation charges) spread on the cavity surface. The cavities are defined as the envelope of spheres centered on the solute atoms, reproduced by small planar sections (tesserae). The parameters of the cavity radii value of these spheres and the magnitude of the tesserae used in this study were the one established by default in the computational programs. As Gaussian do not permit optimization of the CIs using PCM, we reoptimized only the minima, using water as solvent with a dielectric constant of 78.39. We then performed PCM single point calculations on the new minima obtained and on the previous CIs at the CASPT2 level using MOLCAS. In electronic transitions (for example photon absorption or emission) non-equilibrium effects must be included, due to the finite relaxation time of solvent molecules following the sudden change in electronic distribution. This is done by partitioning the reaction field in two components, fast and slow, and equilibrating only the former. Electronic transitions from the ground state were so calculated including this non-equilibrium effect. The energy of that kind of transition should be calculated by the difference between the energy of the ground state taking into account the slow component and the energy of the excited state taking into account only the fast component. To modelize solvent short range effects like H-bonds, we also took into account explicit molecules of water. In this case, a cluster of the solute plus some solvent molecules are treated at the quantum mechanical level, and placed in a cavity in the continuum solvent environment. The analysis of the minimum number of molecules needed and the distribution around the solute molecule was carried out at the DFT level by the group of Dr Improta, from the university of Napoli, expert in the study of the solvent effect with who we maintain a collaboration in this subject [29]. They determined that in the case of uracil four water molecules should be considered. The critical points of the system were then fully reoptimized except the CI due to the high computational cost of this last kind of calculations. At this points we kept the solute geometry fixed and only allowed the reoptimization of the water molecules before recalculating the energy at the CASPT2 level with MOLCAS.

4.3 Uracil

The idea behind this work has been to start with an exhaustive study of the parent system uracil in order to get a global picture of the photochemistry and photophysics. This will allow us to determine the key points of the reaction mechanism on which we will then focus our work on the derivatives with the aim of comparing differences and explain them.

4.3.1 Ground state geometry

The first step of this study was to optimize and analyze the ground state. The equilibrium geometry, optimized at the CASSCF level with an active space of 14 electrons in 10 orbitals as explained before, is shown in Figure 4.5 and compared in table 4.2 with the experimental values obtained by X-ray [5].

Figure 4.5: Ground state geometry of uracil

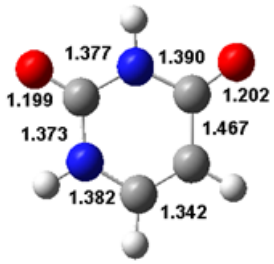

Table 4.2: Geometrical parameters of the ground state geometry obtained at CASSCF level (bond lengths in Angstroms). Experimental values obtained by X-ray are also included for comparison.

parameter	CASSCF(14/10) [a]	Exp [b]
$r(N_1C_2)$	1.373	1.374
$r(C_2N_3)$	1.377	1.381
$r(N_3C_4)$	1.390	1.370
$r(C_4C_5)$	1.467	1.444
$r(C_5C_6)$	1.342	1.343
$r(C_6N_1)$	1.382	1.380
$r(C_2O_7)$	1.199	1.233
$r(C_4O_8)$	1.202	1.219

[a] geometry at the CASSCF(14/10)/6-31G(d) level [b] reference [5]

The geometry is planar. The calculated distances show a good agreement with the experimental results as the standard deviation of the experimental data is about 0.01

Å and the differences do not exceed in any case 0.03 Å for bond lengths. Our result is also in good agreement with previous theoretical results obtained at the B3LYP/6-311G(2df,2pd) level from Matsika et all [30].

4.3.2 Vertical excitation energies

Once the ground state geometry was obtained, we studied the vertical excitation energies, also called Franck-Condon (FC) transition energies. We focused on the singlet excited states and discarded both the Rydberg and the triplet states in this study. The Rydberg states are higher in energy than the bright state that absorbs the excitation so in the decay mechanism these states must not be directly involved. In the same way, the coupling between the triplet states and the ground state, which is a singlet, is low. Even if a triplet state (the $^3(\pi\text{-}\pi^*)$) lies below the singlet excited states of interest, the experimental evidences published up to the moment when this work was developed indicate that the singlet-triplet contribution to the decay mechanism was small. Nevertheless, very recent theoretical studies point out the possible involvement of these two kind of excited states in the decay path of uracil [31, 32].

The energies of the lowest excited states calculated at CASSCF and CASPT2 levels are shown in table 4.3. Given that the ground-state equilibrium geometry is planar, the lowest excited states at this geometry can be classified following their symmetry. The first excited state corresponds to an excitation from a lone pair electron of the O_8 atom to a π^* orbital. The next excited state has a $^1(\pi\text{-}\pi^*)$ character. The third excited state, of $^1(\text{n-}\pi^*)$ character, comes from excitation of a lone pair electron of the O_7 and is quite higher in energy. For this reason we discarded this O_7 lone pair orbital in the active space (12,9) used for CASPT2 calculations as explained in the computational details, after checking that this reduction of the active space does not change the energies obtained for the three first states. The fourth excited states is again of $^1(\pi\text{-}\pi^*)$ character and is only taken into account in initial tests calculations. The second excited state, of $^1(\pi\text{-}\pi^*)$ character, has an oscillador strength of 0.338 which means that it is the state that absorbs the initial excitation, while the other excited states have oscillador strengths negligible and will therefore not be optically active.

To determine the number of roots that should be included in our calculations and analyze the influence of their weights in the results, we performed an initial set of test calculations. When we changed from 5 roots and CAS(14,10) with equal weights to 3 roots and CAS(12,9) with equal weights as well, the maximum difference was of 0.05 eV. We then calculated the energies for the three roots, with a specific weight for each one. In that case, the three roots have a weight respectively of (8,1,1), (1,8,1)

and (1,1,5) for S_0, S_1 and S_2. The differences found were of 0.05 and 0.04 eV for the two lowest vertical excitation energies, which is within the expected precision of the method (see Table 4.3). Consequently, to avoid enlarging the computational costs, we performed all following calculations with equal weights for every state. The MS-CASPT2 results have been also included with the final configuration we chose.

Table 4.3: Comparison of energy differences for the first excited states of uracil considering different number of roots and weights in the calculation.

	S1 (^{1}(n-π*))	S2 (^{1}(π-π*))	S3 (^{1}(n*-π*))	S4 (^{1}(π-π*))
CASPT2(14,10) [a]	5,16	5,53	6,58	6,67
CASPT2(12,9) [b]	5,21	5,56		
CASPT2(12,9) [c]	5,26	5,52		
MS-CASPT2(12,9) [d]	5,16	5,52		

[a] five roots with equal weights [b] three roots with equal weights [c] three roots with specific weights respectively (8,1,1), (1,8,1) and (1,1,5) for S0, S1 and S2 [d] three roots with equal weights

Our results are in good agreement with both previous theoretical and experimental results [30, 33]

4.3.3 Excited states minima and adiabatic energies

Once we got the ground state geometry, we looked for the minima of the PES of the states S_1 and S_2 (see figure 4.6. For the ^{1}(n-π*) state, we found a minimum on the S_1 surface with a geometry which deviate slightly from planarity. Three bond lengths differ considerably from those of the ground state geometry. The largest difference, as it was expected, was found for the C_4-O_8 bond that is elongated by 0.15 Å, changing from 1.202 to 1.358 Å. Other sizable differences are found in the C_5-C_6 bond, which is elongated almost 0.07 Å, and in the C_4-C_5 bond, shortened more than 0.1 Å. These changes correspond well with the excitation of one electron from the n_{O8} orbital to an antibonding π* orbital of the ring. Energies of the three lowest states at each optimised geometry are reported in Table 4.4, together with emission energies (in parenthesis). These energies are calculated as the vertical energy difference with the ground state at the excited state minimum. If the minimum correspond to a singlet excited state species, this energy is the theoretical prediction of the fluorescence energy. Our results are in good agreement with previous theoretical ones. Matsika found an emission energy for the (n-π*) state of 3.17 eV, in good agreement with our result of 3.19 eV.

The ^{1}(π-π*) minimum is more problematic and its existence is still a subject of debate. At the CASSCF level, we found an almost planar minimum for the S_2(π-π*)

state. The increase of the C_5C_6 bond length from 1.342 to 1.487 Å is a consequence of the $^1(\pi\text{-}\pi^*)$ excitation which tends to break the double bond. The elongated length of the C_4O_8 bond (of 1.344 Å) could be due to the fact that the state average geometry optimization has been run with with a nonneglegible weight on the (n-π^*) state. The small energy difference between the first and second excited states does not allows otherwise, so a part of the $^1(\text{n-}\pi^*)$ excitation is included in the description of this S_2 minimum. The character of minimum of this structure was confirmed by a frequency calculation at the CASSCF level.

Figure 4.6: Optimized geometries of the ground state and the two lowest excited states (bond length in Angstroms)

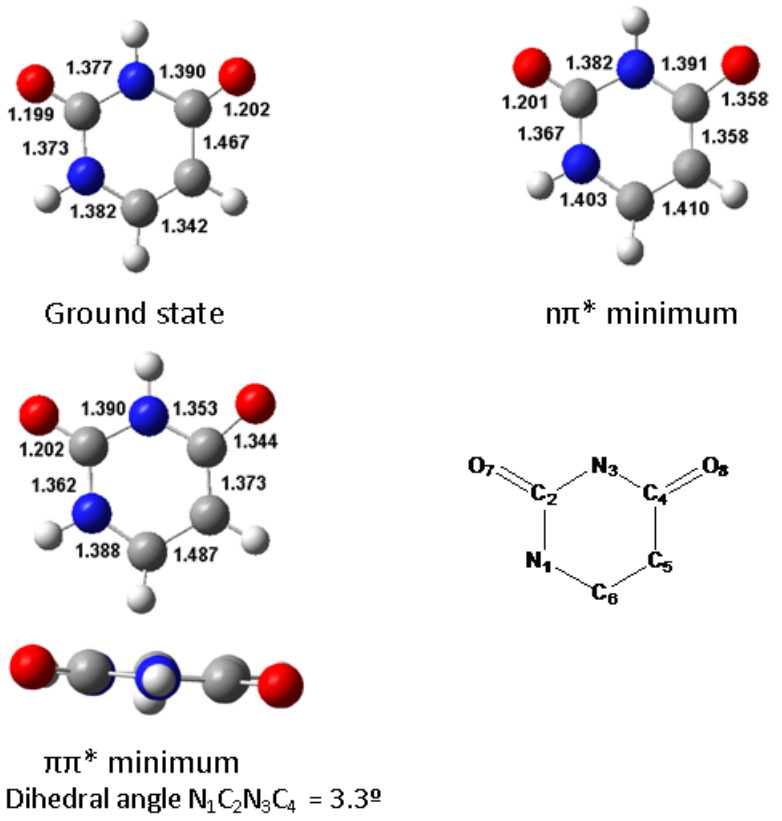

Table 4.4: Energies at optimized geometries (in eV). Fluorescence energies are reported in parenthesis (CASPT2 energies).

	Ground state	n→π* minimum	π→π* minimum [a]
S_0	**0.00** [b]	1.06	1.43
S_1	5.21	**4.25(3.19)**	4.44
S_2	5.56	5.58	**5.32(3.89)**

[a] π→π* pseudo planar minimum, optimised at the CAS-SCF level [b] the energies in bold in each column correspond to the state that was optimized

As said above, the existence and the geometry of the $^1(\pi\text{-}\pi^*)$ minimum is a subject

of debate. Indeed, Matsika and Improta both found a critical point on this area of the PES, but it was a saddle point [30, 33]. Merchàn et al. found a planar minimum at the CASSCF/6-31G(d,p) level [34] but when more dynamic correlation was included in the calculation trough a better basis set or by including $\pi\sigma^*$ excitations inside the active space, the (π-π^*) minimum disapears and a minimum energy path from the Franck-condon region on the (π-π^*) PES goes directly to the CI with the ground state. In order to include the dynamical correlation in our geometry optimization, we looked for the (π-π^*) minimum at the CASPT2 level, a non-standard and computatively expensive procedure. The optimization led to a geometry showing a clear breaking of the ring planarity and with the pyrimidine ring having a "boatlike" formation, with N_3 and C_6 going out of the plane formed by the other four atoms of the ring and some bond lengths of the ring increased (see figure 4.7). But the procedure was not able to converge to a minimum: at that region the energies of the n-π^* and π-π^* states are almost degenerated so this calculations seems to indicate that a real minimum does not exist at this level of calculation. The minimum energy geometry of the π-π^* state on the S_2 PES corresponds to a (π-π^*)/(n-π^*) CI. The optimization of this structure will be presented in the next section.

Figure 4.7: Non-planar (π-π^*) geometry representative of the area where the optimization of the (π-π^*) minimum at the CASPT2 level leads.

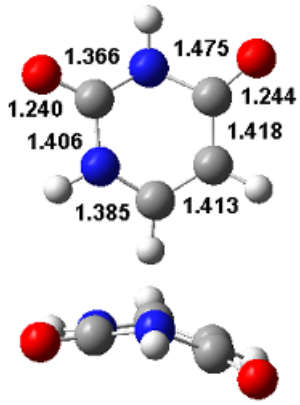

Dihedral angle $N_1C_2N_3C_4$ = -31.7°

Nevertheless, under closer examination of the (π-π^*) minimum localized at the CASSCF level, we found another interesting feature. At that geometry, the second and the fourth CASSCF excited states, both (π-π^*) excited states were strongly mixed in the MS-CASPT2 wave-function, and part of the oscillador strength passes to the second (π-π^*) excited states. It has been recently shown that the lack of dynamic correlation might lead to an artificial mixing of two π-π^* states of different nature (one of them statically neutral but dynamically ionic) [35, 36] and this is what could

happen in this case. This situation was even more marked in the 5-FU molecule, so we had to study this mixing problem more accurately in this later system, as will be shown in the corresponding section.

4.3.4 Conical intersections

After the initial population of the $S_2(\pi\text{-}\pi^*)$ state, the decay to the ground state will require two radiationless transition. We found two conical intersections corresponding to these two transitions, as well as another CI that opens the possibility of a transition from the $^1(\text{n-}\pi^*)$ state to the ground state.

The geometry of the minimum of the $(\pi\text{-}\pi^*)/(\text{n-}\pi^*)$ CI located is shown in Figure 4.8. The main geometrical changes comparing with the GS geometry correspond to a loose of the planarity of the ring that adopts a boat-like conformation. The dihedral angle formed by $N_1C_2N_3C_4$, which accounts for the curvature of the ring, is 19.3º in this case. Nevertheless, this structure presents another peculiar geometrical change, the pyramidalization of C_5, that leads the H bonded to this atom to be placed outside the plane of the ring, with the dihedral angle formed by $C_6C_5C_4H_5$ of 50.3º. The pyramidalization of C_5 also preludes the overlap of its mono-occupied orbital with the π orbitals of the other atoms of the ring. Consequently, the C_4C_5 and C_5C_6 bond distances change. The first one changes from 1.467 Å to 1.381 Å, when the other increases from 1.342 Å to 1.525Å. It indicates a breaking of the C_5C_6 double bond while the C_4C_5 shows now some double bond character. The energy of this conical intersection is lower than the vertical excitation energy to S_2. It is situated at 6.11 eV when S_2 lies at 6.85 eV in the Franck-Condon area (at the CASSCF level) energies. We also must notice that the breaking of the planarity pointed out before destabilizes a lot the ground state, with an energy of 3.26 eV at this conical intersection relative to its equilibrium geometry. Due to the lack of dynamic correlation in the CASSCF calculations, the conical intersection minimum located at this level is not anymore in the conical intersection seam when the energies are recalculated at the CASPT2 level, as $^1(\text{n-}\pi^*)$ and $^1(\pi\text{-}\pi^*)$ energies are not degenerated any longer (see table 4.5). Anyway, the CI must exist in a nearby region.

Due to the inertia of the nuclear movement along the relaxation from the FC area and to the fact that the $(\pi\text{-}\pi^*)$ state is thermodynamically favoured relative to the $(\text{n-}\pi^*)$ state, the system will continue relaxing on this surface that, after this first CI, is now the S_1 state. Continuing the relaxation on this surface, the system reaches the second CI with the ground state. In this CI the main geometrical change, when compared with the previous conical intersection, concerns essentially the position of

Figure 4.8: Geometries of the minima of the conical intersections located among the first three states of uracil. Optimizations carried out at the CASSCF(14/10)/6-31G(d) level, except the (ππ*/GS) CI located with a CAS(10/8)(bond lengths in Angstroms).

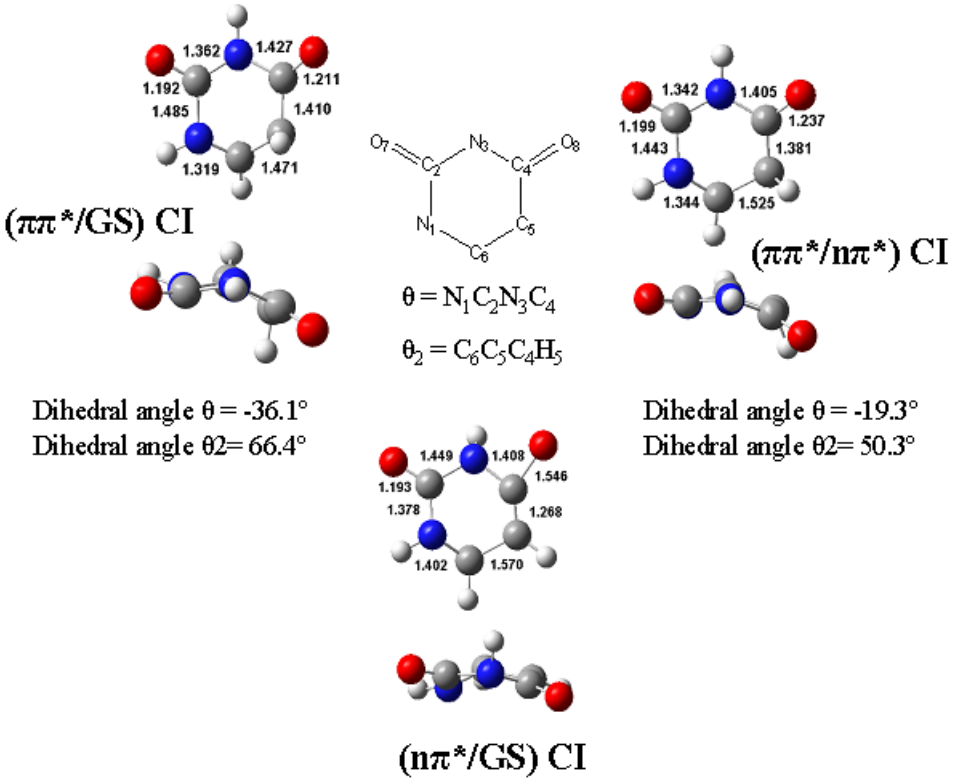

Table 4.5: CASSCF and CASPT2 energies of the conical intersections minimized at the CASSCF (in eV). Active space of (12,9) for CASPT2 calculations and (14,10) for CASSCF optimizations

		(π-π*)/(n-π*) CI	(π-π*)/GS CI[a]	(n-π*)/GS CI
CASSCF	S_0	3.26	5.18	5.97
	^{1}(n-π*)	6.10		6.07
	^{1}(π-π*)	6.11	5.18	9.32
CASPT2	S_0	2.46	4.29	5.72
	^{1}(n-π*)	4.85		5.97
	^{1}(π-π*)	5.56	4.49	7.99
MS-CASPT2	S_0	2.33	4.18	5.61
	^{1}(n-π*)	4.96		6.10
	^{1}(π-π*)	5.95	4.84	8.34

[a] Calculations with an active space (10,8)

the hydrogen atom on C_5, which goes more markedly out of the plane of the ring. The dihedral angle has increased to 66.4º compared with 50.3º of the previous conical intersection. This CI is lying at lower energy than the previous one, about 1 eV down at CASSCF level, at 5.18 eV. For this structure the (π-π*) and ground states are almost

degenerate as well at the CASPT2 level. Indeed, the energy difference between both state is only of 0.2 eV while it was of 0.7 eV in the previous CI. It means that the dynamic correlation affects almost equally to these two states. At this geometry the (n-π*) state is higher in energy, as will be shown later.

The experimental findings of Kohler and his hypothesis of the involvement of the (n-π*) dark state in the mechanism of the slow deactivation reaction [16] made of crucial interest to characterize the point of crossing of this state with the GS. The geometry of the minimum of this CI shows huge changes. First, C_4O_8 bond length increases to 1.546 Å and C_5C_6 to 1.570 Å, while C_4C_5 bond length decreases to 1.268 Å. The planarity of the ring is lost, but in a different way than in the previous CIs located. This time is the hydrogen linked to N_3 atom the one that goes out of the plane. This conical intersection is higher in energy than the initial vertical excitation to the ^{1}(π-π*) state. At CASSCF level, the (n-π*/GS) CI energy is about 6 eV, while the (π-π*) state at this geometry is more than 3 eV higher.

4.3.5 Paths

The structures and energies of the critical points gives a very valuable information about the reaction mechanisms, but it is necessary to know the paths that the system can follow to have the complete knowledge of the (static) reactive possibilities. To get this information, the best option would be to calculate the minimum energy paths between the critical structures involved in the reaction, but this option not always works correctly computationaly speaking. We have calculated linearly interpolated internal-coordinate (LIIC) paths. In some points, it is also convenient to know the gradient of the PES of the reactive states. The CASPT2 potential energy profiles allow to give a qualitative overview on the energetics of the path. The barriers found along a linear interpolation are upper bounds of the actual barriers, thereby if a LIIC path does not show any barrier, the MEP will also be barrierless.

The first path to be considered was the one followed by the system just after the initial excitation. Given that the state populated is the (π-π*) and that the gradient of its PES at the FC geometry leads towards the (π-π*) pseudo-minimum, we calculated the path from the FC region to the S_2(π-π*) planar pseudo-minimum. The energies at the CASSCF level show a barrierless path, but the CASPT2 results are quite different, showing a small barrier of 0.35 eV (Figure 4.9).

If the system relaxes to the region of the (π-π*) planar pseudo-minimum, one of the possible paths from there would be towards the (π-π*)/(n-π*) CI. The situation is similar to that of the previous path: at the CASSCF level this is a barrierless path,

Figure 4.9: LIIC profile for the (π-π*) and (n-π*) PES obtained at the MS-CASPT2 level between the (π-π*) state at the FC geometry and the (π-π*) planar pseudo-minimum.

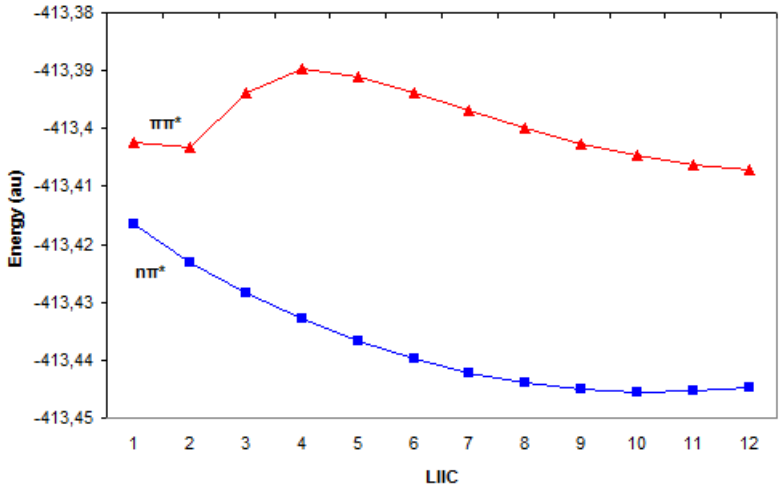

while at the CASPT2 level there is a barrier of 0.13 eV (Figure 4.10).

Figure 4.10: LIIC profile for the (π-π*) and (n-π*) PES obtained at the MS-CASPT2 level between the (π-π*) planar pseudo-minimum geometry and the (π-π*/ n-π*) CI geometry.

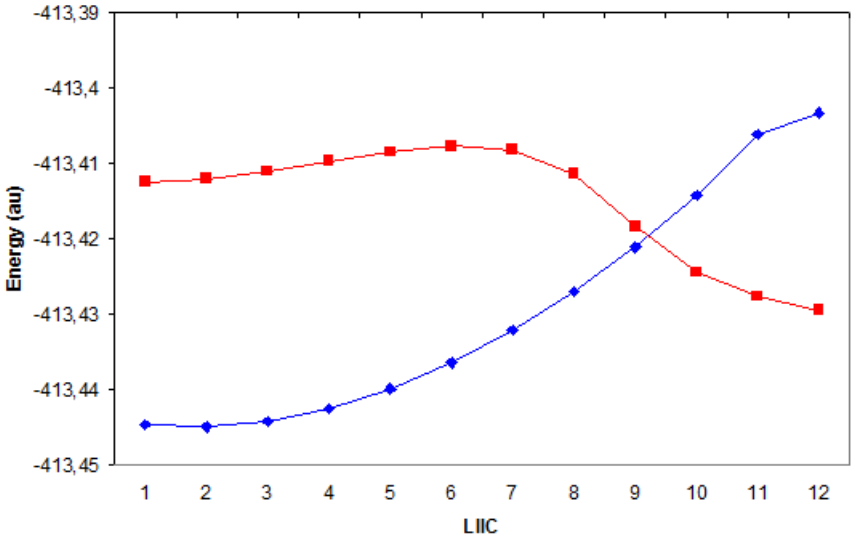

Given that the existence of the (π-π*) planar pseudo-minimum seems to be an artefact of the computational method, another possibility for the relaxation on the (π-π*) PES immediately after the initial excitation that should be considered is the movement towards the (π-π*)/(n-π*) CI, what would yield a change from the S_2 to the S_1 PES. This LIIC path, depicted in Figure 4.11, does not show any barrier, leading

directly to the final structure with a continue decrease of the (π-π^*) energy. We must not forget that the structure of this minimum energy point of the conical intersection was optimised at CASSCF level and that the CI can be located somewhere else at the CASPT2 level. In fact, ^{1}(n-π^*) and ^{1}(π-π^*) cross at point 7 of the path. It does not imply that this structure be a minimum of the CI hipersurface at the CASPT2 level, but it is an upper bound for it. We know indeed that at the CASPT2 level, the minimum energy point of the conical intersection must have a geometry close to that of point 7 and lower energy.

Figure 4.11: LIIC profile for the (π-π^*) and (n-π^*) PES obtained at the MS-CASPT2 level between the FC geometry and the (π-π^*)/(n-π^*) CI geometry.

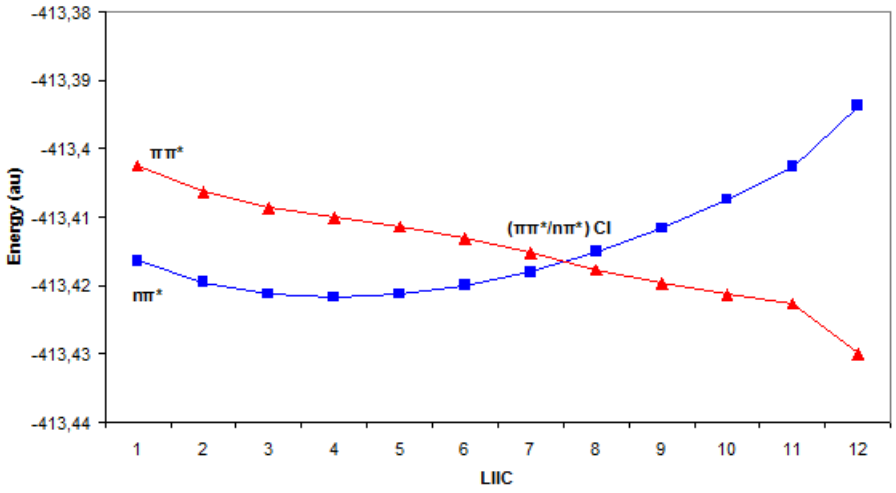

The last possibility considered for relaxation along the (π-π^*) PES from the FC region was the evolution of the system towards the (π-π^*)/GS CI. Obviously, before this crossing, the (π-π^*) PES must cross the (n-π^*) PES, but this does not have to happen necessarily through the (π-π^*/n-π^*) CI minimum energy point. For this reason we also obtained the LIIC path from the FC structure to the (π-π^*)/GS CI (see Figure 4.12). The first points of this path are calculated with an active space (12,9) containing the n_{O8} orbital, so the energy of the ground, (n-π^*) and (π-π^*) states have been obtained. After the (π-π^*) state crosses the (n-π^*) surface at the first stages of the path, the active space was reduced to (10,8), leaving the n_{O8} orbital in the inactive space. This active space is able to describe only the (π-π^*) excited states, so only the ground state and the (π-π^*) state energies are reported in the last part of the path. The path found is barrierless at the CASSCF level as well as at the CASPT2 level as shown in Figure 4.12.

With the whole of the above results we can propose a path for the fast deactivation mechanism of uracil. After the initial population of the (π-π^*) state, the system relaxes

Figure 4.12: LIIC profile for the (π-π*), (n-π*) and GS PES obtained at the MS-CASPT2 level between FC geometry and the (π-π*)/GS CI geometry.

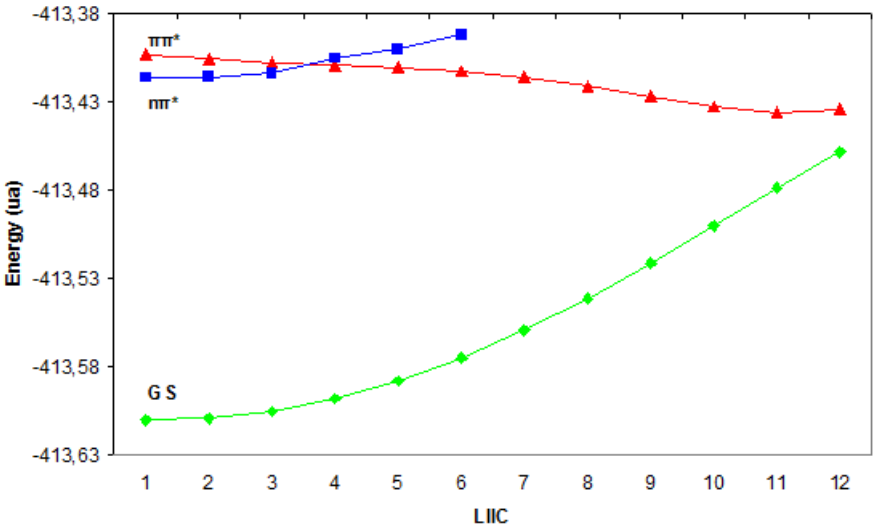

bending the ring. The planar minimum, if it exists, will not be populated because of the presence of a barrier that, although small, will make this path little probable. The system will reach the CI with the (n-π*) system (not necessarily at the minimum of the CI) keeping the (π-π*) electronic distribution that from now on will be S_1 instead of S_2. The vectors of the branching space of the CI, that show the coordinates that will make the system leave the degeneracy, are show in Figure 4.13. They correspond to a stretching of the C_4O_8 bond and a breaking of the ring planarity. The first one will lead to the (n-π*) minimum, as this minimum is characterized by an elongation of the C_4O_8 bond. The second one will lead to the second CI, the (π-π*)/GS one, where the bending of the phenyl ring is even more marked.

From the static point of view, both directions are in principle equally probable but, taken into account the dynamics, we must consider that to arrive to this CI the system is relaxing bending the ring. The inertia of the movement of the nuclei when arriving to the CI will drive the system mainly towards the (π-π*/GS) CI.

To get additional information we also calculated the LIIC path from the (π-π*)/(n-π*) CI minimum to the (π-π*)/GS CI minimum. This path is also barrierless on the (π-π*) surface, the out-of-plane motion destabilizing hugely S_0 (see Figure 4.14). The S_1 surface will have a (π-π*) character along that path, while S_2 will be of (n-π*) character. Once at the (π-π*)/GS CI, the molecule relaxes back to the S_0 minimum.

The small proportion of molecules that relaxes towards the (n-π*) minimum without any barrier at the (π-π*)/(n-π*) CI will be trapped in this dark state, as demonstrated

Figure 4.13: Branching space of the (π-π*)/(n-π*) conical intersection obtained at the CASSCF level.

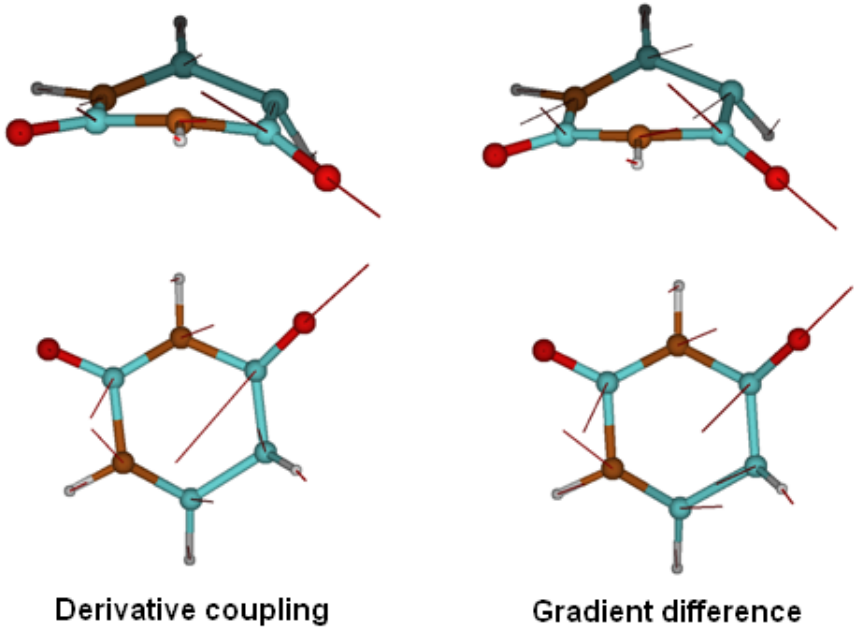

Figure 4.14: LIIC profile for the (π-π*) and GS PES obtained at the MS-CASPT2 level between the (π-π*)/(n-π*) CI geometry and the (π-π*)/GS CI geometry.

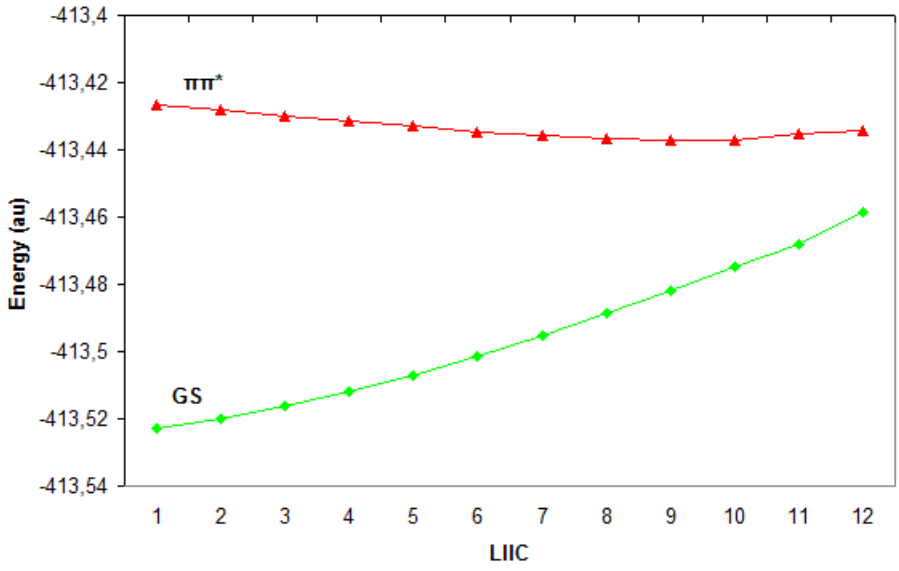

by Kohler.[10] The LIIC path from this ^{1}(n-π*) minimum to the (n-π*)/GS CI (see Figure 4.15) shows a barrier of more than 30 kcal·mol^{-1}. This high energy gap make highly unprobable the decay to the ground state trough this CI. On the other hand, the barrier between the (n-π*) minimum and the (π-π*/n-π*) CI is thermodynamically

accessible and the wave packet might recross to the π-π* PES. In that case, this path would be associated with the longer life-time of the decay mechanism. Moreover, this barrier between (n-π*) state and the conical intersection with the ground state is very small for adenine, and adenine derivatives does not exhibit slow channel decay . It suggests that the slow decay channel must be connected with the presence or not of a barrier on this path.

Figure 4.15: LIIC profile for the (π-π*), (n-π*) and GS PES obtained at the MS-CASPT2 level between the (n-π*) minimum geometry and the (n-π*)/GS CI geometry.

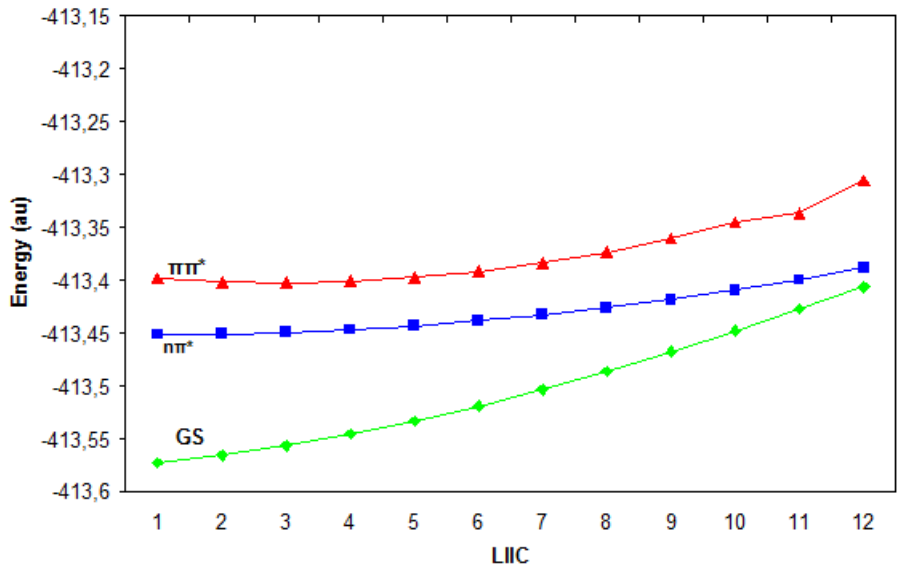

Once we got all these paths, we can draw a general scheme of the reaction profile, as shown in Figure 4.16

It has been proved that the ultrafast decay channel experimentally characterized with subpicosecond lifetime must go from the (π-π*) excited state, the one populated at the FC geometry by the initial excitation, situated on the S_2 PES, to the ground state through a conical intersections that is reached along a barrierless path. This path involves the breaking of the ring planarity as well as a pyramidalization of C_5 that pushes H_5 out of the initial plane of the molecule. For the slower decay channel we propose that at the first (π-π*)/(n-π*) CI which the system reaches along its relaxation path, a small part of the molecules decay along the S_1(n-π*) PES and is trapped into the dark (n-π*) state. The path leading to the deactivation funnel (conical intersection with the ground state) presents a large energetic barrier, so it will be strongly unfavored. The wave packet may then crosses back trough the (π-π*)/(n-π*) CI to come back on the (π-π*) PES, accounting for the longer lifetime. The com-

Figure 4.16: Resume of the reaction path profile, energies in eV

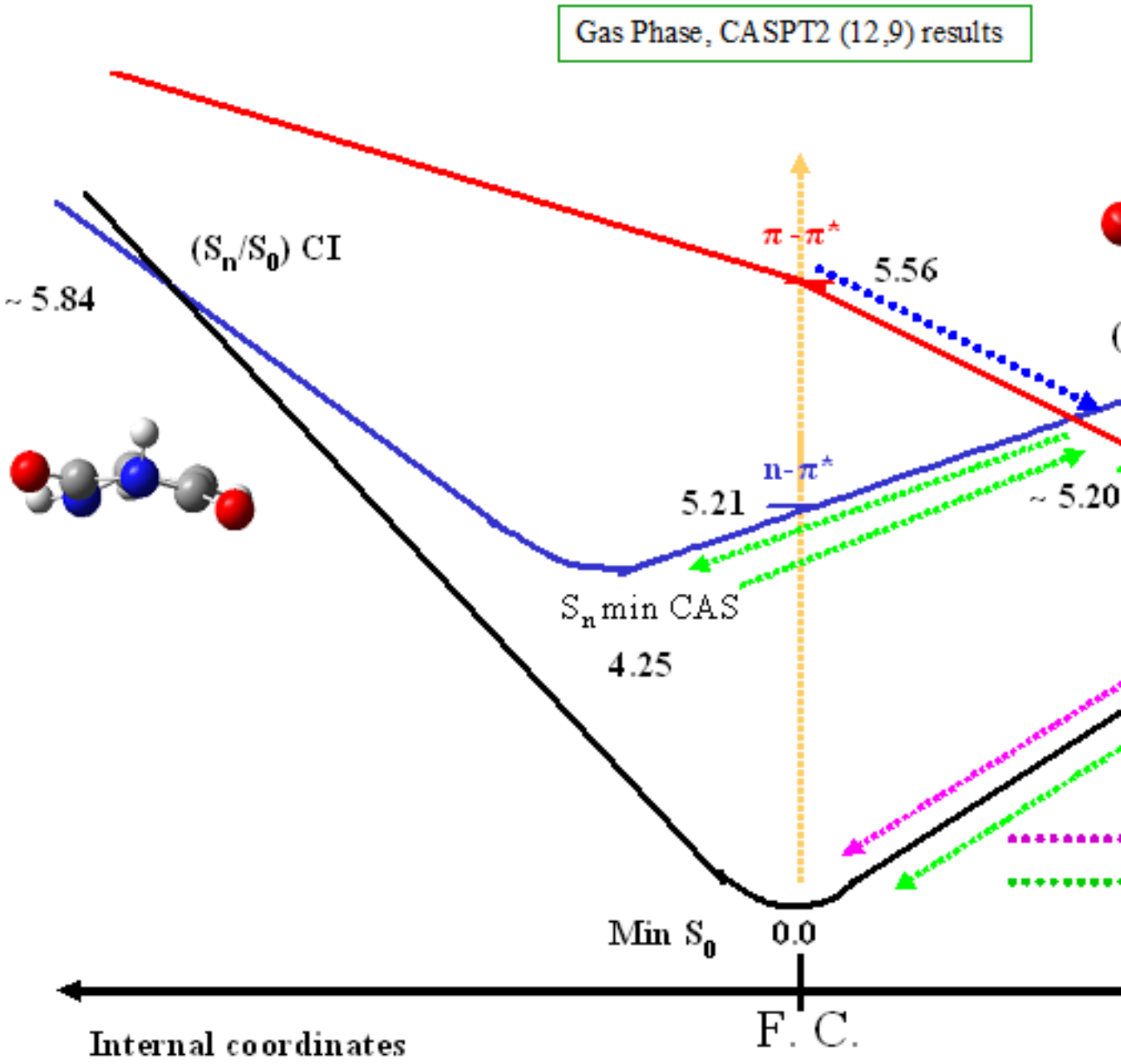

petition between the different pathways will determine the efficiency and rate of the competitive radiationless decays to the ground state.

In order to confirm these global scheme, we have investigate both solvent and substitution effects on different aspects of the reaction mechanism, but focusing mainly on the fast deactivation mechanism. Indeed, the solvent shifts the energy levels and

may change the ordering of these states involved in the photochemistry, as it has been shown that solvent blue-shifts (n_O-π^*) excitation energies much more than (π-π^*) ones. In the same way, the effect of substitution should be investigated, with special attention in C_5, given that changes in this atom are the most important ones along the reactive paths. Consequently, solvent and substitution effects will be the subject of the next sections of this chapter.

4.4 Modelization of the solvent effect: Uracil in aqueous solution.

To reproduce accurately the solvent effects is important in general because most of the experiments are performed in solution. So, to be able to compare directly experimental and theoretical results, the solvent effects should be included in the calculations. To check the importance of the environment in the photochemistry of uracil, we restudied the critical points of the deactivation mechanism presented in the previous section in an aqueous environment. To take into account the solvent, we used the PCM model as explained in the chapter of computational details. In a second step, to modelized short range effects (like H-bonds), we took some explicit water molecules into account in the description of the system.

When using the PCM model, the geometries of the minima found in gas phase were reoptimized in aqueous solution at the CASSCF level (using Gaussian package) and the energies refined at the CASPT2 level with the Molcas package. Unfortunately, the reoptimization of the CI's with PCM was not possible with the commercial version of the Gaussian package available, so for this structures only the PCM energy was recalculated.

The structures obtained for the ground state, ^{1}(π-π^*) and ^{1}(n-π^*) minima in aqueous solution are shown in Figure 4.17. Changes relative to gas phase geometries are very small for all the three geometries, with bond distances changes smaller than 0.01 Angstroms. We can conclude, then, that the solvent does not modify substantially the structure of the critical points.

The energies of the of the lowest states at these structures are collected in Table 4.6.

It can be observed that in the Franck Condon region the (π-π^*) state becomes the first excited state. This state is the one that absorbs the excitation, showing an oscillador strength of 0.40.This inversion (relative to the gas phase ordering of the

Figure 4.17: Geometries of the (a) Ground State (b) (n-π*) minimum and (c) (π-π*) minimum, optimized at CASSCF level. Distance in Angstrom. Gas phase values in parenthesis.

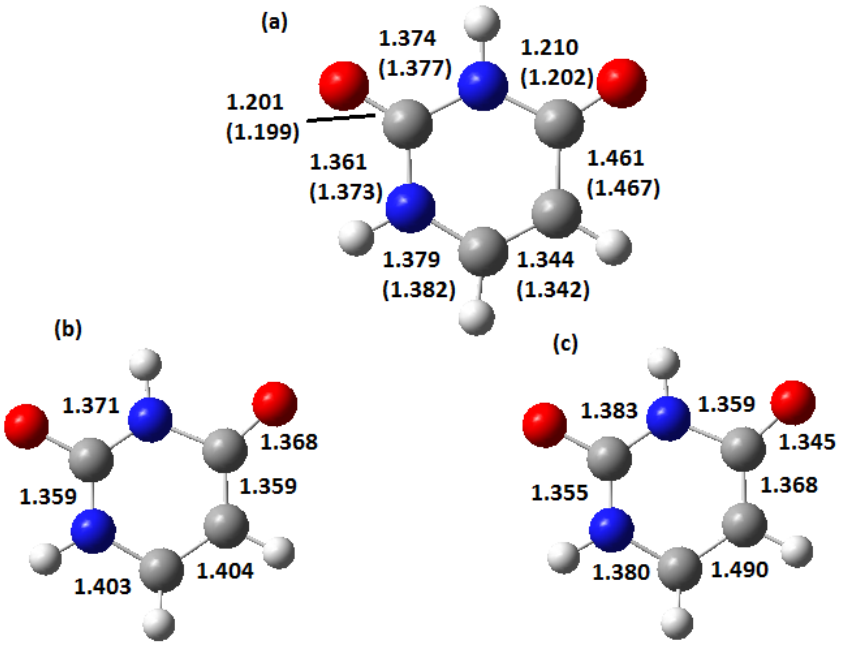

Table 4.6: Energies (in eV) of the critical points at the CASSCF(12,9)/CASPT2 level. Emission energies in parenthesis.

Structure	State	Energy
Ground state	S_0	0.0
	(n-π*)	5.56
	(π-π*)	5.31
(n-π*) minimum	S_0	0.78
	(n-π*)	4.39 (3.61)
	(π-π*)	5.66
(π-π*) minimum	S_0	1.14
	(n-π*)	4.56
	(π-π*)	5.26 (4.12)
(π-π*)/(n-π*) CI		5.54
(n-π*)/S_0 CI		6.12
(π-π*)/S_0 CI		4.51[a]

[a] Calculation with an active space (10,8)

lowest excited states) is due to the fact that the solvent destabilize the (n-π*) state by 0.4 eV while it stabilizes the (π-π*) state by more than 0.2 eV. This result is in agreement with other theoretical studies about the influence of solvent [22, 33]: using TD-DFT method and highly correlated basis set, Improta et al. found a blue-shift of

0.5 eV and a red-shift of 0.2 eV for the (n-π^*) and (π-π^*) excitation respectively.

Regarding the energy of the excited state minima, we also observe some differences relative to the gas phase. Although absolute energies of both minima does not change substantially from those of uracil in gas phase, the emission energies are both blue-shifted. While in gas phase the (π-π^*) bright state has an emission energy of less than 4 eV, it increases up to 4.12 eV in water. The same occurs with the dark state, whose vertical decay energy is blue-shifted from 3.20 eV to 3.61 eV. The Stokes-shift is larger than 1 eV, which is in good agreement with experimental data: Gustavsson et al. found an emission energy for the bright state of 31301 cm^{-1} (3.88eV) and a Stoke shift of 0.91 eV (7242 cm^{-1}).[22] Improta et al found with the TD-DFT method that the fluorescence energy of the bright state is blue-shifted by almost 0.4 eV relative to the gas phase results.[33] It should be pointed out that even if in solution at the ground state geometry the (π-π^*) state is more stable than the (n-π^*) state, the minimum of the first is more energetic than the (n-π^*) minimum, like in gas phase.

The similarity of the relative energies of the excited state minima on the gas and aqueous phase indicate that the decay mechanism must not be modified drastically in solution. Indeed, the (π-π^*)/(n-π^*), (π-π^*)/S_0 and (n-π^*)/S_0 CIs shows energies comparable with those in gas phase. The (π-π^*)/S_0 CI lays 4.51 eV above the electronic ground state at the ground state geometry, while the crossing between both excited states lays at 5.54 eV, which is almost iso-energetic with the (n-π^*) state in F.C. As the initially populated state, the (π-π^*) one, is the first excited state at the ground state structure, the system must relax directly on this surface. Like in gas phase, it can decay directly to the ground state trough the CI, without passing by the corresponding minimum, but a part of the wave packet might go to the (n-π^*) surface trough the (π-π^*)/(n-π^*) CI. The recrossing from the (n-π^*) surface to the (π-π^*) PES and further cross to the ground state, would account for the longer decay lifetime, like in the gas phase.

In order to modelize better the influence of solvation, taking into account short-range effects, calculations should be done using explicit water molecules. We performed some test calculations in this way. The number and position of the water molecules was decided based on a previous study performed by Improta et al [29], who showed that four water molecules were adequate to modelize this system. The ground state geometry was then reoptimized at CASSCF level using the cluster shown in figure 4.18 and PCM as well. Once more, bond distances do not change significantly relative to the previous models. Absorption energies, collected in table 4.7, do not show either substantial differences from those obtained with the PCM model. The (π-π^*) state is even more stabilized by the addition of the four explicit water molecules, but this

change will not modify the deactivation mechanism. It should be pointed out that even with the water molecules and PCM, at the CASSCF level, the (π-π^*) state still lies in the second excited state.

Figure 4.18: Geometry of the Ground State minima of Uracil with four water molecules, optimized at the CASSCF level. Distances in Angstroms.

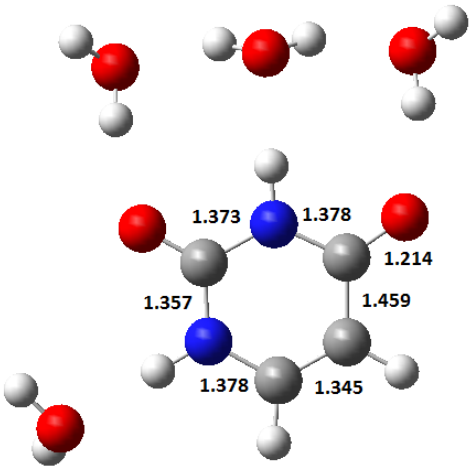

Table 4.7: Absorption energies of Uracil with 4 water molecules at the CASSCF(12,9)/CASPT2 level (in eV), oscillador strength in parenthesis.

State	Energy
S_0	0.0
(n-π^*)	5.52
(π-π^*)	5.24 (0.56)

Further exploratory calculations with explicit water molecules have been performed in other critical points. The preliminary results show the same trends than the results presented here for the ground state geometry, with non-crucial qualitative changes. Nevertheless, it can be interesting to develop with further details this study, although it is beyond the scope of this thesis.

4.5 5-fluorouracil

As said before, 5-fluorouracil is the uracil derivative that shows the longest decay time. For this reason, it is an interesting case to see how the substitution modifies the topology of the PES of the low-lying states to predict the effect of these changes according with the deactivation mechanism proposed in our work on uracil. If the changes agree with the experimental observations, our hypothesis on Uracil will be

validated. For 5-FU we developed a similar study to that on uracil, but making emphasis on the differences that might explain the longest decay time in 5-FU. The procedure followed, then, is the same than in the previous case, that means geometry optimization at CASSCF level using Gaussian package and then energy calculations at CASPT2 level with MOLCAS.

4.5.1 Ground state

The ground state geometry obtained for 5-FU is quite similar to the one obtained for uracil (see figure 4.19)

Figure 4.19: Ground state geometry of 5-fluorouracil optimized at the CAS-SCF level.

The change of the hydrogen atom by a fluor one does not modify significantly the ground state geometry. The bond distances are basically the same than those for uracil and the molecule is planar as well. Our results are in good agreement with the few theoretical works published about 5-FU in gas phase [38, 39].

4.5.2 Vertical excitation energies

The absorption energies of the singlet excited states have been calculated using an active space of 12 electrons and 9 orbitals, in order to use the same active space for all critical points, except some of the CIs that have been optimized with an active space of 10 electrons in 8 orbitals. In these cases we excluded from the active space the lone pair of O_8 given that, like in uracil, the excited states that involves excitation from this orbital is too high in energy. We found, like for uracil, that at the CASSCF level, the first excited state in the FC zone has $^1(n\text{-}\pi^*)$ character while the second one is of $^1(\pi\text{-}\pi^*)$ character (see table 4.8). The third excited state has as well a $^1(\pi\text{-}\pi^*)$ character.

The two $(\pi\text{-}\pi^*)$ states are characterized by the combination of two $(\pi\text{-}\pi^*)$ excitations with non-negligible weights in both states. Although in principle only the first three

Table 4.8: Vertical excitation energies

	S_1(n-π^*)	S_2(π-π^*)	S_3(π-π^*)
CASSCF (basis set 6-31G)*	5.72	6.84	8.45
MS-CASPT2 (basis set 6-31G)*	5.14	5.59	7.05
MS-CASPT2 (basis set ANO)	5.22	5.21	7.27

states are involved in the deactivation mechanism, test calculations including 4 roots show that in the Perturbed Modified CAS-CI (PM-CAS-CI) functions obtained at the MS-CASPT2 level there is some mixing of the two CASSCF wavefunctions of the (π-π^*) excited states. When the same kind of calculations are performed at other critical points of the (π-π) PES (see latter), this mixing is shown to be much more important, so this MS-CASPT2 results show the need of taking into account the two (π-π^*) states in the CASSCF calculations to get an accurate global description of the first (π-π^*) excited state. For this reason the rest of the study was performed including four roots in the state average of the CASSCF calculations. A consequence of the mixing of the CASSCF wavefunctions is that the PM-CAS-CI functions are characterized mainly by a unique (π-π^*) excitation. It is interesting to point out that the mixing of (π-π^*) states in 5-FU is more pronounced when this calculations are performed with a 6-31G(d) basis set, in such a way that even at the MS-CASPT2 level, both (π-π^*) states have a non-negligible contributions of the two different (π-π^*) excitations. It seems that the inclusion of correlation helps to get a cleaner description of the states of interest, based on an unique excitation. For that reason we switched to the ANO basis set. At the MS-CASPT2 level of theory with ANO basis set, the absorbing state (the state with the largest oscillator strength) is the first (π-π^*) excited state, which is practically degenerate with the (n-π^*) excited state. This is a differential feature between U and 5-FU, given that for the first system the energies of these states computed at the CASSCF(12,9)/MS-CASPT2/ANO-S level (using for these comparative calculations the same basis set than for the 5-FU) are 5.08 eV and 5.22 eV for the (n-π^*) and (π-π^*) states respectively, not degenerate. The degeneracy between (π-π^*) and (n-π^*) states in uracil is only found when an aqueous environment is considered and a certain number of explicit water molecules are included in the cluster (together with the solute molecule) treated at the quantum mechanical level.[22] The stabilization of the (π-π^*) state relative to the (n-π^*) state in 5-FU can be explained by the inductive effect of the fluorine atom that destabilize the π orbital involved in the (π-π^*) excitation that gives place to the (π-π^*) state, as have also been observed in previous studies. [22, 40]

The value for the absorption energy for 5-FU (5.21 eV at the MS-CASPT2 level) can only be compared with the experimental data of the absorption maximum in water,

of 4.66-4.68 eV.[22, 40] It has to be taken into account that the polar media of the experimental measurement stabilizes the excited (π-π^*) state relative to the ground state.

4.5.3 Excited states minima

Minima of the PES corresponding to the states S_1 and S_2 were located. Once again, the geometrical differences when compared with the ground state are in line with the excitation (see figure 4.20). For the (n-π^*) state, we found a minimum with a geometry which deviate very little from planarity. Three bond lengths differ significantly from those of the ground state geometry, one of them being logically the C_4O_8 bond, which is elongated by 0.17 Å. The other two are the bond distance (C_5C_6), which is elongated by almost 0.06 Å, and the bond distance (C_4C_5), shortened by 0.1 Å. These changes correspond well with an excitation of one electron from the n_{O8} orbital to an antibonding π^* orbital of the ring. About the (π-π^*) minimum, the geometry shows a slight break of the ring's planarity. The excitation breaks the double bond (C_5C_6) which is elongated by 0.085 Å while the (C_4C_5) is shortened by almost 0.12 Å. Once more, due to the state-average of the three first states used in the procedure of the optimization, we still have an elongation of the (C_4O_8) bond. This minimum, opposite to the one of the uracil case, is not subject of debate. Indeed, contrary to the results for U, for 5-FU this minimum was located at both CASSCF and CASPT2 levels of theory. The MS-CASPT2 geometry is very similar to the CASSCF geometry, with the breaking of the C_5-C_6 double bond slightly more marked. This structure is almost planar, with a slight pyramidalization of C_5 and C_6. It is interesting to observe the elongation by 0.14 Å of the C_4-O_8 bond. This geometrical change favours the (n-π^*) state so at this geometry this is more stable than the (π-π^*) state. At this geometry we found a strong mixture of the (π-π^*) CASSCF states in the PM-CAS-CI wavefunctions obtained at the MS-CASPT2 level. Also in this case the (π-π^*) CASSCF functions are characterized by two (π-π^*) excitations, while in the MS-CASPT2 functions only one excitation in each state has a large weight. The orbitals involved in the first excitation are mainly the π and π^* orbitals of the C_5-C_6 ethylenic moiety while in the second excitation the orbitals involved are the π_O orbital of the C_4-O_8 bond and the same π^* that before, which explains the lengthening of the C_4-O_8 bond. The need of the inclusion of dynamic correlation to obtain a correct description of the (π-π^*) state is more evident in this calculation.

The adiabatic and vertical energies of the excited state minima are shown in table 4.9. As said before, there are few studies on 5-FU, both from the experimental and

Figure 4.20: Excited states minima of 5-fluorouracil

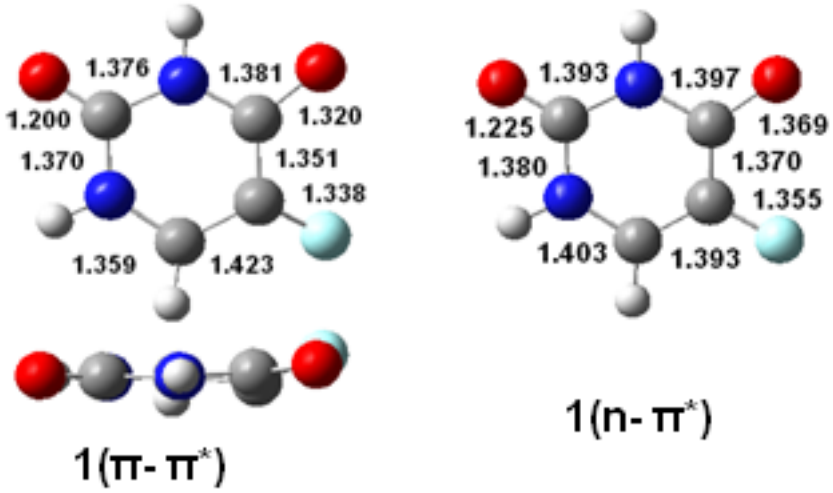

theoretical point of view and the few theoretical studies have been done in solvent. Anyway, as solvent will both stabilize the (π-π^*) minimum and destabilize the (n-π^*) minimum, we can consider that our results show a good agreement with those of Gustavsson et al.[41] The fluorescence energy show a small red-shift from 3.89 to 3.80 eV, values predicted by Gustavsson et al. in water.[22]

Table 4.9: MS-CASPT2 energies (in eV) at optimized geometries. The energies in bold in each column correspond to the state that was minimized. Fluorescence energies are reported in parenthesis.

	Ground state	(n-π^*) minimum	(π-π^*) minimum
S_0	**0.00**	0.68	1.20
S_1	5.22	**4.15(3.47)**	4.38
S_2	5.21	4.85	**4.75(3.55)**

4.5.4 Conical intersections

The conical intersections between the S_0, ^{1}(π-π^*) and ^{1}(n-π^*) states have been optimized also for 5-FU and their geometries and energies are shown in figure 4.21 and in table 4.10.

Table 4.10: MS-CASPT2 energies (in eV) of the conical intersection minima.

		($\pi\pi^*$/nπ^*) CI	($\pi\pi^*$/GS) CI[a]	(nπ^*/GS) CI
MS-CASPT2	S_0	2.35	4.21	5.44
	Sπ	4.56	3.93	
	Sn	5.47	7.36	5.86

[a] Calculations with an active space (10,8)

Figure 4.21: Geometries of the conical intersections located between the lowest-energy states of the 5-fluorouracil

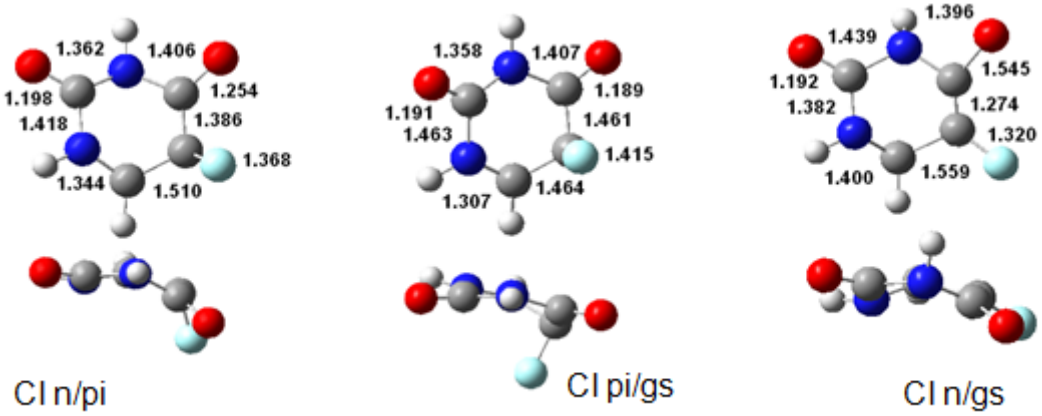

The (π-π^*)/(n-π^*) CI is quite similar to that obtained for uracil. It has a "boatlike" formation with a dihedral angle formed by $N_1C_2N_3C_4$ of 28.5°, to be compared with the value of 19.3° for uracil. Bond distances are also quite similar of those found for uracil. The (n-π^*)/GS CI has as well the same structure than in uracil, and its energy is much higher as well than the (n-π^*) minimum by almost 1.3 eV

The (π-π^*)/GS CI geometry optimized for 5-FU shows remarkable differences from that found for U. For 5-FU the bend of the ring is smaller (28° for 5-FU to compare with 36° for U) while the dihedral angle formed by the F atom with the ring is larger (101° for 5-FU to compare with 66° for U). According to this, the C_4-C_5 bond distance is larger than that found in U (1.461 Å for 5-FU to compare with 1.410 Å for U). The influence of the fluorine substitution is larger in this geometry than in any other because this structure is mainly characterized by the out-of-plane movement of this atom. A similar effect was found in another study performed by our group on 5- and 6-aminouracil (5-AU and 6-AU) as will be shown in the next section of this chapter.

4.5.5 Mechanistic overview

The direct involvement of the (π-π^*) planar minimum in the radiationless deactivation path has been checked by a MEP calculation on the ^{1}(π-π^*) PES from the Franck-Condon region. Due to the computational requirements of this calculation, it has only been performed at the CASSCF level. The minimum energy path obtained in this way leads the system directly to the (π-π^*) minimum, confirming the involvement of this species in the deactivation mechanism. To complete the profile of the deactivation path, a LIIC path was calculated between this minimum and the (π-π^*/GS) CI. The profiles of the S_0, ^{1}(n-π^*) and ^{1}(π-π^*) PES calculated at the MS-CASPT2 level are

shown in Figure 4.22. We can observe that the minimum of the (π-π*) state appears, at the CASPT2 level, slightly displaced relative to the geometry optimized at the CASSCF level (the minimum MS-CASPT2 energy point corresponds to step no. 3). After an extended plateau, a barrier of 0.22 eV relative to the initial ^{1}(π-π*) energy (0.32 eV relative to the minimum energy point) appears before a pronounced slope that directs to the (π-π*/GS) CI. The involvement of the minimum in the deactivation mechanism and the existence of a barrier to reach the funnel of deactivation to the ground state, explains the enlargement of the excited states lifetimes observed in 5-FU relative to U.

Figure 4.22: Evolution of the (π-π*) excited state from (π-π*) minimum to the (π-π*/GS) CI geometry along a linear interpolation intrinsic coordinates (LIIC) path, MS-CASPT2 energies.

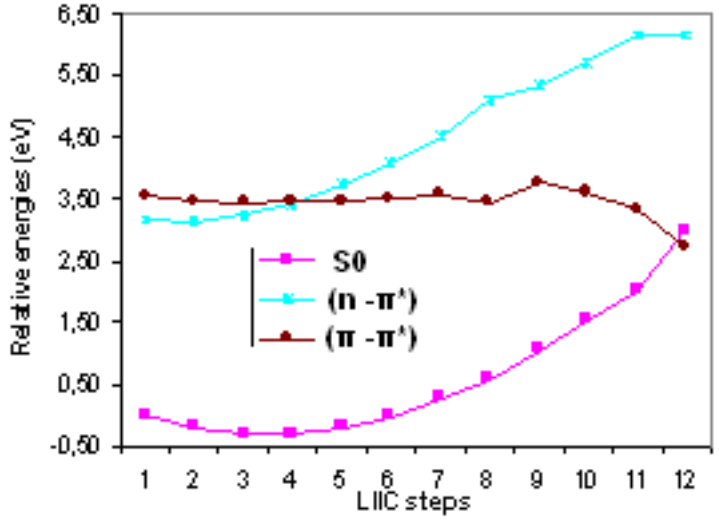

Although the MEP from the FC region directs to the Sπ minimum, it is convenient to check if there exist a direct and barrierless path from the FC region to the Sπ/S0 CI avoiding the well of the minimum. For this reason, we obtained the profile of the ^{1}(π-π*) PES between those two geometries by means of a LIIC path calculation. The results obtained at the MS-CASPT2 level are shown in figure 4.23.

In the case of the 5-FU, contrary to uracil, this path shows a small barrier of around 0.30 eV that slows down the relaxation process. A small barrier similar to this has also been found in previous studies.[17]

As said before, the minimum of the ^{1}(n-π) state is quite similar to that of U and, like in that case, it is the lowest energy excited minimum also for 5-FU. Again, the geometry of the minimum energy point of the CI of this state with the ground state is quite similar to that of U. The energy of this point is higher than that of the initial

Figure 4.23: Evolution of the (π-π*) excited state from FC geometry to the (π-π*/GS) CI geometry along a linear interpolation intrinsic coordinates (LIIC) path, MS-CASPT2 energies.

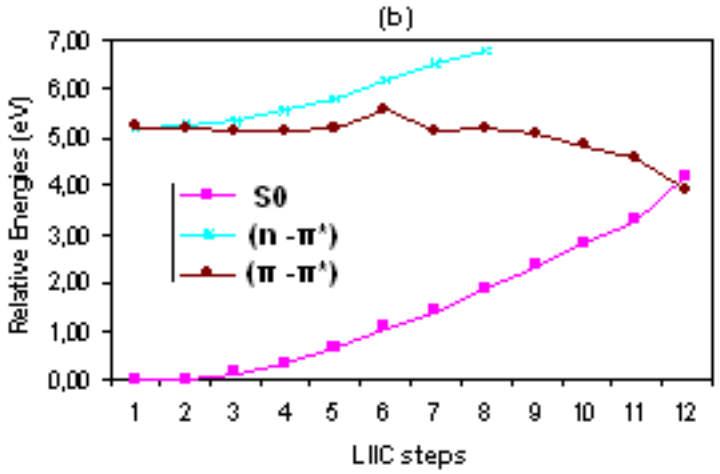

absorption energy, so this deactivation path can be ruled out. Nevertheless, it could be possible that the ^{1}(n-π) minimum were populated, given that it is thermodynamically favoured. This process would proceed through a (π-π*)/(n-π*) CI. The geometry optimized for this CI at the CASSCF level is very similar to that obtained for U, but when the energies of the ^{1}(π-π*) and ^{1}(n-π*) states at this geometry are recalculated at the MS-CASPT2 level, it is found that these states are far from degenerate. This is due to the different contribution of the dinamic correlation effect to the energy of these states. The effect of the correlation leads to the opposite effect at the Franck Condon region: while at the CASSCF level these states are far from degenerate, we found that they have the same energy when recalculated at the CASPT2 level. We have, then, a point of the CI hypersurface and, although this geometry does not have to be the minimum energy point of the CI, it provides useful information because it indicates that the crossing of these PES occurs very early in the deactivation process. Nevertheless, given that the state populated in the initial excitation is the (π-π*) state and that the forces of this PES at the FC geometry are far from negligible, it can be expected that the preferential evolution of the system will be the relaxation on the ^{1}(π-π*) surface instead of the internal conversion to the ^{1}(n-π*) state. In fact, some dynamic studies based on DFT calculations of the PES of U and 5-FU, predict the percentage of the wavepacket populating the Sn minimum.[42] In the case of U this is of a 10-25%, weakly dependent on the solvent, while for 5-FU the ^{1}(π-π*) → ^{1}(n-π*) decay channel is open in acetonitrile but closed in water, where the ^{1}(π-π*) state is more stable that the ^{1}(n-π*) state.

The global picture of the deactivation mechanisms that our results draw for 5-

FU, depicted in Figure 4.24, shows that the excited state populated after the initial excitation, the $^1(\pi\text{-}\pi^*)$ state, overcome a radiationless deactivation to the ground state via a $^1(\pi\text{-}\pi^*)$/GS CI that is reached following the geometry relaxation of the system on the $^1(\pi\text{-}\pi^*)$ surface after the initial excitation. Opposite to uracil, for 5-FU there is not a direct path because the initial relaxation of the system on the $^1(\pi\text{-}\pi^*)$ surface directs towards a minimum that corresponds to an almost planar geometry. To reach the $^1(\pi\text{-}\pi^*)$/GS CI from there, the system must overcome a small barrier, high enough to slow down the deactivation process. The alternative path, leading directly from the FC geometry to the CI avoiding the minimum, also shows a barrier, so also in this case the process will be slower than in the case of U.

Figure 4.24: Schematic representation of the radiationless deactivation mechanism of 5-fluorouracil. Energies in eV, distances in Angstroms.

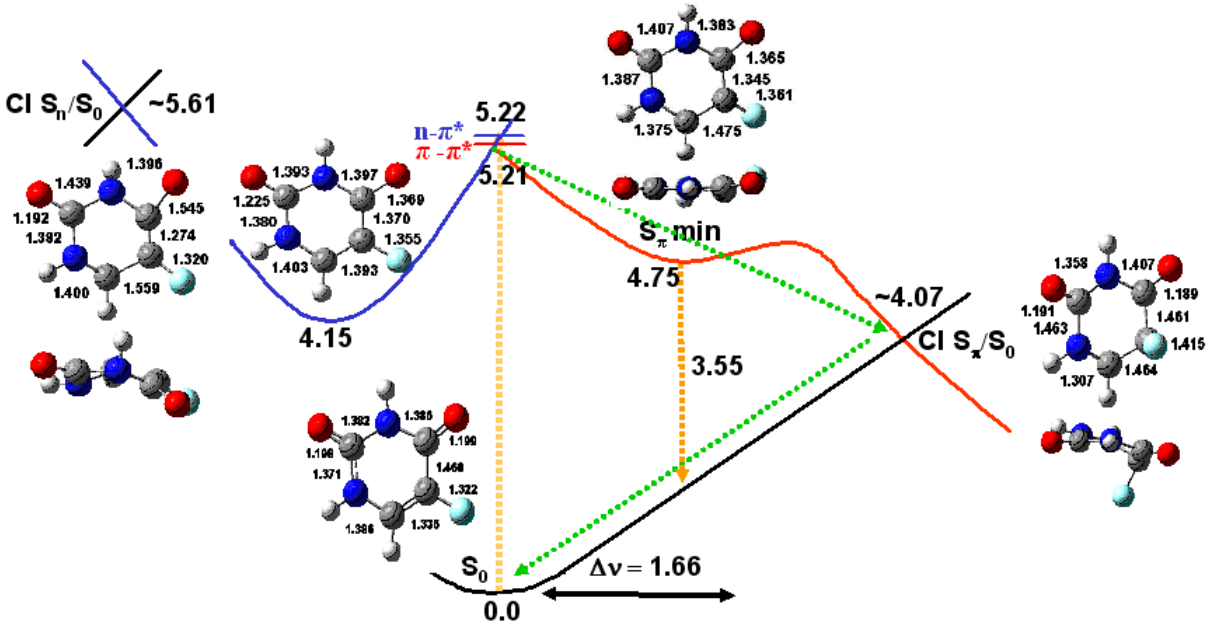

The characteristics of the deactivation mechanism of 5-FU derived from our computational results compared with that of the parent system, uracil, correlate well with the experimental measurements that assign longer excited state lifetimes to the fluoro derivative. The good agreement of the mechanistic hypothesis derived from our results with the experimental observations supports the suitability of the methodology used to perform this study. At the same time, the hypothesis proposed in our previous work of the absence of a planar minimum in the $^1(\pi\text{-}\pi^*)$ excited state of U is reinforced.

4.6 Aminouracil

As said in the introduction of this chapter, the amino substitution in position 5 and 6 of the uracil ring modifies in different ways the photochemical properties of the amino derivatives compared with the parent uracil. While 6-AU has an excited state lifetime as short as uracil, about 100 fs, 5-AU shows a slower decay of about several picoseconds, that depends on the wavelength of the excitation source. Moreover, both molecules show very different shifts in their absorption and emission bands relative to uracil. This differential influence in the luminescent behaviour of the amino-uracil derivatives is the main point of interest of this study.

4.6.1 Ground state geometry and absorption spectra

For the ground-state structure of 5-AU, two minima were found, one with the amino group almost coplanar to the ring, and another with the substituent rotated in an almost perpendicular orientation (see figure 4.25 a) and b)). Although the first geometry is in agreement with the experimental results, it is an unstable structure, as it corresponds to a shallow minimum 1.4 kcal·mol^{-1} less stable (at the CASSCF/6-31G* level) than the rotated minimum. The inclusion of an explicit water molecule in the description of the system was shown to avoid this problem, making the planar minimum more stable, so all the calculations have been done in this way. To keep the comparability, this water molecule was also included in the 6-AU system. To check the possible influence of this water molecule in the results, several test calculations were performed of the "nude" uracil derivatives. First of all, some geometries of stationary points of the 6-AU PES were reoptimized without the explicit water molecule, finding negligible changes in the geometrical parameters. Then the relative energies of different states at fixed geometries and relative energies of different areas of the PES were compared for both 6-AU and 5-AU, with and without the explicit water molecule, and again no significant differences were found. Consequently, given that the results show that the inclusion of one water molecule does not change significantly the relative energies for both systems or the geometries in the case of 6-AU, all the energetic data reported in this paper at the CASPT2/CASSCF level are referred to the 5-AU·H_2O and 6-AU·H_2O systems. The geometry of the ground state for both molecules and the position of the water molecule can be seen in figure 4.25 c) and d).

Once obtained the ground state geometries, we calculated the vertical excitations energies, shown in table 4.11. Calculations indicate that the two lowest energy excited states of 6-AU and 5-AU are qualitatively similar to that of U.[22, ?, ?, 29] A bright

Figure 4.25: Geometry of the ground state optimized at CASSCF(16,11)/6-31G* level for (a) 5-AU planar (b) 5-AU rotated (c) 5-AU·H2O and (d) 6-AU·H2O. Distances in Angstrom.

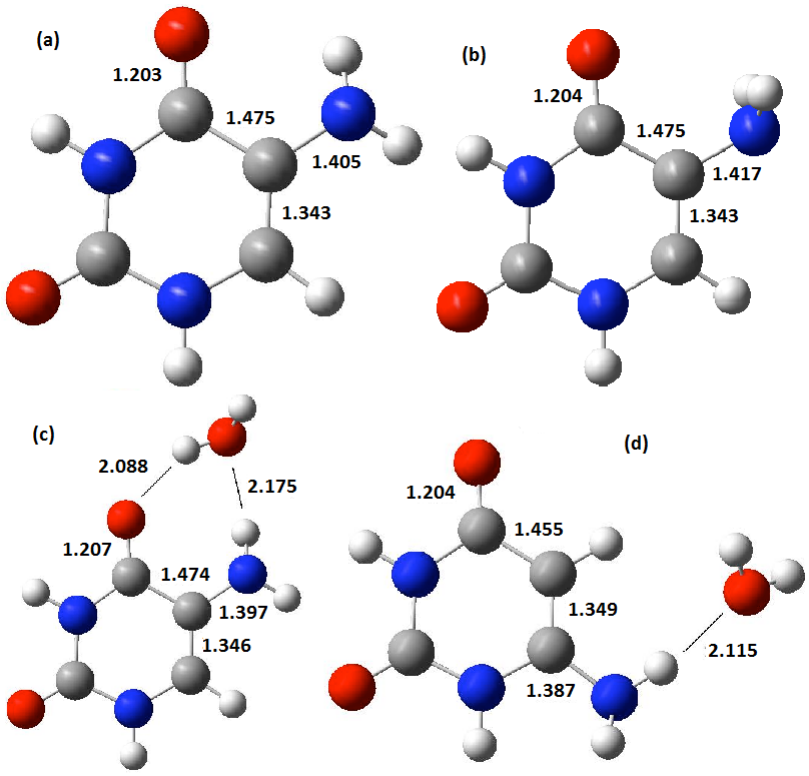

transition with (π-π^*) character is predicted, and close in energy, calculations predict the existence of a dark transition with (n-π^*) character. Another (π-π^*) state, labelled $(\pi\text{-}\pi^*)_2$, is found with a small but non-negligible oscillator strength, more than 1.5 eV higher in energy than the first (π-π^*) state. These calculations are in agreement with the experimental results that indicate that the amino substituent significantly affects the properties of the lowest energy excited states of U. For 5-AU calculations predict that the lowest energy excited state is $^1(\pi\text{-}\pi^*)$, whose transition energy is significantly red-shifted (by 1 eV) relative to the corresponding transition in U. The presence of another bright transition ($S_0 \rightarrow {}^1(\pi\text{-}\pi^*)_2$), blue-shifted by 1.5 eV with respect to ($S_0 \rightarrow {}^1(\pi\text{-}\pi^*)$) is also correctly predicted. 5-amino substitution alters also the energy ordering of the $^1(\pi\text{-}\pi^*)$ and $^1(\text{n-}\pi^*)$ excited states. While in U the latter is significantly more stable than the former, at least in the gas phase, for 5AU $^1(\pi\text{-}\pi^*)$ is predicted to be the lowest energy excited state in vacuo. From the quantitative point of view, it is noteworthy that computations significantly overestimate the effect of the 5-amino substituent on the absorption spectra, since the predicted red-shift of the ($S_0 \rightarrow {}^1(\pi\text{-}\pi^*)$) transition energy is twice as large as that found experimentally in water Calculations confirm instead that an amino substituent in position 6 does not have a dramatic effect

on the uracil absorption spectrum so the energy of the ($S_0 \rightarrow {}^1(\pi\text{-}\pi^*)$) transition in 6-AU is rather similar to that found in U. On the other hand, a quantitative disagreement is found for 6-AU: the ($S_0 \rightarrow {}^1(\pi\text{-}\pi^*)$) transition is predicted to be slightly blue-shifted (by 0.2 eV according to MS-CASPT2) with respect to U, while the experimental band maximum is red-shifted by 0.1 eV. Regarding the ${}^1(\text{n-}\pi^*)$ state, MS-CASPT2 results predict that this state is the lowest energy excited state of 6-AU, like in U.[22, ?, ?, 29] Calculations fully agree with the experiments, instead, concerning the substituent effect on the intensity of the lowest energy bright transitions. Steady-state absorption spectra indicate that the extinction coefficient of 6-AU band is remarkably larger than that of U, whereas that of the 5-AU band is smaller. This trend is fully reproduced by our results values of the oscillador strength of the (π-π^*) states °already in the gas phase, although the experimentally observed substituent influence on the intensities is much more important.

Table 4.11: Vertical excitation energies (eV) computed at the CASPT2(14,10)/ANO level on CASSCF(16,11)/6-31G(d) optimized geometries (state averaged results for four roots of equivalent weight).

	CASSCF	CASPT2	MS-CASPT2	f [a]
		5-AU		
${}^1(\pi\text{-}\pi^*)$	6.29	4.40	4.42	0.256
${}^1(\text{n-}\pi^*)$	5.47	5.45	5.50	0.000
${}^1(\pi\text{-}\pi^*)_2$	7.57	6.38	6.58	0.109
		6-AU		
${}^1(\pi\text{-}\pi^*)$	6.66	5.23	5.42	0.544
${}^1(\text{n-}\pi^*)$	5.45	5.51	5.61	0.000
${}^1(\pi\text{-}\pi^*)_2$	7.73	6.80	6.93	0.040
		U [b]		
${}^1(\pi\text{-}\pi^*)$	6.56	5.14	5.22	0.390
${}^1(\text{n-}\pi^*)$	5.00	5.00	5.08	0.000
${}^1(\pi\text{-}\pi^*)_2$	7.09	6.19	6.28	0.020

[a] oscillador strength from CASCI
[b] Calculations with an active space (12,9)

4.6.2 Emission energies

The next step on this study was the location and optimization of the minimum of the two first excited states. In fact, to interpret the experimental fluorescence spectra, it is more important to focus on the lowest energy bright state. This state, ${}^1(\pi\text{-}\pi^*)$, is expected to play a dominant role in fluorescence for two reasons; (1) it corresponds to an allowed ('bright') transition and (2) calculations predict the 'dark' ${}^1(\text{n-}\pi^*)$ state to be located well above the ${}^1(\pi\text{-}\pi^*)$ state for both 5AU and 6AU. We thus center

our analysis to the study of the $^1(\pi\text{-}\pi^*)$ minima. Energies of the optimized structures found for 5-AU and 6-AU are shown in table 4.12. For 5AU and 6AU our calculations predict a behaviour rather different with respect to that depicted for U. For 5-AU, calculations indicate that a stable minimum exists on the $(\pi\text{-}\pi^*)$ surface, with a slightly bent geometry. The most relevant changes are seen in the C_5C_6 bond length (increase of 0.05 Å relative to the ground state geometry) and for C_4C_5 (decrease of 0.02 Å). The C_4O_8 bond length increases also of 0.02 Å. One interesting feature is the change of the bond length of the amino substituent: it is shortened by 0.03 Å, which shows that the coupling between the amino part and the ring is stronger in the excited state. The C_5 atom is not pyramidalized, differently from the case of uracil. For 6-AU, optimizations of the $(\pi\text{-}\pi^*)$ state do not lead to a stable minimum, although DFT calculations show the presence of a pseudo-minimum in a flat region of the PES when the ring is constrained to planar geometries. Afterwards the ring bends strongly, leading to a region of a conical intersection with the ground state where the NH_2 substituent undergoes a large out of plane motion. The experimental fluorescent spectra of 6-AU shows a very broad band, which may indicate that it contains contributions from the planar geometries of the region of the PES close to the Franck Condon point. Only a multidimensional quantum dynamical study could assess the involvement of this region in the excited state deactivation path.

Table 4.12: Energies (in eV) computed at the CASPT2(14,10)/ANO level on CASSCF(16,11)/6-31G(d) optimized geometries (state averaged results for four roots of equivalent weight) .

geometry	state	5-AU	6-AU
Ground-state	S_0	0.00	0.00
	$^1(\text{n-}\pi^*)$	5.50	5.61
	$^1(\pi\text{-}\pi^*)$	4.42	5.42
$^1(\text{n-}\pi^*)$ minimum	S_0	1.31	1.73
	$^1(\text{n-}\pi^*)$	4.46	4.65
	$^1(\pi\text{-}\pi^*)$	6.41	5.80
$^1(\pi\text{-}\pi^*)$ minimum	S_0	0.20	[b]
	$^1(\text{n-}\pi^*)$	5.48	
	$^1(\pi\text{-}\pi^*)$	3.54 (3.34)	

[a] Fluorescence energies in parenthesis.
[b] no real minimum, leads to the CI region with the ground state.

As a whole, our computational results, schematically depicted in figure 4.26, can explain the main differences observed experimentally between these two aminouracil derivatives and uracil. While our calculations for uracil indicate that after the initial excitation, the wave-packet on the $^1(\pi\text{-}\pi^*)$ should go directly to the CI with the

ground state, explaining the ultrafast decay, the case of 5-AU is different. The presence of a minimum on the $^1(\pi\text{-}\pi^*)$ surface, with planarization of the amino group and partial formation of a double bond for the C_5N bond obviously affects the emission energy, explaining the significantly larger Stokes shift of 5-AU and its larger fluorescence quantum yield and the consequent longer life time of the excited state when compared to U. Regarding 6-AU, CASPT2 calculations predict a very fast departure from the ring planarity, with a simultaneous out-of-plane motion of the 6-amino substituent, which finally leads to a CI with S_0. No real energy barrier is predicted for this process, in line with the ultrafast decay shown by time-resolved experiments.

Figure 4.26: Schematic profile describing the absorption and the emission processes of the bright S(π-π^*) state in U (green), 5 AU (blue), and 6 AU (red). Energy differences are not in scale.

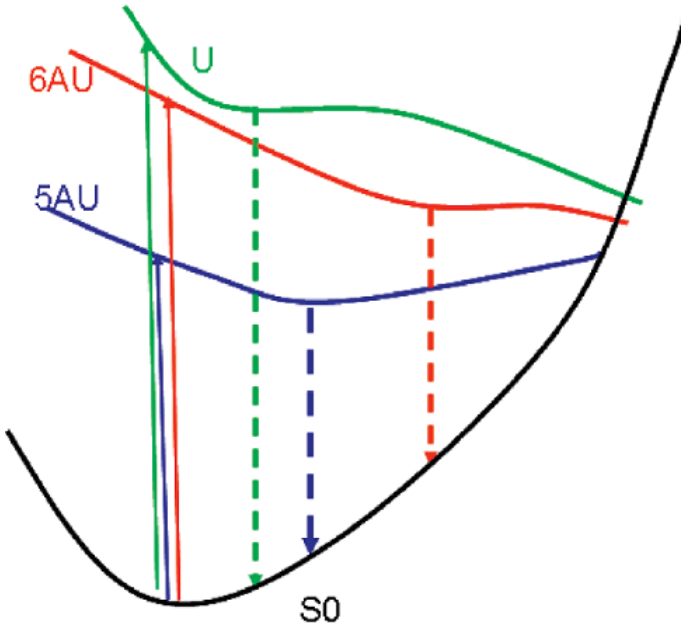

The picture provided by our calculations is thus in qualitative agreement with the experimental trends concerning both the steady-state absorption and fluorescence spectra as well as time-resolved experiments. On the other hand some quantitative discrepancies can be found, mainly on the shift of the absorption bands.

4.7 Conclusions

We can now resume the results presented in this chapter and compared the different systems studied. The presence of a substituent on uracil C_5C_6 double bond has a dramatic effect on the absorption and the fluorescence spectra of U. Furthermore, the spectral features strongly depend on the position of the substituent, as shown by the

very different behaviour exhibited by 5-AU and 6-AU. Actually, substitution in C_6 leads to smaller differences relative to the parent system: our results show no barrier in the decay processes of U and 6-AU, that experimentally shows as short excited state lifetimes as those of U. On the other hand, both 5-AU and 5-FU, show well defined minima in the $^1(\pi\text{-}\pi^*)$ surface and a barrier in the decay path, what correlates well with the experimental measurements that assign longer excited state lifetimes to these compounds. In fact, substitution in C_5 could hinder the out-of-plane motion of the C_5 substituent which, for U and its derivatives, is necessary to reach the CI between the bright excited and the ground state. As a consequence, we can expect that the deactivation mechanism result to be more complex than that found for U. Anyway, significant differences may exist between different 5-substituted derivatives: the dark $^1(\text{n-}\pi^*)$ state, which can take part into the $^1(\pi\text{-}\pi^*)$ dynamics of U and 5-FU, should not be involved in 5-AU, since it is significantly less stable than $^1(\pi\text{-}\pi^*)$ in the FC region. Another theoretical prediction that can be compared with experimental measurements is the Stokes shift. The values obtained theoretically (in the gas phase) for U, 5-FU and 5-AU (1.63, 1.66 and 2.05 eV respectively) reproduce the trend found in the experimental results in aqueous solution (0.9, 1.0 and 1.5 eV respectively). The good agreement of the mechanistic hypothesis derived from our results with the experimental observations reinforce the hypothesis proposed in our work of the absence of a planar minimum in the $^1(\pi\text{-}\pi^*)$ excited state of U. At the same time this agreement supports the suitability of the methodology used to perform this study.

Regarding this last point, the analysis of the results shows that it is necessary to include the dynamic correlation in the calculations for several reasons. To begin with, the effect of the inclusion of the correlation is different for the different states involved in the mechanism, so to calculate relative energies and localize crossing points, the correlation must necessarily be taken into account. An appropriate choice of the basis set used, like the ANO-S basis set in our case (defined to optimize the inclusion of the correlation energy), will further improve the results. On top of this, we have seen (in a more explicit way in the case of 5-FU, but also for AU derivatives) that the description of the $^1(\pi\text{-}\pi^*)$ state changes when the coupling among states is considered (at the MS-CASPT2 level of calculation). It precludes a correct description of this state at the CASSCF level, which provides a good approximation in other cases, so the MS-CASPT2 treatment is essential in this case, together with the inclusion of at least 4 roots in the initial CASSCF calculations. These results are another illustration of the fact that the CASPT2 method can not be used like a "black box" without a convenient initial study of the computational parameters to be used, and a subsequent detailed analysis of the results. Anyway, in order to have a complete description of the ultrafast deactivation mechanism, a dynamical treatment of the problem is necessary.

But to get accurate results, a good description of the PES is essential, so high level quantum methods must be used to obtain it.

Bibliography

[1] Pfeifer, G., You, Y.-H., and Besaratina, A. *Mutat. Res.* (571), 19–31 (2005).

[2] Middleton, C. T., de La Harpe, K., Su, C., Law, Y. K., Crespo-Hernández, C. E., and Kohler, B. *Annual Rev. of Phys. Chem.* **60**, 217–39 (2009).

[3] Dreyfus, M., Dodin, G., Bensaude, O., and Dubois, J. *J. Am. Chem. Soc.* **97**, 2369 (1975).

[4] Holmen, A., Broo, A., Albinsson, B., and Norden, B. *J. Am. Chem. Soc.* **119**, 12240 (1997).

[5] Voet, D. and Rich, A. *Prog. Nucl. Acid. Res. Mol. Biol.* **10**, 183 (1970).

[6] Mons, M., Dimicoli, I., Piuzzi, F., Tardivel, B., and Elhanine, M. *J. Phys. Chem. A* **106**, 5088 (2002).

[7] Weinkauf, R., Aicher, P., Wesley, G., Grotemeyer, J., and Schlag, E. *J. Phys. Chem.* **98**, 8381.

[8] Grun, C., Heinicke, R., Weickhardt, C., and Grotemeyer. *J. Int. J. Mass Spectrom. Ion Processes* **187**, 307 (1999).

[9] Crespo-Hernández, C. E., Cohen, B., Hare, P. M., and Kohler, B. *Chem. Rev.* **104**(4), 1977–2019 (2004).

[10] Pecourt, J. M., Peon, J., and Kohler, B. *J. Am. Chem. Soc.* **125**, 13594 (2003).

[11] Gustavsson, T., Sharonov, A., Onidas, D., and Markovitsi, D. *Chem. Phys. Lett.* **106**, 11367 (2002).

[12] Voet, D., Gratzer, W., Cox, R., and Doty, P. *Biopolymers* (1), 193–208 (1963).

[13] Callis, P. *Annu. Rev. Phys. Chem.* , 329–357 (1983).

[14] Bearpark, M. J., Robb, M. A., and Schlegel, H. B. *Chem. Phys. Lett.* **223**, 269 (1994).

[15] Daniels, M. and Hauswirth, W. *Science* **171**, 675–677 (1971).

[16] Hare, P. M., Crespo-Hernández, C. E., and Kohler, B. *Proceedings of the Nat. Acad. Sc. of the U.S.A.* **104**(2), 435–40 (2007).

[17] Serrano-Andrés, L. and Merchán, M. *J. Photochem. Photobiol. C: Photochem. Rev.* **10**(1), 21–32 (2009).

[18] Langer, J. *Annals of Physics* **110** (1969).

[19] Sagan, C. *J. Theor. Biol.* **39**, 195 (1973).

[20] Yoney, a., Bati, Y., Akboru, H., Isikli, L., and Unsal, M. *Cancer radiothérapie : journal de la Société française de radiothérapie oncologique* **14**(1), 19–23 (2010).

[21] De Angelis, P. M., Svendsrud, D. H., Kravik, K. L., and Stokke, T. *Molecular cancer* **5**, 20 (2006).

[22] Gustavsson, T., Bányász, A., Lazzarotto, E., Markovitsi, D., Scalmani, G., Frisch, M. J., Barone, V., and Improta, R. *J. Am. Chem. Soc.* **128**(2), 607–19 (2006).

[23] Clark, L. and Tinoco, I. *J. Am. Chem. Soc.* **87**, 11–15 (1965).

[24] Kleinwachter, M., Drobnik, J., and Augenstein, L. *Phtochem. Photobiol.* **5**, 579–586 (1966).

[25] Lohmann, W. *Z. Naturforsch* **29**, 493–495 (1974).

[26] Aaron, J. and Gaye, M. *Talanta* **35**, 513–518 (1988).

[27] Bányász, A., Karpati, S., Mercier, Y., Reguero, M., Gustavsson, T., Markovitsi, D., and Improta, R. *J. Phys. Chem. B* (2010).

[28] Bányász, A., Gustavsson, T., Keszei, E., Improta, R., and Markovitsi, D. *Photochemical & photobiological sciences : Official journal of the European Photochemistry Association and the European Society for Photobiology* **7**(7), 765–8 (2008).

[29] Mercier, Y., Santoro, F., Reguero, M., and Improta, R. *J. Phys. Chem. B* **112**(35), 10769–72 September (2008).

[30] Matsika, S. *J. Phys. Chem. A* **108**(37), 7584–7590 (2004).

[31] Sobolewski, A. L. and Domcke, W. *Phys. Chem. Chem. Phys.: PCCP* **12**(19), 4897–8 (2010).

[32] González-Luque, R., Climent, T., González-Ramírez, I., Merchán, M., and Serrano-Andrés, L. *J. Chem. Theory. Comput.* (2010).

[33] Improta, R. and Barone, V. *J. Am. Chem. Soc.* **126**(44), 14320–1 (2004).

[34] Merchán, M., González-Luque, R., Climent, T., Serrano-Andrés, L., Rodríguez, E., Reguero, M., and Peláez, D. *J. Phys. Chem. B* **110**(51), 26471–6 (2006).

[35] Angeli, C. *J. Comp. Chem.* **30**(8), 1319–33 (2009).

[36] Angeli, C. *Int. J. Quant. Chem.* **00** (2010).

[37] Santoro, F., Barone, V., Gustavsson, T., and Improta, R. *J. Am. Chem. Soc.* **128**(50), 16312–22 (2006).

[38] Shukla, M. *J. Mol. Struct.: THEOCHEM* **535**(1-3), 269–277 (2001).

[39] Alcolea Palafox, M., Tardajos, G., Guerrero-Martínez, A., Vats, J. K., Joe, H., and Rastogi, V. K. *Spectrochimica acta. Part A, Molecular and biomolecular spectroscopy* **75**(4), 1261–9 (2010).

[40] Billinghurst, B. E., Yeung, R., and Loppnow, G. R. *J. Phys. Chem. A* **110**(19), 6185–91 (2006).

[41] Gustavsson, T., Coto, P. B., Serrano-Andrés, L., Fujiwara, T., and Lim, E. C. *J. Chem. Phys.* **131**(3), 031101 (2009).

[42] Improta, R., Barone, V., Lami, A., and Santoro, F. *J. Phys. Chem. B* **113**(43), 14491–503 (2009).

UNIVERSITAT ROVIRA I VIRGILI
AB-INITIO INSIGHT INTO THE ORGANIC PHOTOCHEMICAL DIVERSITY: NON-RADIATIVE DECAY IN URACIL AND DERIVATIVES AND INTRAMOLECULAR CHARGE TRANSFER MECHANISMS IN THE BENZONITRILE FAMILY
Yannick Mercier
DL:T. 1371-2011

UNIVERSITAT ROVIRA I VIRGILI
AB-INITIO INSIGHT INTO THE ORGANIC PHOTOCHEMICAL DIVERSITY: NON-RADIATIVE DECAY IN URACIL AND DERIVATIVES AND INTRAMOLECULAR CHARGE TRANSFER MECHANISMS IN THE BENZONITRILE FAMILY
Yannick Mercier
DL:T. 1371-2011

We are faced with the paradoxical fact that education has become one of the chief obstacles to intelligence and freedom of thought.

Bertrand RUSSELL

Education is a condition of imposed ignorance!

Noam CHOMSKY

UNIVERSITAT ROVIRA I VIRGILI
AB-INITIO INSIGHT INTO THE ORGANIC PHOTOCHEMICAL DIVERSITY: NON-RADIATIVE DECAY IN URACIL AND DERIVATIVES AND INTRAMOLECULAR CHARGE TRANSFER MECHANISMS IN THE BENZONITRILE FAMILY
Yannick Mercier
DL:T. 1371-2011

UNIVERSITAT ROVIRA I VIRGILI
AB-INITIO INSIGHT INTO THE ORGANIC PHOTOCHEMICAL DIVERSITY: NON-RADIATIVE DECAY IN URACIL AND DERIVATIVES
AND INTRAMOLECULAR CHARGE TRANSFER MECHANISMS IN THE BENZONITRILE FAMILY
Yannick Mercier
DL:T. 1371-2011

Chapter 5

Charge transfer reaction

5.1 Introduction

One of the most frequent photochemical reactions is the Charge Transfer(CT) process in which, following the initial excitation, an electron is transferred from a donor group (D) to an acceptor one (A). It can occur between two separate molecules (intermolecular CT) or between two regions of a single molecule (intramolecular CT, ICT). The prototype of ICT reaction involves an organic molecule with two π systems linked by a single bond. The photochemical excitation can be localized in one of the π systems of the molecule, leading to a called Locally Excited (LE) state, or produce the charge transfer leading to an ICT excited state like depicted in Figure 5.1. The ICT reaction leads to both geometrical and electronic changes, and possibly to a decoupling between the donor and acceptor parts. Following Platt's nomenclature, established for benzene and its mono- or di-substitued derivatives [1], these states are classified as ^1L_b and ^1L_a respectively.

Figure 5.1: Scheme of the LE and ICT state of a D-A system

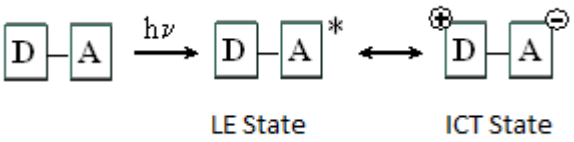

One interesting property of these systems was found by Lippert et al. almost fifty years ago [2, 3] in 4-(N,N-dimethylamino)-benzonitrile (DMABN, see figure 5.2). In this system the donor moiety is the amino group while the acceptor part is the benzonitrile. DMABN was the first molecule found that showed dual fluorescence, that is, it can fluoresce simultaneously at two different frequencies, depending on the solvent

polarity and temperature. These two fluorescence bands correspond to the radiative desexcitation from both types of excited state, LE and ICT. The emission from the LE excited state is named normal fluorescence while the one from the ICT excited state is called anomalous fluorescence (see figure 5.3 for a scheme of the fluorescence spectra).

Figure 5.2: Scheme of the DMABN molecule

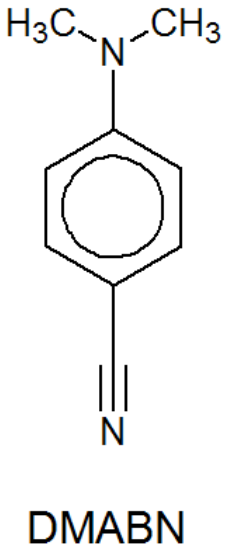

Figure 5.3: Scheme of the dual fluorescence spectra

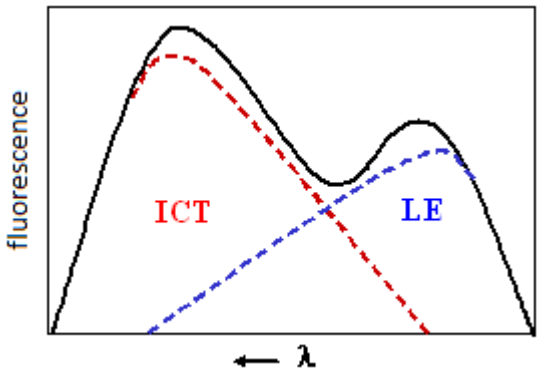

For DMABN, Lippert et al. observed that in nonpolar solvents only the normal fluorescence appears, while in strongly polar solvents both bands are present, with the long-wavelength fluorescence growing in intensity with the increase of the polarity of the solvent. After determining that the fluorescent species of this anomalous band show a high dipole moment, they attributed this band to the ^1L_a state, on the belief that its structure should have a highly dipolar quinoid character. Their hypothesis was that due to the reorientation of the polar solvent, the ^1L_a state is stabilized and turns into the lowest excited state allowing it to emit.

In general, this kind of systems could emit from both excited states, depending on the relative equilibrium between them (that can be tuned by the polarity of the solvent) and on the activation energy of the CT process (see figure 5.4). That means that for the anomalous band to appear, the cinetic and thermodynamic conditions must be favourable to the ICT state. Since the discovery by Lippert, DMABN has become the prototype of the systems showing dual fluorescence and the most studied one.

Figure 5.4: Schematic representation of the LE and CT states leading to a fluorescence spectra a) with only a normal band, b) with dual fluorescence.

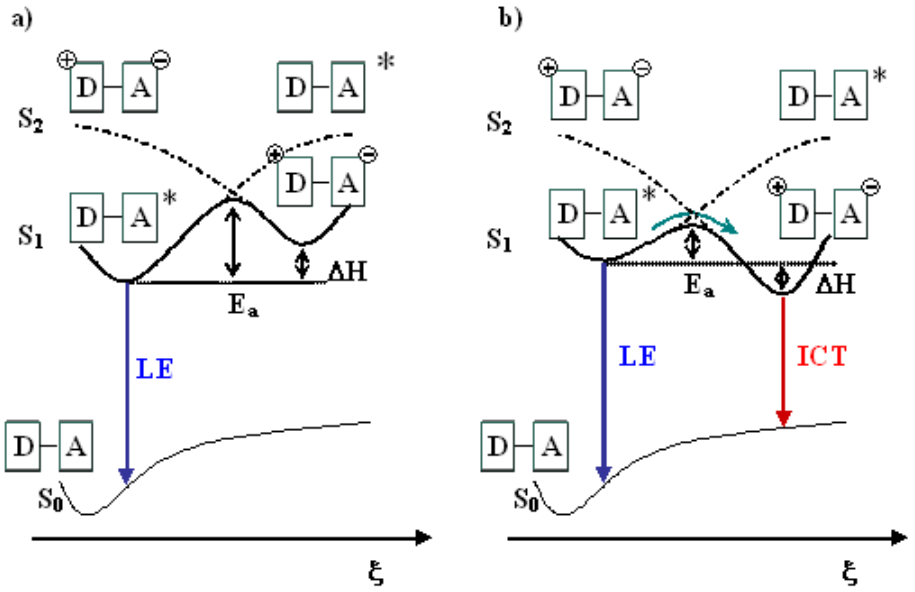

The systems presenting ICT are of great interest in many field, as fluorescence indicators [4, 5] or as potential molecular logical gates [6]. With the interest arisen by this molecule, experimental as well as theoretical data started to accumulate and other hypothesis regarding the fluorescent species and the mechanism of the ICT reaction appeared, as can be read in the extensive review of Grabowski et al. [7]. At the same time, other D-A systems with dual or anomalous fluorescence have been found, and the debate about the ICT process has become more entangled. Although the last years have permitted to clarify some aspects of the long-running controversy, there are still some points that are subject of debate. Basically, two issues of the reaction are always investigated. First, the reaction path that leads from the Franck-Condon region to the ICT state and then the geometrical and electronic structure of the ICT state responsible for the anomalous band.

From the schematic picture of the global reaction shown in figure 5.4, one can see that the reaction take place on two excited surfaces. An early theoretical ab-initio

study by Serrano-Andrés et al. on DMABN [8] demonstrated, based on the high value of the oscillador strength of this excited state, that the second excited state S_2, ^1L_a, is the one that absorbs the initial radiation. As emission is only possible from the first excited state (according to Kasha Rules), there must be a non-adiabatic path leading from the S_2 to the S_1 surface. Then, once on the S_1 surface, an adiabatic path must connect both LE and ICT excited states. The profile of this path will be the key of the fluorescence pattern. The main hypothesis about the first part of the path, leading from the S_2 to the S_1 surface, is that after the initial excitation, an ultrafast internal conversion occurs through a funnel. A study of the DMABN at ab-initio level made by Gomez et al. [9] confirmed that after population of the S_2 state in FC, a quick relaxation without a significant barrier leads to a S_2/S_1 CI where the deactivation can occur. Moreover, they found that this nonradiative decay can take place along an extended conical intersection seam. Anyway, some of the DMABN derivatives studied experimentally that show dual fluorescence present very small energy difference between the S_2 and the S_1 state, which might indicate that part of the decay might occur trough vibrionic coupling as well. About the adiabatic path, it has been considered for a long time that after the internal conversion the ICT state is populated directly from the LE state. An extensive experimental work on DMABN and derivatives suggested, based on time-resolved picosecond emission techniques, that the rise time of the ICT fluorescence corresponds to the decay time of the LE emission [10], although both processes were quicker (4 ps) than the instrument response functions (>20 ps). Recent studies using femtosecond time-resolved techniques suggest that the mechanism of this reaction might be more complex than thought, with the involvement of a $\pi\sigma^*$ state along the path to the ICT state. This hypothesis has been supported as well by recent femtosecond transient absorption measurements [11, 12, 13].

The second controversial point lies on the structure of the emitting species. On this point many theories have been postulated during the last thirty years, and even if most of then are now discarded, it is of interest to revisit them. As we have said earlier, both geometrical and electronic structure must be characterized. Some considerations about the electronic character should then be explained before talking about the proper ICT structure.

The Valence Bond (VB) theory is useful to describe the different excited state that are present in this reaction. Indeed, it allows to differentiate not only the LE and ICT states in terms of the electronic distribution, but also the different possible ICT states. As shown in figure 5.5, the ground and LE states have a covalent structure derived from the combination of the typical two resonant electronic structure of the benzenic ring (structure (I) and (II) for the ground and the LE states respectively).

Figure 5.5: Scheme of the electronic structures of the different state of DMABN according to VB descriptions

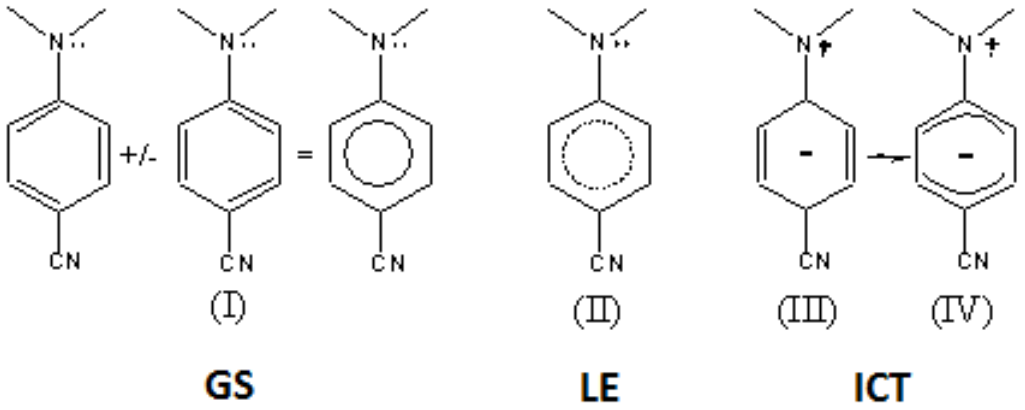

On the other hand, the CT structures have a zwiterionic character (structures (III) and (IV)). This CT state can be described in terms of quinoid (Q) or antiquinoid (AQ) structures. The quinoid structure, labelled (III) in figure 5.5, is characterized by shorter C-C central bonds of the benzene ring as well as shorter $C_{benzene}$-$N_{pyrrolo}$ bond. In the AQ structure (IV), stabilized by two resonant structures, the two central C-C bonds of the benzene ring and the $C_{benzene}$-$N_{pyrrolo}$ bond are elongated while the others are shortened.

Different ICT structures have been proposed in the last thirty years as potential ICT emitting species. They are basically differentiated and named by their geometrical structure (see Figure 5.6). The Twisted ICT (TICT) was proposed by Grabowski and co-workers [14]. It is characterized by a twist of the amino group relative to the plane of the phenyl ring. In the second one, proposed by Zachariasse et al. [15, 16], the nitrogen atom of the donor group (the amino group) is rehybridized, adopting a pyramidal conformation. This model is called Wigged ICT (WICT). Later, Zachariasse proposed another model with a planar structure (Planar ICT (PICT)), with the amino group being coplanar to the phenyl ring [17, 18]. The last model is the Rehybridization by ICT (RICT) [19, 20] where the cyano donor group is rehybridized, from a sp to a sp^2 configuration, leading to a closure of the C-C-N angle.

Today, the controversy lies essentially between the PICT and TICT models for the numerous derivatives of the DMABN that have been studied. Some experimental studies and almost all the theoretical calculations indicate that the twist angle is the reaction coordinate for the population of the ICT state [9, 21], but there are experimental works that support the PICT model. One of the arguments to support one or the other is based on the relation between the electronic and geometrical structures.

Figure 5.6: Scheme of the structures of the different ICT models

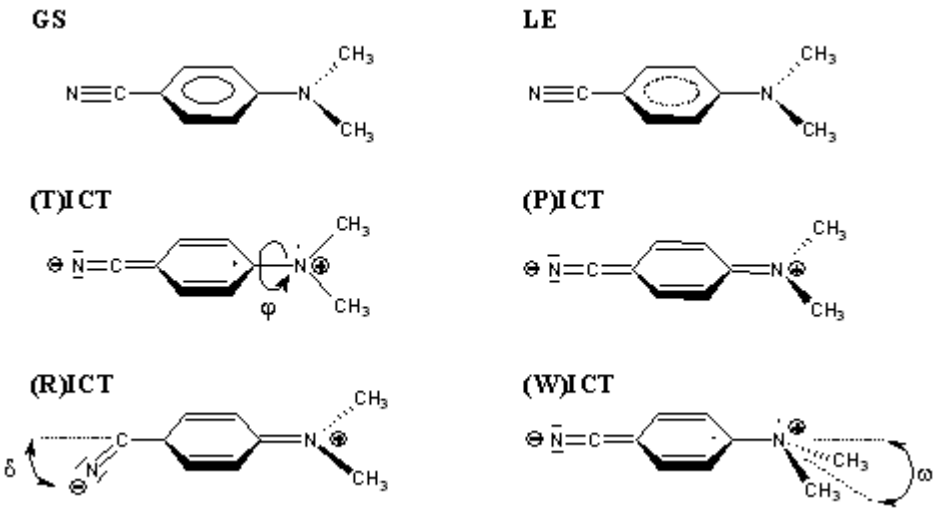

In a twisted configuration, the electronic coupling between the donor and acceptor parts must be very small due to the zero overlap of the molecular orbitals of the two moieties. The N-Phenyl bond that join them has for this reason a single bond character so this distance is long. On top of this, the spectrum of the ICT state should be equal to the addition of those of the donor and acceptor moieties. On the other hand, in a PICT geometry, the coupling of the donor and acceptor parts should be strong leading to an N-Phenyl bond with a double-bond character and consequently shorter. Several experiences confirmed the benzonitrile radical character of the ICT emitting state, supporting so the TICT model. For example, the ICT-state absorption at 420 and 320 nm shows the same kind of absorption spectrum than this radical anion [22], and picosecond time-resolved resonance Raman spectra of the ICT state show similar characteristic modes than the benzonitrile anion as well [23].

Another set of experiments studied DMABN derivatives with geometrical constrains. Derivatives with a pretwisted amino group that show dual fluorescence support the TICT hypothesis [7], but other rigid derivatives that can twist only partially, and still show the anomalous band, support the PICT structure as emitting species [24].

The aim of the work presented in this chapter is to clarify some of the controversial points regarding the ICT phenomena. With this idea in mind, we choose for our study DMABN derivatives with different characteristics. First of all, we studied a set of bicyclic systems of increasing rigidity that exhibit different fluorescence patterns. The possible relation between geometrical constrains and dual vs. normal or anomalous fluorescence can help to elucidate the geometrical structure of the emitting species. On top of this, the agreement between the experimental observations and

the theoretical predictions can be used to corroborate the adequacy of the theoretical methodology used to develop this study. Following, we studied different isomers of the di-tert-butylaminobenzonitrile (DTABN). First of all, we were interested in studying the influence of the bulky aminosubstituent that imposes a non-planar ground sate geometry. Secondly we also studied the influence of the position of the substituents, studying the orto- meta- and para-DTABN isomers. In the last part of this chapter we present the results of the study of the tetrafluoro-DMABN (4F-DMABN). We were interested in studying the influence of fluoro substitution because it has been observed experimentally that the presence and number of fluor atom modifies strongly the spectral features of both absorption and emission. In fact, the 4F-DMABN shows only a CT band, strongly red-shifted, even in non-polar solvents [25].

5.2 Computational details

The different electronic states of the molecules named before have been studied with the CASSCF method using a 6-31G(d) basis set. The 12 electrons and 11 orbitals that constitute the active space include the benzene π and π^* orbitals, the amino nitrogen lone pair, and the four π and π^* orbitals of the cyano group. Full geometry optimizations were performed without any symmetry constraint. Numerical frequency calculations were carried out to determine the nature of the stationary points. Intrinsic reaction coordinates (IRCs) were also computed to determine the pathways linking the critical structures (stationary points and CI). Conical intersections were optimized using the algorithm of Beapark et al.[26] State averaged orbitals were used, and the orbital rotation derivative correction to the gradient (which is usually small) was not computed.

To incorporate the effect of the dynamic valence-electron correlation on the relative energies of the lower excited states, we made CASPT2 calculations based on the CASSCF(12,11) reference function. CASPT2 single-point energies were calculated at the CASSCF (12,11)/6-31G(d) optimized geometries using an average of states between the three lowest-energy singlet states $S_0/S_1/S_2$. Nevertheless, in some zones of the potential energy surfaces where the S_1 and S_2 states were almost degenerate and very high with respect to the ground state, an average 0.5/0.5 between the S_1/S_2 states was used. This is the case for the S_2/S_1 conical intersection. All CASPT2 computations were performed using the completed Fock matrix to define the zero-order Hamiltonian together with an imaginary level shift of 0.2 to prevent incorporation of intruder states [27, 28]. The CAS state interaction method (CASSI) [29, 30] was used to compute the transition dipole moments of the various excited states in the Franck-Condon region,

which were then used together with the excitation energies to determine the values of the oscillator strength. Valence bond (VB) structures were determined using the results of the computation of the second-order exchange density matrix Pij and the diagonal elements of the electronic density matrix [31]. The elements of Pij have a simple physical interpretation, which is related to the spin coupling between the electrons localized in the orbitals residing on the atoms i and j. An illustration of the meaning of these matrix elements can be found in ref [31].

In the case of the DTABN, due to the size of the system, we also made some QM/MM calculations, as it will be explained in the corresponding section. The CASSCF calculations were carried out with either the Gaussian 98 or the Gaussian 03 set of programs, whereas the CASSI and CASPT2 computations were performed with the MOLCAS 6.0 and Molcas 7.0 program packages.

5.3 Bicycle derivatives of DMABN

The main reasons why in recent years the TICT model has been the most postulated explanation of the ICT mechanism are, apart from the theoretical results, the experimental observation of only ICT fluorescence in systems with a twisted ground-state equilibrium geometry (like for example, in 3,5-dimethyl-4-(dimethylamino)benzonitrile [16]) even in nonpolar solvents, and the absence of ICT fluorescence in the emission spectra of rigidized systems such as 1-methyl-5-cyanoindoline (NMC5) [18], 1-methyl-6-cyano-1,2,3,4-tetrahydroquinoline (NMC6) [18, 32], and 1-ethyl-5-cyanoindoline (NEC5) [33], even in strongly polar solvents like acetonitrile or methanol. However, when the aliphatic ring becomes more flexible, as in the case of 1-methyl-7-cyano-2,3,4,5-tetrahydro-1H-1-benzazepine (NMC7) [18, 34], fast and efficient ICT emission is observed both in polar and nonpolar solvents. Furthermore, a recent Density Functional Theory study performed by Jamorski et al. [35, 36] demonstrates that NMC7 is already twisted around 60^{o} in its ground-state geometry. These authors, therefore, suggest that only the twisted ICT model can explain the fluorescence characteristics of this kind of compounds since the high rigidity of the cycle in NMC5 and NMC6 prevents the TICT structure from forming whereas it forms easily in the more flexible NMC7. Nevertheless, not long ago Zachariasse et al. again proposed the PICT model because they observed fast and efficient ICT emission in 1-ter-butyl-6-cyano-1,2,3,4-tetrahydroquinoline (NTC6) [37] in all solvents investigated, from nonpolar n-hexane to polar acetonitrile or methanol. They suggested that the ICT emitting species is planar in NTC6 because the torsion of the amino group is sterically hindered. They also suggested that the different luminescence behavior in these systems is attribut-

able to a different magnitude of the initial energy gap between the two excited states, $\Delta E(S_1,S_2)$, in the Frank-Condon region. For NTC6, this energy gap must be small so it allows vibronic coupling, while for NMC6 and NMC5 the ΔE must be large. On the other hand, Köhn and Hättig [38] suggest that NTC6 may still be able to twist in its ICT state and that data in ref [37] do not necessarily exclude a TICT mechanism. Although in a previous work of our group a TICT structure was found to be the ICT emitting species for DMABN, this result can not be generalized for every system showing dual fluorescence. For this reason we chose a set of systems with different rigidity to study their excited states and analyze the energetics in relation with their fluorescence patterns. In particular, we have studied 5-cyanoindoline (NHC5), 6-cyano-1,2,3,4-tetrahydroquinoline (NHC6), NMC6, NTC6, 7-cyano-2,3,4,5-tetrahydro-1H-1-benzazepine (NHC7), and NMC7 (see figure 5.7).

Figure 5.7: Structures of the systems of the series studied

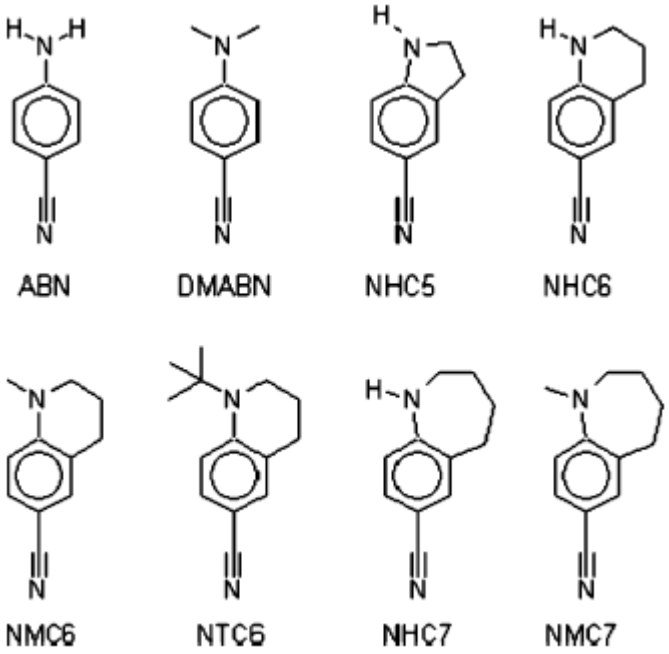

For the sake of comparison, the results previously obtained for the more flexible ABN and DMABN systems are also included. We will show that the topology of the potential energy surfaces in NXC6 and NXC7 do not change in comparison with their more flexible counterparts ABN and DMABN, since NXC6 and NXC7 are able to twist. Actually, the energy gap between the two initial excited states, $\Delta E(S_1,S_2)$, and the energetics of the LE and ICT minima are the key to explain why the luminescence behaviour is different in the systems studied.

5.3.1 Excitation energies in the Franck-Condon region

Table 5.1 shows the computed excitation energies of NHC5, NXC6, and NXC7 in the gas phase, together with the dipole moments and the oscillator strengths of the lowest excited states determined by CASSCF and CASPT2 calculations.

Table 5.1: Excitation energies (kcal·mol^{-1}), dipole moments (μ, in Debyes), and oscillator strengths (f) obtained at the Franck-Condon region in the gas phase for the different systems studied

molecule	state	ΔE_{SCF}	ΔE_{PT2}	exp [a]	$\Delta E(S_1,S_2)_{PT2}$	μ	f
ABN	LE	111.0	101.9	>92[b]		5.3	0.068
	CT	152	118.1	>109[b]		11.8	0.478
DMABN	LE	111.0	99.1	92-102[c]	16.2	6.0	0.006
	CT	140.7	106.3	99-106[c]		13.8	0.608
NHC5	LE	110.5	99.1		7.2	5.3	0.063
	CT	146.1	110.4			14.5	0.399
NHC6	LE	109.9	98.4		11.3	5.7	0.006
	CT	144.6	109.7			12.8	0.500
NMC6	LE	109.9	97.2		6.7	5.9	0.006
	CT	139.3	103.9	99.5[d]		13.5	0.556
NTC6	LE	109.4	95.3		-0.7	6.1	0.005
	CT	137.9	94.6	95.7[d]		14.0	0.508
NHC7	LE	111.8	102.3		10.4	5.2	0.000
	CT	145.9	112.7			11.8	0.398
NMC7	LE	111.2	101.7		0.3	5.2	0.000
	CT	147.3	102.0	96.4[e]		13.8	0.388

[a] Experimental values of absorption energies are included for comparison
[b] Absorption energy in *n*-heptane [16]
[c] Absorption energy in the gas phase [39]
[d] Absorption energy in *n*-hexane [37]
[e] Absorption energy in *n*-hexane [18]

The corresponding excitation energies of ABN and DMABN are also included for comparison. These energies were calculated as the vertical difference between the excited state and the ground-state energies, at the ground state optimized geometry that will be discussed in the next section. No qualitative or quantitative differences are observed between these systems at the CASSCF level. The first excited state is the LE (L_b-like) one in all cases with very similar dipole moments of around 5-6 D. The oscillator strengths for this excitation are very small, indicating its weakly allowed character. The CT (L_a-like) state is the second excited state, characterized by a high dipole moment of around 12-14 D and a strong oscillator strength, which indicate that it should be considered as the initially promoted state. This state will

carry most of the energy after absorption because of the allowed character of the transition. Although the CASSCF results agree qualitatively with the experimental data in nonpolar solvents [18, 37], the energies are highly overestimated, particularly for the CT state, where the disagreement is larger than 30 kcal·mol^{-1}. To obtain more accurate results, we recalculated the energies with the CASPT2 method to include the dynamic correlation. As can be seen from the results shown in Table 5.1, the dynamic electron correlation has a different quantitative effect on the LE and CT states. For both states the CASPT2 excitation energies are smaller than the CASSCF ones, but the LE state undergoes a smaller stabilization of around 10 kcal·mol^{-1}, whereas the CT state is stabilized by around 30 kcal·mol^{-1}. These CASPT2 results are now in reasonable agreement with the available experimental data. It seems that dynamic electron correlation effects are of critical importance for obtaining quantitatively accurate results, especially in the computation of the excitation energies. A direct consequence of this discriminatory effect of the dynamic electron correlation is that the energy gap between the two excited states decreases. The variation of the CASPT2 energy difference between the LE and CT states throughout the series of compound studied is depicted in Figure 5.8. The energy difference is smaller when the alkyl chain is larger (for example, $\Delta E(S_1,S_2)$ in ABN is more than twice the gap in DMABN), as the charge transfer state is stabilized in molecules with long, more polarizable chains attached to the nitrogen atom of the amino group. This effect is surprisingly strong for NTC6 and NMC7, where the CT state is degenerate with the LE. It should be pointed out that these are the only systems in the series that present anomalous fluorescence even in nonpolar solvents. Zachariasse suggested that the efficiency of the ICT reaction in n-hexane was much greater for NTC6 and NMC7 than for DMABN because of the decrease in the energy gap.[37] Our results seem to confirm this. The fact that the energy of the CT state is almost degenerate with that of the LE state in the Franck-Condon region in NTC6 and NMC7 could be explained by (a) the geometry of the ground state in these systems and (b) the effect of the substituents in the amino group. As we will discuss in the next section, the ground state in NTC6 and NMC7 displays a pretwisted geometry that favours the CT over the LE state because it is strongly stabilized by the twisting mode. Additionally, replacement of methyl by tert-butyl (NMC6/NTC6) or of hydrogen by methyl (NHC7/ NMC7) enhances ICT efficiency because the charge generated by the electron transfer is delocalized by the interaction between the amino nitrogen lone pair orbital and the molecular orbitals of the alkyl substituents. This assumption was also made by Serrano-Andrés et al. [8] in an extensive theoretical study on DMABN, where the main component of the reaction pathway was assumed to involve an amino group twist.

Figure 5.8: (a) Excitation energies of the LE and ICT states at the Franck-Condon region for the compounds of the series studied. (b) Energies of the LE, PICT, and TICT minima for the different systems studied relative to their corresponding ground-state minima.

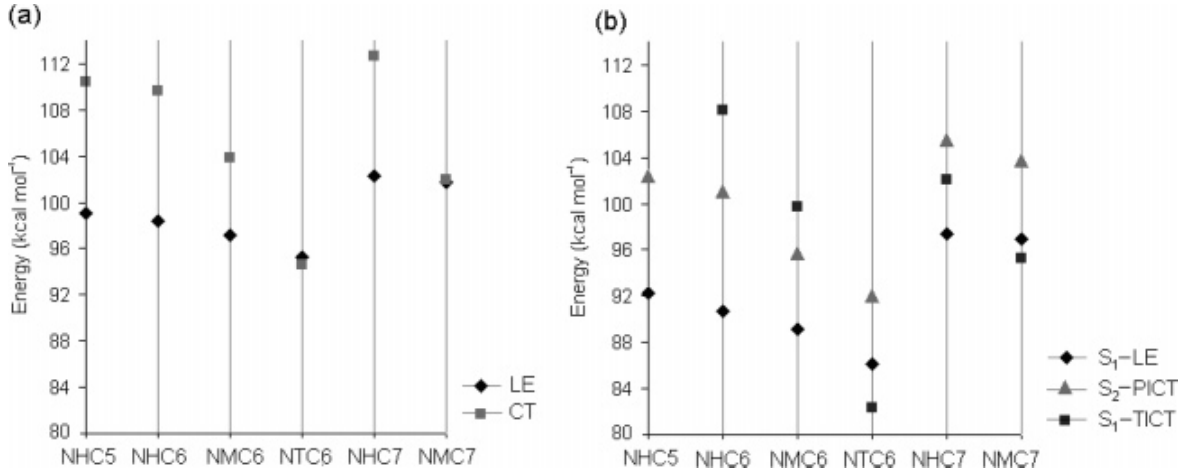

5.3.2 Critical points

We discuss now the geometry of the various critical points located on different PES and describing their wave functions in terms of VB language. Actually, the structural and electronic descriptions of the various minima are at the heart of the ICT controversy. First, we located (at the CASSCF level) the various minima on the S_0, S_1, and S_2 PES of NHC5, NXC6, and NXC7 that correspond to the ground-state, LE, TICT, and PICT stable species. As in ABN and DMABN [9], we found a planar ICT stable species lying on the S_2 potential-energy surface but could not locate a S_1-PICT minimum. Twisted ICT minima were located on the S_1 surface of every compound of the series studied except for NHC5, which cannot adopt this structure because of its greater rigidity. The S_1-RICT minima, too high in energy in ABN and DMABN to be mechanistically interesting, were not looked for. The geometries of the minima located are shown in Figure 5.9 together with the VB structures derived from the analysis of the corresponding wave function. This VB structure derive from the values of the second-order exchange density matrices and the one electron matrices which are shown in Figure 5.10.

These results show that the electronic structure of the ground state minimum (S_0-GS) corresponds to an in-phase combination of the two Kekulé structures. It is clear that this covalent nature is retained in the S_1-LE state, with similar dipole moments but with an anti-Kekulé benzene moiety. The S_2-PICT and S_1-TICT minima have similar zwitterionic characters with a partial or net positive charge on the nitrogen

atom of the amino group and a resonant quinoidal phenyl anion, giving rise to large dipole moments. The values of this property obtained here are systematically lower than the experimental data because the latter were measured in polar solvents while the former were calculated in the gas phase (see table 5.3 further down). The major difference between S_2-PICT and S_1-TICT is the magnitude of the charge transfer (fraction of electron transfered), which, as expected, is slightly greater in TICT (see Figure 5.10). The values of the second order exchange density matrixes collected in figure 5.10 show that the coupling between the nitrogen lone pair and the phenyl ring is larger in the ICT structures, PICT and TICT, than in the more covalent ones, GS and LE.

Let us now discuss the relaxed geometries shown in figure 5.9. We will pay special attention to the wagging angle ϑ (angle between the plane of the amino group and the phenyl ring) and the twist angle. The values of these parameters for the optimized minima are collected in table 5.2.

Table 5.2: Selected geometrical parameters of the optimized structures: wagging angle (ϑ) and twist angle (φ)

	ABN		DMABN		NHC5		NHC6		NMC6		NTC6		NHC7		NMC7	
Structure	ϑ	φ	ϑ	φ	ϑ	φ	ϑ	φ	ϑ	φ	ϑ	φ	ϑ	φ	ϑ	φ
S_0-GS	43	0	26	0	33	0	24	0	19	0	0	33	0	38	0	46
S_1-LE	40	0	21	0	31	0	20	0	19	0	0	35	0	36	0	44
S_1-TICT	0	90	0	90	-	-	0	62	0	65	0	69	0	82	0	85

The ground-state geometries of ABN and DMABN are untwisted with a pyramidal amino group with wagging angles of 43° and 26°, respectively. This geometric feature is retained in NHC5, NHC6, and NMC6 (see Table 5.2). However, NTC6, NHC7, and NMC7 possess somewhat twisted ground state equilibrium geometries with twist angles of 33°, 38°, and 46°, respectively, and a practically nonpyramidal amino group (near sp^2 hybridization). This finding can be explained by the strong steric hindrance between the tert-butyl group, in NTC6, and the o-hydrogen in the phenyl ring. In NXC7, the conformation of the aliphatic ring imposes a pretwisted ground-state geometry rather than a planar one.

The optimized geometries for the S_1-LE minima closely resemble those of the ground state. Similar wagging and twist angles are found in the corresponding geometries (Table 5.2). The main difference is that the phenyl CC bonds in the excited state are expanded, as expected from the out-of-phase combination of two Kekulé structures.

One of the main arguments against the TICT model, in which the amino group is perpendicular to the benzene ring, is the general agreement that it can only be adopted by very flexible 4-aminobenzonitriles, like ABN and DMABN. Actually, in the five-membered ring compound NHC5 no TICT structure was located because of the restricted flexibility of the amino group, which was structurally fixed to be nearly coplanar to the ring. However, in the NXC6 systems the alkyl chain is long enough to allow a partial rotation of the amino group. Thus, we located twisted ICT minima in NHC6, NMC6, and NTC6 at 62°, 65°, and 69°, respectively. The more flexible the aliphatic ring is, the larger the twist angle, which reaches values of 82° and 85° in the TICT structures of NHC7 and NMC7, respectively. Our calculations show that, as in ABN and DMABN, these TICT species are slightly bent with the nitrogen of the amino group and the carbon of the phenyl ring taking the group out of the ring plane and in an anti position. As in ABN and DMABN, the phenyl ring of all the S_1-TICT and S_2-PICT structures exhibits a quinoidal geometry: the two CC central bonds of the benzene ring are much shorter than the other four CC bonds. However, in the S_1-TICT structures, the N-C_{phenyl} bond length is larger than in the ground-state one (almost single bond length) whereas in S_2-PICT the N-C_{phenyl} bond is shorter (practically double bond length).

Figure 5.9: Geometries of the ground-state, LE, PICT, and TICT minima and VB structures of the different systems studied

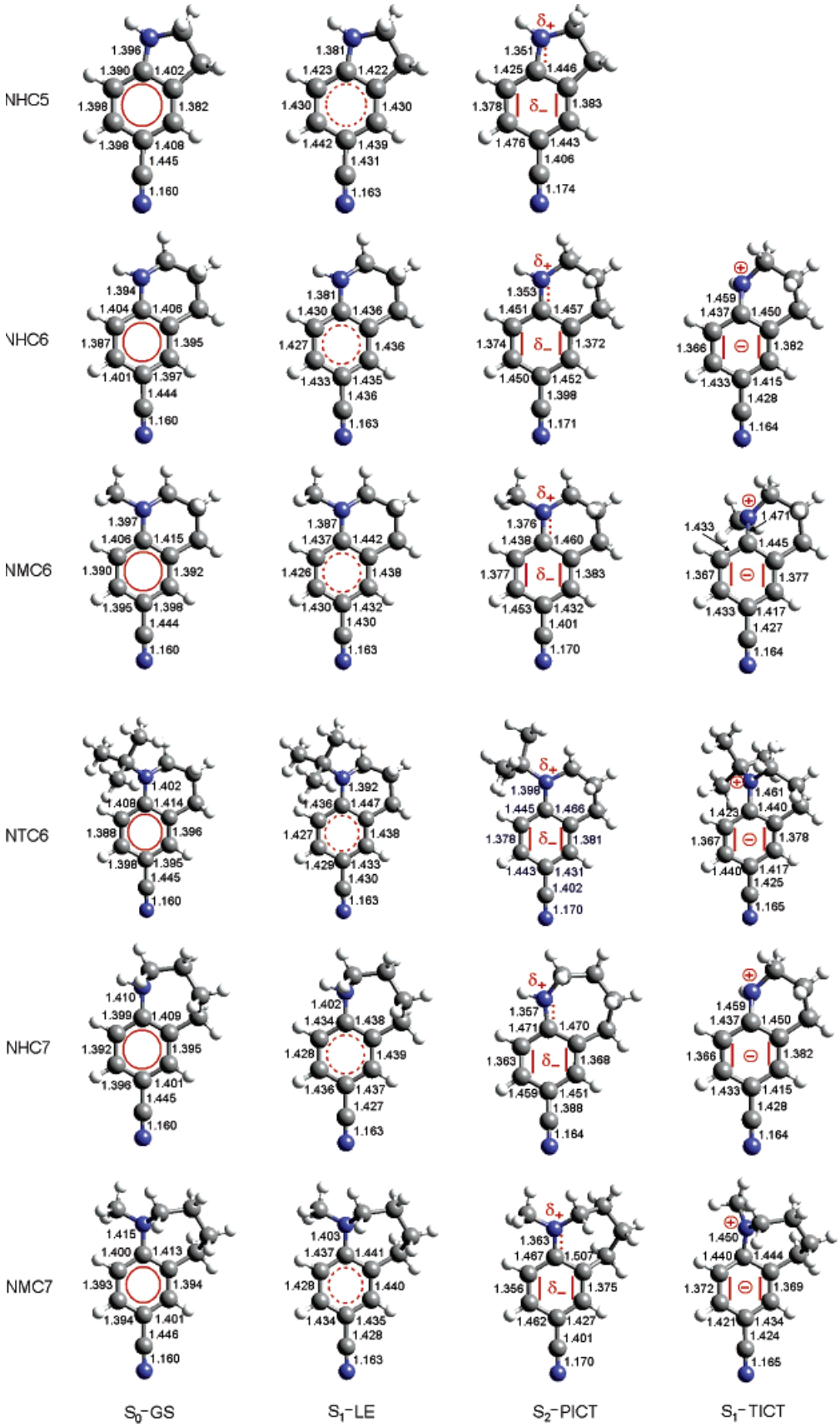

Figure 5.10: Values of the second-order exchange density matrix (in italic blue) and the one-electron density matrix (in black) of the ground state, LE, TICT, and PICT minima of the different systems studied.

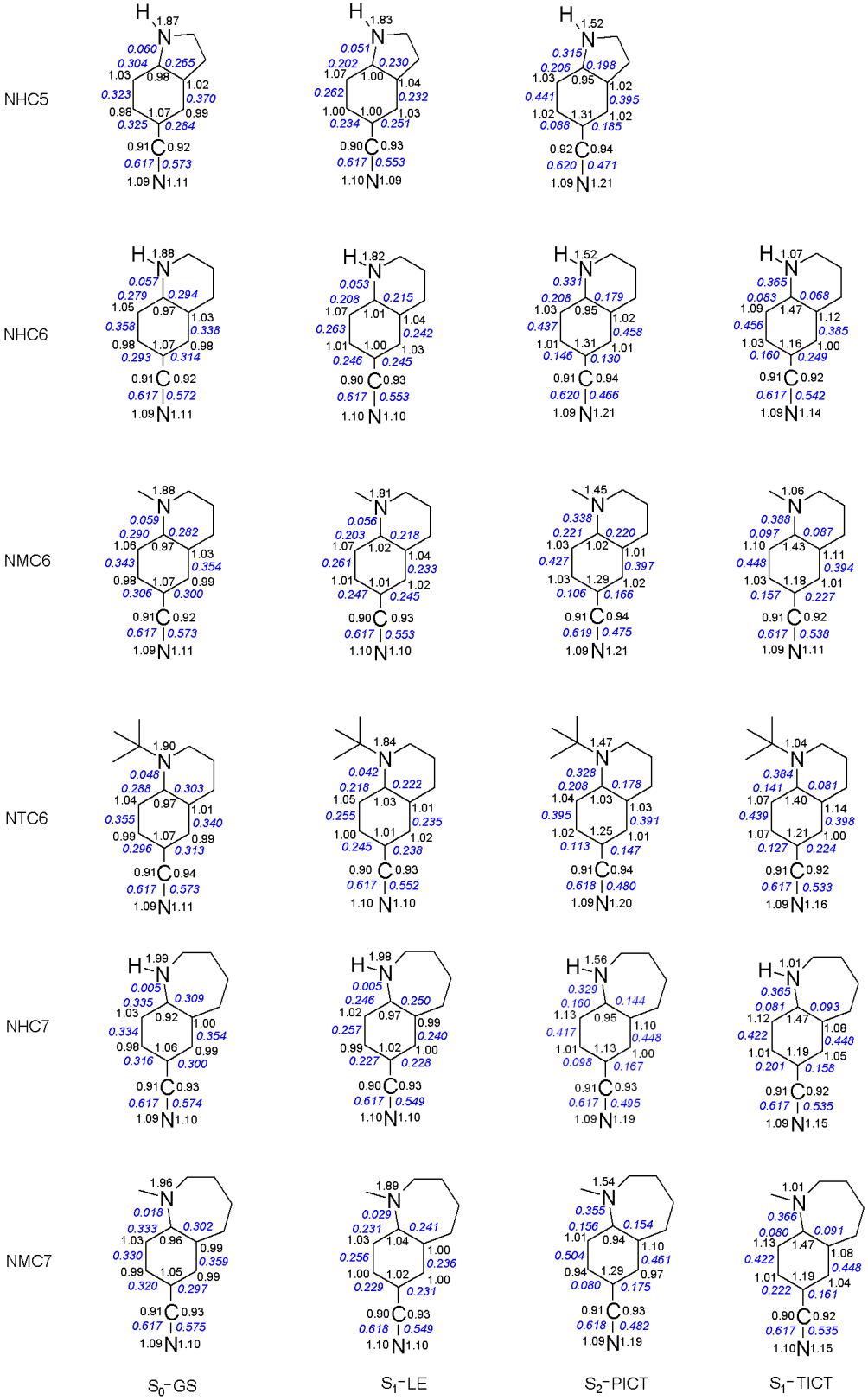

5.3.3 Mechanistic overview

The luminescent characteristics of the π-electron donor-acceptor systems studied here will be determined by the relative energies and the connection between the potential energy surfaces of the low-lying excited states LE and ICT. As we will use the CASPT2 energies obtained for the NHC5, NXC6, and NXC7 systems in this study, CASPT2 calculations for DMABN (not included in reference [9]) have also been run for comparative purposes. The CASSCF/CASPT2 relative energies and the dipole moments of the structures located are shown in table 5.3. The LE minima of all the molecules of the series studied (including ABN and DMABN) lie on the S_1 surface (S_1-LE). For the ICT, the planar minimum was found to be always on the S_2 surface (S_2-PICT) while the twisted one was always located on the S_1 surface (S_1-TICT). It is worth noting that although at the CASPT2 level some of the PICT species are more stable than the TICT ones, the emission will never take place from the second excited-state potential-energy surface, so the PICT species cannot emit. Two elements force the geometry of the ICT species and determine their relative energies. First, let us consider the restricted flexibility of the aliphatic ring. The shorter the alkyl chain is, the more difficult it is for a stable TICT structure to form, to such an extent that this structure has not been located for NHC5. The population of the LE and PICT minima, therefore, is favoured for compounds with short alkyl chains. Second, we must take into account the steric hindrance between the substituents of the amino group and the o-hydrogen in the phenyl ring. This hindrance enforces pretwisted geometries for the ground-state and LE species, destabilizing them relative to the TICT species. In fact, in those systems with a pretwisted ground-state structure (NTC6, NHC7, and NTC7) the high energy of the PICT species (that is, higher than the energy of the TICT structure) indicates that the planar geometry is very unfavourable. On the other hand, in systems with a planar ground state (i.e., ABN, NHC6, and NMC6) the PICT structure is more stable than the TICT structure, although the former lies on the S_2 potential-energy surface and the latter on the S_1 one. These results can be seen in Figure 5.8, which shows a diagram of the CASPT2 energies of the LE, PICT, and TICT structures for each system.

Because the CT state is S_2 in the Franck-Condon region but S_1 in the TICT structure at the CASSCF level, the first part of the reaction path after light absorption must be nonadiabatic. That is, at this level of theory the S_1 and S_2 surfaces must cross. We have located the lowest energy point on the S_1/S_2 conical intersection in these systems. Their energies are collected in Table 5.3. Because the geometry optimization of these critical points is carried out at the CASSCF level, when the energies are recalculated at the CASPT2 level it is found that the S_1 and S_2 states are no

longer degenerate. Unfortunately, although Molcas package allow to recalculate these geometries at CASPT2 level, it is computationally too expensive to do it as a routinary procedure. Given that for the purpose of this study it is not necessary a quantitative determination of the minimum energy point (MEPt) of the S_2/S_1 CI, we have analyze these points at the CASSCF level. Figure 5.11 shows the MEPt of the S_2/S_1 CI together with the two degeneracy-lifting coordinates that define the branching space (the derivative coupling vector and the gradient difference vector) in all systems studied. The characteristics of the conical intersections found for NHC5, NHC6, NMC6, NTC6, NHC7, and NMC7 are the same as those reported for ABN and DMABN [9]: there is an extended seam that runs parallel to the $CN(Me)_2$ torsion coordinate. The branching space does not involve either the amino group twist or the pyramidalization coordinates; rather, it is dominated by skeletal deformations of the phenyl ring coupled with C-N stretch, so the S_1/S_2 degeneracy is preserved along the amino group torsion. Thus, $S_2 \rightarrow S_1$ internal conversion can take place at the full range of torsion angles depending on the vibrational energy in torsional coordinates following photoexcitation, but the highest probability corresponds to the minimum energy point of the seam. This structure has different twist and pyramidalization angles for the different alicyclic derivatives of the series, as will be discussed below. The deexcitation will be followed by an adiabatic equilibration between the LE- and ICT-emitting species on the S_1 potential energy surface. The energy of the TS of this adiabatic path will be similar to that of the S_1/S_2 CI, as the TS is generated in the neighbourhood of the CI due to the associated avoided crossing. For all systems the initial excitation energy is larger than the energy of the minimum of the CI seam, which means that the TS of the LE-ICT interconversion is always accessible. The luminescence behaviour will also depend on the relative energy of the LE- and ICT-emitting species. As Figure 5.8 shows, the TICT structure is thermodynamically favoured over the LE structures only for NTC6 and NMC7, which are the only structures capable of producing the anomalous fluorescence band in nonpolar solvents.

Our computational results show that the overall topology of the potential-energy surfaces of the LE and ICT states in these 4-aminobenzonitrile alicyclic derivatives do not change substantially in comparison with the ones of the more flexible ABN and DMABN. Thus, the S_1 LE-TICT equilibration and dual fluorescence will be controlled in this series of compounds by (a) the position along the amino group twist coordinate where the S_2/S_1 CT-LE internal conversion takes place and (b) the S_1 adiabatic reaction path between the LE and TICT minima. Taking this into account we can distinguish several types of systems. For ABN, NHC5, NHC6, NMC6, and NHC7, the amino group is untwisted at the lowest point of the S_2/S_1 conical intersection seam, so the branching at the CI favors population of the LE state. Moreover, the S_1-LE

species are much more stable than the S_1-TICT ones (see Figure 5.8 and Table 5.3), so the equilibrium will favour the LE species. This explains why, in these molecules, ICT emission cannot be observed in the fluorescence spectra. Note that in NHC5 the S_2/S_1 conical intersection will lead directly to the S_1-LE structure since this system cannot adopt any other stable structure on the S_1 potential-energy surface.

On the other hand, the lowest energy point of the S_1/S_2 conical intersection located at the CASSCF level for NTC6 and NMC7 shows the amino group slightly twisted (21.2º and 31.9º, respectively), so branching at the CI favours formation of the TICT state. Nevertheless, in these cases, the energy gap between the two excited states in the Franck-Condon region is small enough to allow vibronic coupling between the CT and LE states, so both minima would be populated simultaneously. The adiabatic S_1 reaction path connecting them will displace the equilibrium toward the TICT minimum because it is less energetic. Consequently, observation of dual fluorescence emission in nonpolar solvents is in very good agreement with our results. It is worth pointing out that the LE and CT states are degenerate in the Franck-Condon region only for NTC6 and NMC7. This, together with the fact that the stability of the TICT species is greater than that of the LE species, is the key to explaining the ICT emission of these molecules in nonpolar solvents. These characteristics are clearly reflected in Figure 5.8.

A polar solvent will stabilize the ICT state even further, so in this case the initial excitation will populate the CT state that will correspond to the first excited state. The system will relax over the S_1 surface directly to the S_1 minimum, the TICT emitting species, without undergoing any internal conversion. This direct mechanism explains why the ICT reaction is much more efficient in these systems than in DMABN in polar solvents. The DMABN is a halfway case. The geometry of the minimum energy point of the S_1/S_2 conical intersection minimum is a pyramidal untwisted structure, but the LE and TICT minima are almost degenerate in the gas phase. This is in good agreement with its luminescent behaviour, which presents only the LE normal band in nonpolar solvents and dual fluorescence in polar ones, where the TICT minimum will be stabilized further than the LE one.

Figure 5.11: S_1/S_2 conical intersection geometries and branching space coordinates of the different systems studied.

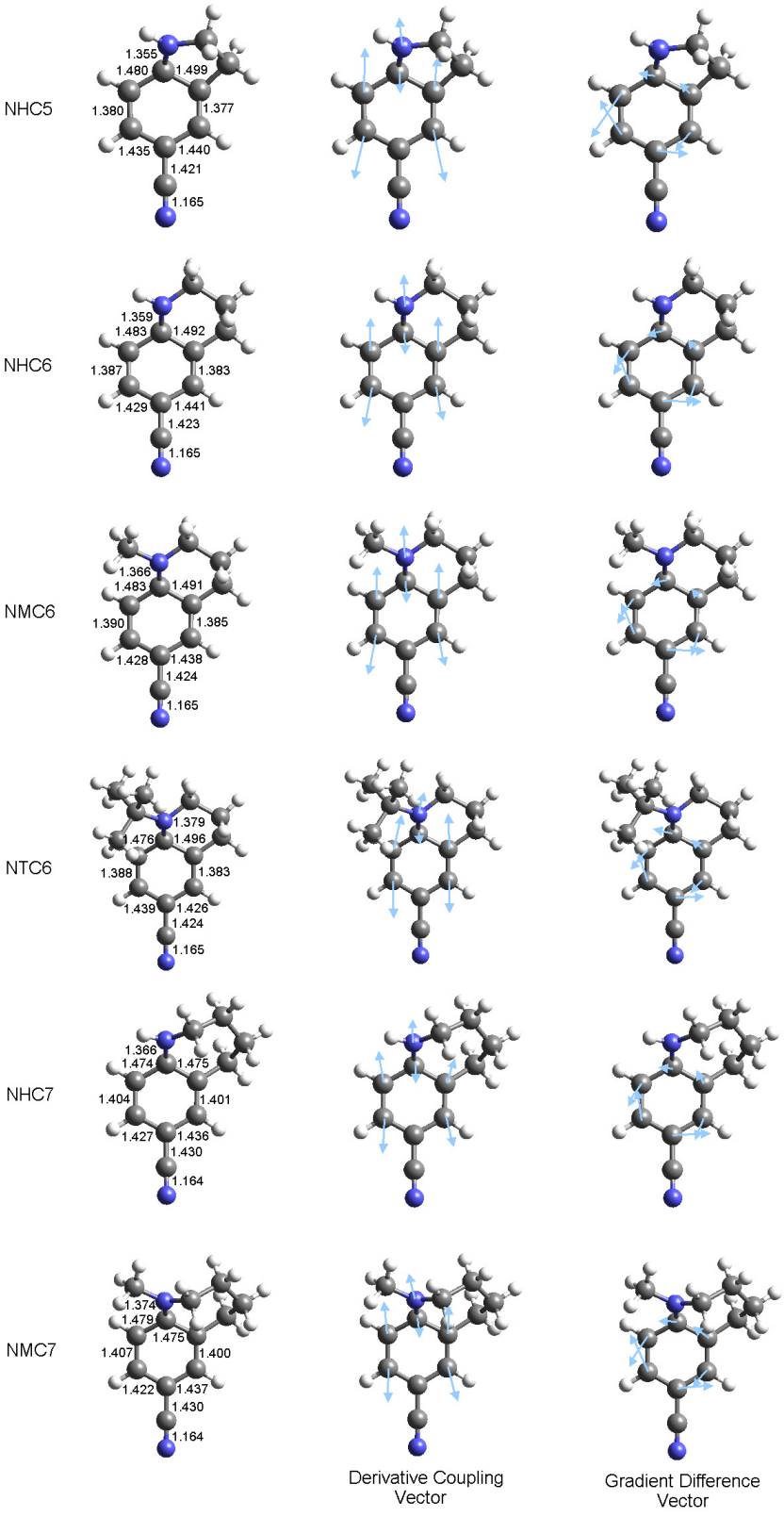

Table 5.3: CASSCF and CASPT2 relative energies (kcal·mol^{-1}) and dipole moments (μ, in Debyes) of the critical points (minima on the S_1 and S_2 PES and CI's) of the systems studied in the gas phase.

Molecule	Structure	ΔE CASSCF	ΔE CASPT2	μ	μ_{exp}
ABN	S_0-GS	-109.4	-95.6	5.5	6.6[b]
	S_1-LE	0.0	0.0	5.4	8[b]
	S_1-TICT	25.2	15.7	11.7	
	S_2-PICT	35.0	14.5	12.1	
	S_1/S_2-CI	26.9	[8.1,21.2][a]	6.1	
DMABN	S_0-GS	-106.6	-91.5	6.1	6.6[b]
	S_1-LE	0.0	0.0	6.1	9.9[b]
	S_1-TICT	2.4	0.4	13.5	17[b]
	S_2-PICT	28.5	7.1	13.8	
	S_1/S_2-CI	23.8	[6.1,18.3][a]	7.1	
NHC5	S_0-GS	-105.6	-92.3	5.6	
	S_1-LE	0.0	0.0	5.5	
	S_1-TICT	-	-	-	
	S_2-PICT	30.8	10.2	12.7	
	S_1/S_2-CI	29.9	[11.8,22.3][a]	7.2	
NHC6	S_0-GS	-105.3	-90.7	5.9	
	S_1-LE	0.0	0.0	5.9	
	S_1-TICT	23.4	17.4	11.3	
	S_2-PICT	35.3	10.4	12.9	
	S_1/S_2-CI	28.0	[10.9,22.8][a]	7.6	
NMC6	S_0-GS	-105.4	-89.12	6.1	6.8[c]
	S_1-LE	0.0	0.0	6.0	10.6[c]
	S_1-TICT	14.0	10.6	12.1	
	S_2-PICT	32.6	6.6	13.4	
	S_1/S_2-CI	25.9	[9.8,16.2][a]	7.6	
NTC6	S_0-GS	-104.9	-86.1	6.1	6.8[c]
	S_1-LE	0.0	0.0	6.0	
	S_1-TICT	5.9	-3.8	13.0	17.6[c]
	S_2-PICT	33.1	5.9	13.8	
	S_1/S_2-CI	23.3	[3.9,15.2][a]	8.7	
NHC7	S_0-GS	-107.0	-97.4	5.3	
	S_1-LE	0.0	0.0	5.1	
	S_1-TICT	12.3	4.7	12.9	
	S_2-PICT	36.8	8.1	12.4	
	S_1/S_2-CI	22.9	[1.9,13.3][a]	7.0	
NMC7	S_0-GS	-106.4	-96.9	5.4	
	S_1-LE	0.0	0.0	5.3	
	S_1-TICT	3.0	-1.6	13.6	17[d]
	S_2-PICT	38.2	6.7	12.5	
	S_1/S_2-CI	22.9	[3.6,5.3][a]	7.4	

[a] CASPT2 energies corresponding to the S_1 and S_2 states.
[b] [15] [c] [37] [d] [18]

5.3.4 Conclusion

According to our results, two factors rationalize the photophysical differences between the systems studied. First, the position of the TICT and LE potential-energy surfaces in the first stages of the ICT reaction must be considered. If the CT state is higher in energy than the LE in the Franck-Condon region and the lowest energy point on the CI is located at a planar geometry, the LE minimum will be populated first. On the other hand, if the CI lowest energy point has a twisted geometry or the CT state is lower in energy than the LE in the Franck-Condon region, the TICT minimum will be populated first. In the next stage of the reaction the second factor plays its role. The relative energies of the LE and TICT minima will determine the displacement of the equilibrium between the two species along the adiabatic path that connects them over the S_1 surface. The minimum that is not reached in the first stages of the reaction can now be populated if it is more stable than the other one. This factor is strongly sensitive to the presence of polar solvents that will preferentially stabilize the CT state. Thus, our conclusions agree partially with Zachariasse's generalization that relates the efficiency of the ICT process to the energy gap between the S_1 and S_2 states in the Franck- Condon region.[37] On the other hand, and in contrast to Zachariasse's hypothesis, our results suggest that the ICT species responsible for the anomalous fluorescence band in the NTC6 and NMC7 spectra must have a twisted structure. We present computational evidence that a twisted ICT structure can very well be adopted by these bicyclic but still slightly flexible molecules. A full perpendicular twist of the amino group is not necessary to get a stable ICT structure on the S_1 surface when the alkyl chain is long enough. Therefore, the experimental results in ref [37] do not necessarily exclude a TICT fluorescence emission. Nevertheless, it is possible that in other systems structural or environmental changes (in the donor or acceptor moieties with the addition of further substituents and/or the inclusion of solvent effects) could modify the relative energies of the key structures or their location. This, in turn, can modify the outcome of the CT reaction and change the fluorescence behaviour in different compounds. In particular, the PICT structure can stabilize to such an extent that it becomes a first excited-state structure. In this case, it could be a radiative species of the anomalous fluorescence band in competition with the TICT species. This qualitative modification of the interplay between the LE and ICT surfaces would explain why there is so much contradictory evidence in favour of the TICT and PICT models. As a result, it is not advisable to propose a general mechanism for the CT reaction, and each particular case must be studied in detail.

5.4 DTABN

In the previous section, we studied some bicyle derivatives of DMABN in order to check how the rigidity influence the LE/ICT equilibrium and the structure of the emitting specie. With the same idea, in this section we study DMABN derivatives, but in this case, with bulky substituents on the amino group that modify the structure of the molecules by means of steric effects that enhance the twist of the amino group relative to the benzene ring. In particular, we will study three isomers of the (di-tert-butylamino)benzonitrile : 4-(di-tert-butylamino)benzonitrile (p-DTABN), 3-(di-tert-butylamino)benzonitrile (m-DTABN) and 2-(di-tert-butylamino)benzonitrile (o-DTABN). This study will also allow us to analyze the influence of the position of the substituent on the luminescent patterns. Another goal of this work, on a different line of interest, was the analysis of the applicability of ONIOM methodology to this kind of problems. The size of the system studied here is at the limit of the applicability of the CASSCF/CASPT2 methodology (given the size of the molecule and, more crucially, the size of the active space used in these calculations). This situation makes convenient the use of less expensive methods, ONIOM in this case, but still allows us the use of the more reliable CASSCF/CASPT2 method to check the accuracy of the lower level calculations in some test points.

To our knowledge, there is up to now only one experimental work published on these molecules,[40] where Zachariasse et al studied the photochemistry of p-DTABN and m-DTABN. Both molecules show a similar absorption spectra in n-hexane and MeCN, with a structured benzonitrile-like absorption band between 35000 and 40000 cm^{-1} and a weaker unstructured band at lower energies. Absorption is in both cases around 25 times weaker than that of p-DMABN. In the fluorescence spectra, p-DTABN as well as m-DTABN show a broad emission band. For p-DTABN the maximum of this band is located at 25630 cm^{-1} in n-hexane and at 20900 cm^{-1} in MeCN, while for m-DTABN it appears at 26290 cm^{-1} in n-hexane and at 21280 cm^{-1} in MeCN. It is interesting to note that the red-shift is the same in both isomers. The fluorescence originates in the ICT with a minor or null contribution from the LE state. The fluorescence quantum yields are low, increasing as the polarity increases from 0.0053 to 0.039 in the case of p-DTABN and from 0.013 to 0.027 for m-DTABN. This is the first case reported of a meta-ABN derivative that shows anomalous fluorescence. This work also reports the ground state geometry of the meta isomer determined by X-ray crystal analysis. In particular, they report a value for the twist angle of 86.5°. They also predict a value of 75-79° for he twist angle of the para isomer, based on the correlation established with other systems between the extinction coefficient of the maximum of the lowest-energy absorption band and the amino twist angle determined from X-ray crystal analysis.

These molecules show, then a twisted geometry even at the ground state.

5.4.1 Peculiarities of the computational method used in this study

DTABN has 39 atoms and the active space needed in these calculations is, like in the case of DMABN, of 12 electrons in 11 orbitals. The computational cost of the calculations for systems of this size makes advisable the use of a cheaper method at least for the most expensive calculations of the study. Given the nature of the system to study, we considered that the ONIOM method (explained in Chapter 3) could be a convenient choice. This method is one of the hybrid methods that mixes ab-initio (QM) and Molecular Mechanic (MM) methods and are especially designed for large systems for which a complete ab-initio treatment would be cost-prohibitive. In our case, the CASSCF method was used for the ab-initio calculation of the benzene ring with the amino group and cyano group, but both tert-butyl substituents were replaced by methyl groups. The low-level method used was the UFF force field. In this way, the sterical interaction of the tert-butyl substituents is taken into account, but not their electronic influence in the moiety where the excitations are located. The active space used was the same than that used for DMABN, that is an active space of 12 electrons in 11 orbitals, including orbitals of the benzene ring, both π orbitals of the cyano group and the doubly occupied orbital of the amino's nitrogen. Once the geometries were optimised with the ONIOM method, the energies were recalculated using the CASSCF/CASPT2 method for the whole system. In order to check the accuracy of this choice, we also optimized some structures with a full CASSCF method as will be commented later. The basis set used was the 6-31G(d) in all calculations. Gaussian03 and Molcas7.0 were the two packages used in this study.

5.4.2 Ground State geometries and absorption spectra

We first optimized the ground state geometry for the three isomers in the gas phase with the ONIOM method. The geometries of the minima on the ground state PES located in this work are shown in figures 5.13, 5.14 and 5.12. All three of them show a strongly twisted di(ter-butyl)amino group with angles of 89.5º, 88.2º and 90.6º respectively for the para-, meta- and ortho-isomers. We only can compare the theoretical structural parameters obtained with experimental X-ray data of the meta-isomer, the only one for which this information is provided. [40] The theoretical twist angle is in good agreement with the experimental value of 86,5º found for the meta-isomer. On

the other hand, the agreement is not so good for the value predicted in reference [40] for the twist angle of the para-isomer, of 75-79°, to be compared with our result of 89.5°.

The amino N is also pyramidalized in the geometries determined theoretically, with angles of 17.1° (para-), 20.1° (meta-) and 16.6° (ortho-), values to be compared with the experimental data for the meta-isomer of 32.4°. For this geometrical parameter, the agreement is not very good. Comparison of the experimental and computational bond distances for the meta-isomer (see figure 5.13) shows a good agreement with deviations in general smaller than 0.01 Angstrom. The dipole moments of the ground states are 3.9 Debye for p-DTABN and 4.6 Debye for both m-DTABN and o-DTABN.

Figure 5.12: para-DTABN geometries (distances in Angstrom) and VB structures obtained at the ONIOM (CASSCF(12,11)/UFF) level.

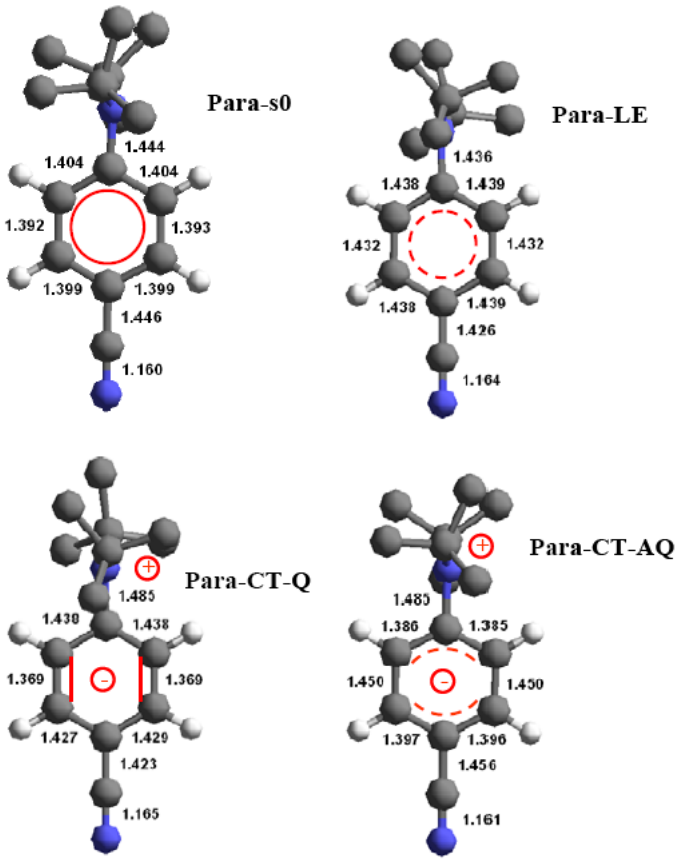

In order to check the accuracy of the ONIOM method, we also optimized the ground state geometry of the meta-isomer at the CASSCF level to be compared also with experimental results. The differences between structures optimised using ONIOM and CASSCF are very small. The largest difference is found for the C-N bond distance between the benzene ring and the amino group, but even in this case the difference is small: 1.431 Å obtained with the CASSCF method, to be compared with the value

of 1.444 Å obtained with the ONIOM method. The experimental value, 1.437 Å, is intermediate between the theoretical ones. These results validate the use of ONIOM method.

Figure 5.13: meta-DTABN geometries (distances in Angstrom, X-Ray experimental values in red) and VB structures obtained at the ONIOM (CASSCF(12,11)/UFF) level.

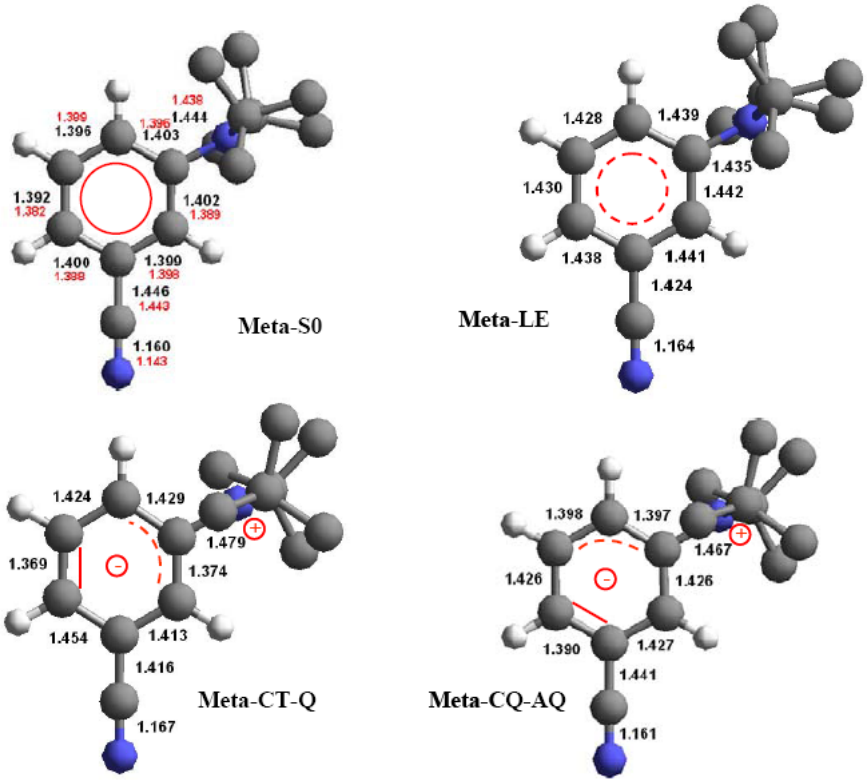

From the optimized ground state geometries, we calculated the excitation energies to the first eight singlet excited states. The character of the excited states is determined analyzing the excitations that give place to their electronic configurations. Among the first four excited states, the ones involved in the processes of interest, there are two LE states (originated by π-π^* excitations, with both π orbitals located mainly in the benzene ring) and two excited states of charge transfer character. On these states, an electron from the lone pair of the amino nitrogen (n_N), is promoted to a π^* orbital located on the ring. In the para-isomer, thanks to the local symmetry of the ring, the excited CT states can be classified into quinoid (CT-Q) or antiquinoid (CT-AQ) following the Valence-Bond terminology, depending on the location of the nodes of the π^* orbital. We will keep this classification also for the ortho and meta isomers (relative to the cyano group), although it could not be applied strictly in these cases.

The relative energies and oscillator strengths of the first excited states of the three isomers calculated at the CASSCF/CASPT2 level are shown in Table 5.4. For all three

Figure 5.14: ortho-DTABN geometries (distances in Angstrom) and VB structures obtained at the ONIOM (CASSCF(12,11)/UFF) level.

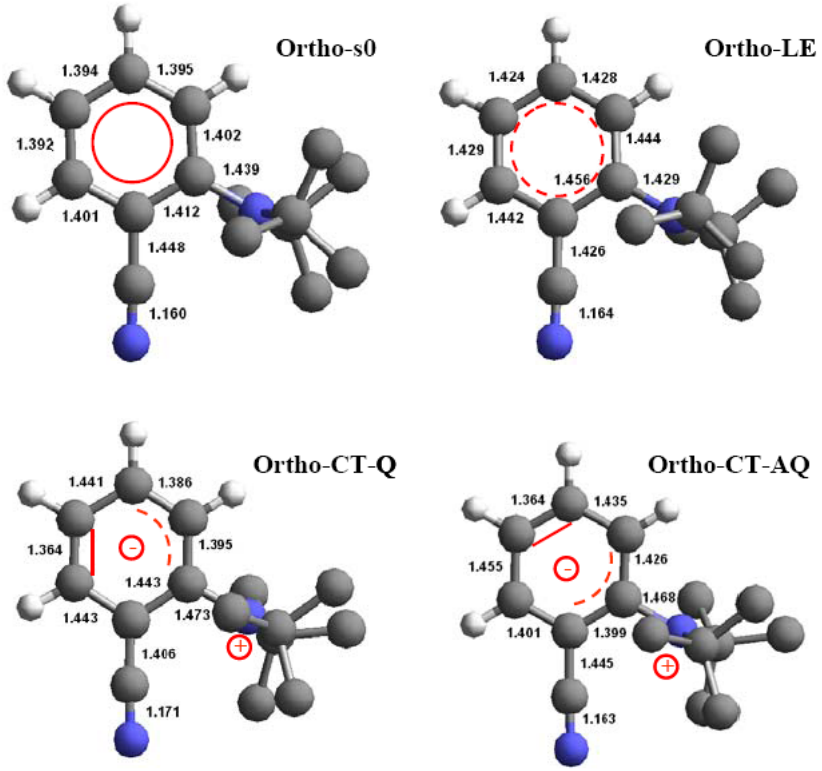

isomers both CT states, CT-Q and CT-AQ, are the excited states of lower energy, followed by two states of LE character. The state with the largest oscillator strength is the fourth excited state, the second LE state, located 140-149 kcal·mol^{-1} above the GS. These results contrast with the ones obtained previously by our group for the DMABN: in that case the lowest excited state had LE character and a low oscillator strength (0.006) while the second excited state had CT character and a high transition probability (f=0.608), with an excitation energy of 106.3 kcal·mol^{-1} (obtained at the CASPT2(12,11)/6-31g(d) level).

With these data, the absorption spectra computationally predicted for the DTABN isomers are in good agreement with the experimental findings reported in reference [40] and with the differences found between the DMABN and DTABN spectra. In reference [40], very weak absorption is reported for the para- and meta-DTABN in the range of the 27000-40000 cm^{-1}, with extinction coefficients 25 times lower than those of DMABN that has the maximum of the absorption band at around 35500 cm^{-1}. Our calculations predict that for all DTABN isomers absorption will hardly take place in the range studied experimentally, given that the main absorption band is located at higher energies, around 50000 cm^{-1}. For the DMABN, though, our calculations locate the main absorption band within the range studied, near the one observed

experimentally, at 37000 cm^{-1}. The differences between the absorption spectra of the para- and meta-DTABN isomers observed experimentally are also reflected in the computational results: there is a blue-shift of the CT absorption-band and a small red-shift of the LE band in the m-DTABN spectrum relative to that of DTABN [40].

Table 5.4: Excitation energies (in kcal·mol^{-1}) obtained at CASPT2 level (CASSCF values in parenthesis) and oscillator strengths (f).

	p-DTABN		m-DTABN		o-DTABN	
root	ΔE CASPT2	f	ΔE CASPT2	f	ΔE CASPT2	f
r2 CT-Q	91.7 (142.9)	0.001	94.6 (147.3)	0.002	89.1 (140.2)	0.001
r3 CT-AQ	107.9 (163.5)	0.001	101.5 (156.2)	0.001	102.1 (156.0)	0.001
r4 LE	112.1 (109.7)	0.001	111.7 (109.3)	0.003	111.4 (109.1)	0.003
r5 LE2	149.1 (176.8)	0.277	149.9 (178.8)	0.226	140.3 (177.4)	0.250
r6	160.2 (171.6)	0.063	165.3 (174.0)	0.032	173.9 (175.2)	0.010
r7	176.2 (195.0)	0.000	176.6 (195.4)	0.000	173.6 (192.3)	0.000
r8	184.2 (184,8)	0.029	183.3 (183.1)	0.025	184.0 (183.1)	0.017

5.4.3 Excited state minima and emissions

Optimised geometries for the lowest excited states of the para-, meta- and ortho-isomers obtained using the ONIOM method are shown in figures 5.12, 5.13 and 5.14. Valence Bond (VB) structures were determined using the results of the computation of the second-order exchange density matrix Pij and the diagonal elements of the electronic density matrix shown in figure 5.15. This information allows us to make clear the LE or CT character of a state attending to the occupancy of the n_N orbital (doubly occupied in the ground and LE states, singly occupied in the CT states) and the Q or AQ character attending to the P_{ij} values of the bonds of the benzene ring.

Structures corresponding to the lowest energy LE, CT-Q and CT-AQ have been located. All of them show strongly twisted geometries. LE minima show anti-kékulé benzene moieties (in contrast with the in-phase combination of the two Kekulé structures of the ground state) and consequently an elongation of the C-C bonds of the ring. CT minima show changes relative to the ground state geometry, modifying the ring C-C distances according to their Q or AQ character (the two central C-C bonds are shorter/larger than the other four for the Q/AQ species). Both CT states have an elongated N-phenyl bond, due to the charge transfer from the nitrogen to the benzene ring and the subsequent weakening of the bond. The geometries of DTABN isomers are very close to those of DMABN, except for the twist angle, that is much larger in

Table 5.5: Energies (in kcal·mol^{-1}) of the optimized structures of the low-energy states of the p-, m- and o-isomers of DMABN. The state optimized is in bold, vertical energies to the ground state in parenthesis and experimental absorption and emission energies in parenthesis and italics.

	p-DTABN		m-DTABN		o-DTABN	
	E CASPT2	μ	*E* CASPT2	μ	*E* CASPT2	μ
GS	0.0	3.9	0.0	4.6	0.0	4.6
CT-Q	95.4 *(88.8)*	15.4	99.0 *(97.6)*	13.7	93.6	9.1
CT-AQ	111.4	14.9	105.8	13.6	106.4	9.0
LE	112.1 *(102.6)*	3.7	111.6 *(101.7)*	4.5	111.3	4.6
GS	4.1	4.0	4.1	4.6	4.3	4.6
CT-Q	94.7	15.5	98.6	13.7	92.5	9.1
CT-AQ	111.2	14.9	105.2	13.4	106.0	9.0
LE	107.6 (103.5)	3.6	107.0 (102.9)	4.5	106.4 (102.1)	4.6
GS	13.2	3.7	7.9	4	8.9	4.2
CT-Q	88.3 (75.1) *(73.3)*	13.7	91.1 (83.2) *(75.2)*	14	86.1 (77.2)	9
CT-AQ	118.8	14.5	109.9	13	111.3	8.7
LE	119.6	4.6	116.0	3.8	115.9	4.3
GS	9.8	3.7	5.5	3.9	9.6	4.3
CT-Q	101.7	15.6	97.4	14.1	98.7	8.7
CT-AQ	103.2 (93.4)	15.0	100.6 (95.1)	12.8	100.9 (91.3)	8.6
LE	119.0	3.4	113.6	3.8	117.5	4.3

DTABN due to the steric repulsion of the di-tert-butyl group that precludes the existence of planar low-energy minima. The electronic structures are as well very similar to the ones found previously for DMABN. Dipole moments of the CT-Q species are 15.4 D for p-DTABN and 13.7 D for m-DTABN, which are lower than the experimental values, 17.1 ± 0.4 and 17.0 ± 0.7 D respectively. The o-DTABN CT species show a dipole moment much lower that the other two, 9 D, due to the ortho-position of the cyano group. The CT-AQ species show similar trends (15.0 D, 12.8D and 8.6D for the p-, m- and o-isomers) while the predicted values for the LE species are as expected much lower (3.6, 4.5 and 4.6 D respectively).

A schematic representation of the energetics of the excited state minima for all the isomers is shown in figure 5.16. The CT-Q state is the lowest excited state for all the geometries localized here and its minimum is located as well on the S_1 PES for all isomers. On the other hand, the CT-AQ minimum lies for all isomers on the S_2 PES, with energies 0.40-0.65 eV higher than the corresponding CT-Q minimum. LE minima of the meta- and ortho- isomers lies on the S_3 PES while for the para-isomer it is located on the S_2 PES. In all cases LE state is almost degenerate at its minimum geometry with the CT-AQ state, inverting the relative energies only in the case of the para-isomer.

Figure 5.15: Electronic structures: values of one-electron density matrix (in black) and of the second-order exchange density matrix (in blue) of the optimized structures of the lowest energy states of the p-, m- and o-isomers of DTABN.

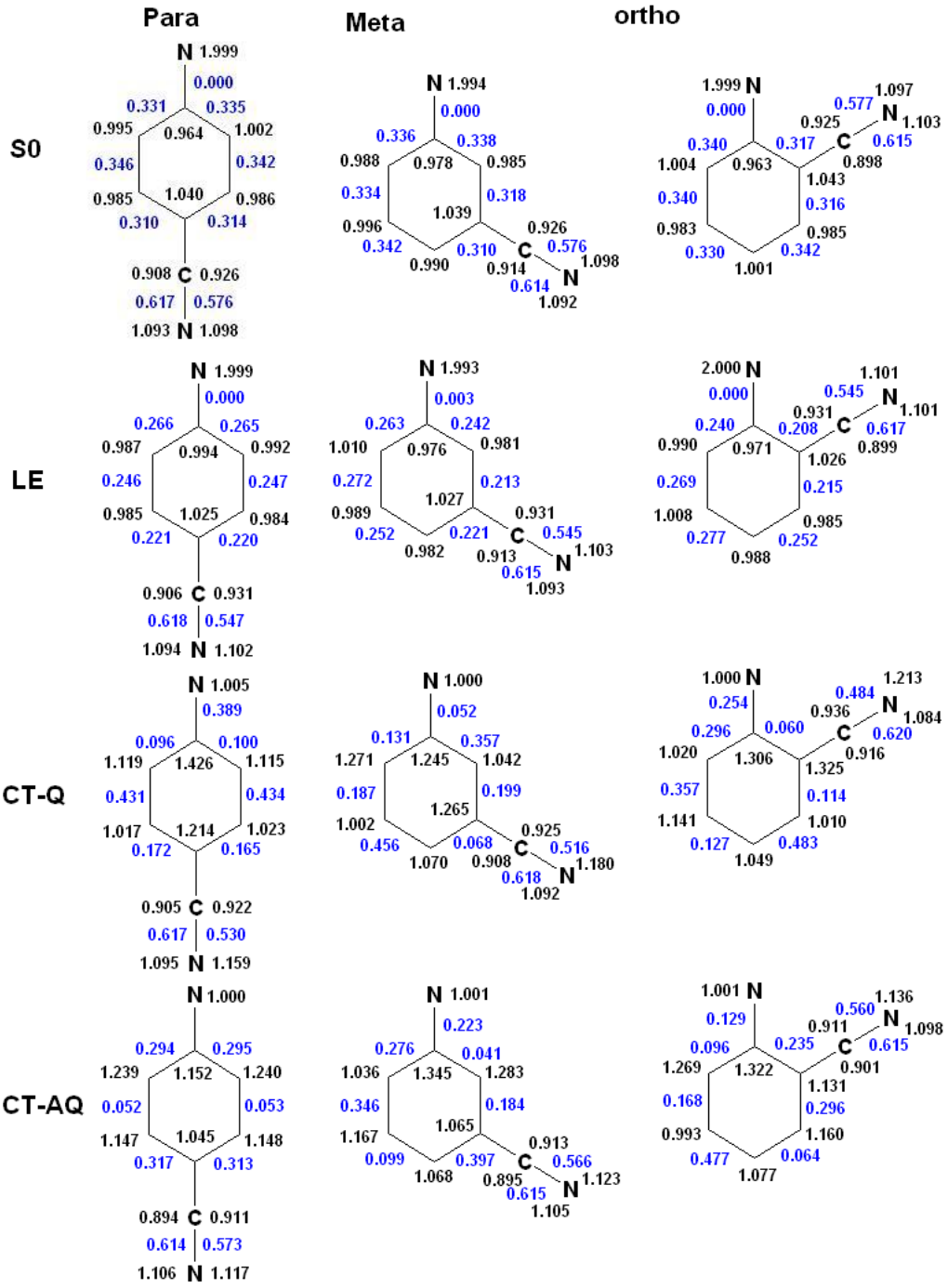

According to Kasha's rule [41], it is expected that emission takes place only from the first excited state, so for DTABN we can only expect fluorescence from the CT-Q species in all three isomers. Our results are in perfect agreement with the experimental spectra that show only CT emission bands for both p- and m-DTABN. We predict a

Figure 5.16: Schematic representation of the energetics of the excited state minima for all three isomers. Relative energies in kcal·mol^{-1}, dipole moments in D in parenthesis.

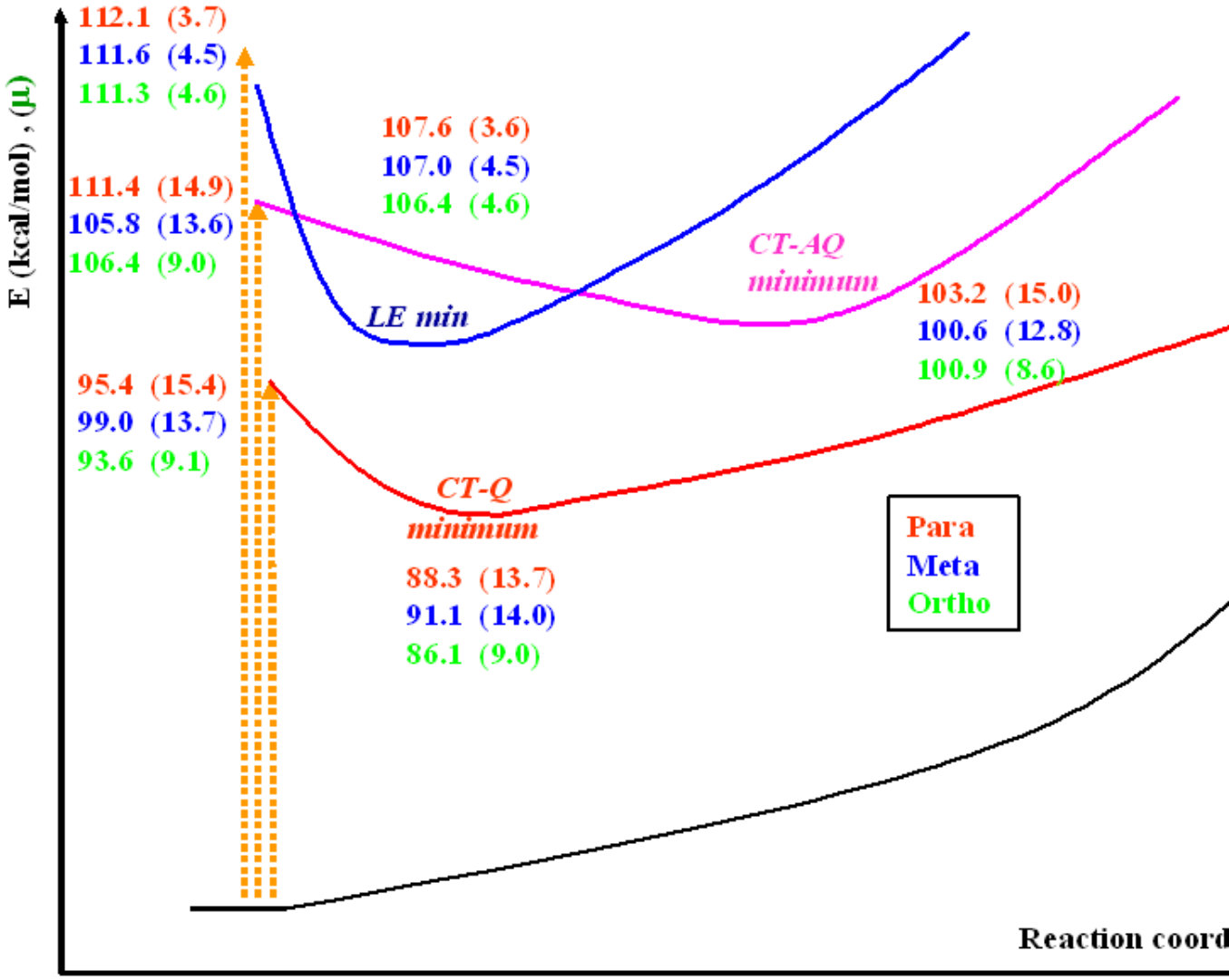

similar emission pattern also for the ortho isomer. The vertical energy from the CT-Q minima to the ground state can be compared with the emission energies measured experimentally. We found 75.1 kcal·mol^{-1} vs. 73.3 kcal·mol^{-1} for the p-isomer and 83.2 kcal·mol^{-1} vs. 75.2 kcal·mol^{-1} for the m-isomer. The agreement is quite satisfactory, taken into account that we compare gas phase theoretical results with measurements obtained in n-hexane. For o-DTABN, for which no experimental data are available up to now, our results predict an anomalous emission of 77.2 kcal·mol^{-1}.

To check that the CT-Q state is the lowest energy excited state in the whole range of geometries involved in the ICT process, we calculated the profile of the 4 lowest

Figure 5.17: CASPT2 energy profiles of the first excited states of p-DTABN from the FC zone to the LE minimum obtained by a LIIC path. Energies in eV.

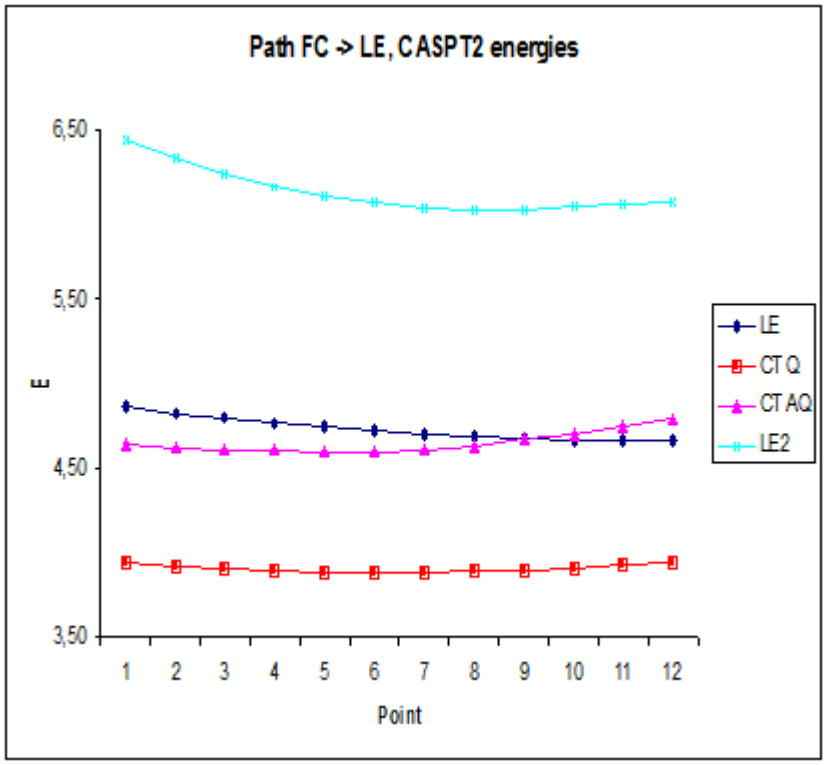

excited states of DTABN along the interpolated paths connecting the F.C. region with the LE minimum and from the LE minimum to the CT-Q minimum for the para-isomer. As can be observed in figures 5.17 and 5.18, the CT-Q state is always the lowest energy excited state. This characteristic is expected to be also found for both m- and o-isomers. This result points out clearly that the only species susceptible of fluorescence (following Kasha's rule) is the CT-Q in all DTABN isomers.

5.4.4 Conclusions

The global topology of the lowest excited states of DTABN isomers is in general similar to that of DMABN, but at the same time there are some important differences in the interplay between PES that lead to a very different luminescent behaviour. The origin of the differences is the steric hindrance of the amino substituents of DTABN that impose rotated geometries. This rotation favours the twisted CT state, that becomes the lowest-energy excited state, in contrast with the DMABN system. For DMABN, planar geometries are possible where the LE state is the lowest-energy excited state. Consequently, while in DMABN there are two S_1 minima of very different character

Figure 5.18: CASPT2 energy profiles of the first excited states of p-DTABN from the LE minimum to the CT-Q minimum obtained by a LIIC path. Energies in eV.

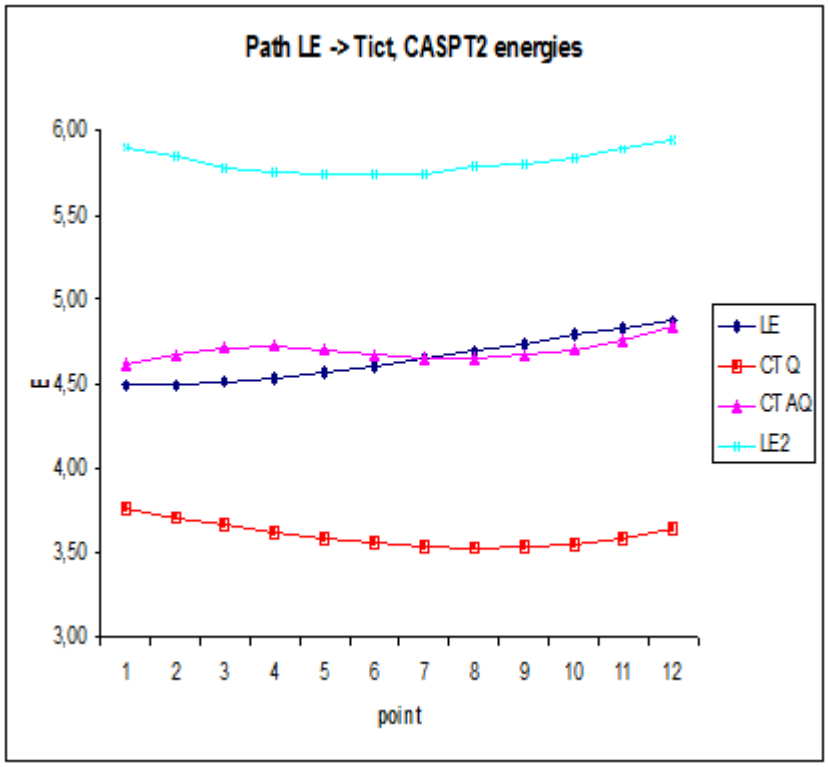

that can be populated and can then give place to two different fluorescence bands (normal and anomalous) depending on the conditions of emission, in DTABN only the CT-Q minimum is located on S_1. This is then the only minimum that can eventually be populated after the initial excitation and produce the anomalous fluorescence observed experimentally in polar and non-polar environments.

5.5 DMABN-4F

Recently, Zachariasse et al.[25] investigated the introduction of a fluorine atom in different positions of the benzene ring in 4-aminobenzonitrile derivatives, and stated that there is no indication of ICT emission in alkane solvents but the internal conversion (IC) is enhanced by the fluoro substituent. Neither the introduction of two F-substituents in the phenyl ring of ABN to get 2,5-difluoro-4-aminobenzonitrile (ABN-2F), are sufficient to induce an ICT reaction [42]. However, for the tetrafluoroaminobenzonitriles, unlike ABN and DMABN, the fluorescence spectra, both in polar and non-polar solvents, consist only of an ICT emission while the fluorescence band from the LE state cannot be detected [42, 25, 43].

Figure 5.19: Scheme of DMABN and DMABN-4F

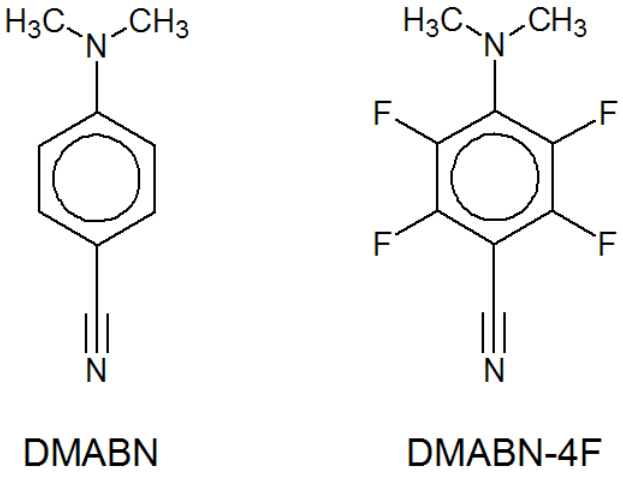

The aim of the study of this section is to understand how the substitution of the four hydrogen atoms in the benzene ring by fluorine atoms can modify the luminescent behaviour of these compounds. We have studied the 2,3,5,6-tetrafluoro-4-(dimethylamino)benzonitrile (DMABN-4F) (see figure 5.19) and compared our results with those of DMABN. Our computational results show that the global topology of the potential energy surfaces (PES) of the LE and ICT states do not change substantially in comparison with the DMABN but the CT state is stabilized in such a way that the different interplay with the LE state induces strong qualitative changes. This stabilization is evident only when dynamic electron correlation is taken into account in the calculations.

5.5.1 Critical points

The first step on this study was to obtain the geometries of the stable species and the critical points of the PES of DMABN-4F. They were optimised at the CASSCF(12,11)/6-31G(d) level, and the energetics were refined at the CASPT2/cc-pVDZ level. These structures of the minima localized are shown in figure 5.20. The values of the second order density matrix and the one electron density matrix were also calculated to generate a Valence-Bond (VB) picture of the systems and get the charges over the atoms. These results are also shown in figure 5.20. At the CASSCF level, we located the S_0-GS, S_1-LE, S_1-TICT and S_1-RICT stable species with the same electronic characteristics as in DMABN [9]. Because of the strong steric hindrance between the two methyl substituents of the amino group and the fluorine atoms in the benzene ring, the S_0-GS structure has a twist angle of 55°, very different from the planar geometry of DMABN. This angle is slightly larger than the 33° obtained from the X-ray data.[44]

However, previous theoretical results predict twist angles ranged from 30° to 54° depending on the computational method employed [43]. The vertical excitations from this geometry were then calculated, to obtain the energies and the electronic character of the first excited states. Table 5.6 shows these computed CASSCF and CASPT2 absorption energies of DMABN-4F in the gas phase together with the experimental data obtained in nonpolar solvents. The corresponding DMABN spectrum is also shown for comparison.

Figure 5.20: Geometries and electronic structures (in red), values of the second-order exchange density matrix (in italic blue) and the one-electron density matrix (in black) of the ground state, LE, TICT, and RICT minima in DMABN-4F. All bond lengths are given in Å and dipole moments in Debyes.

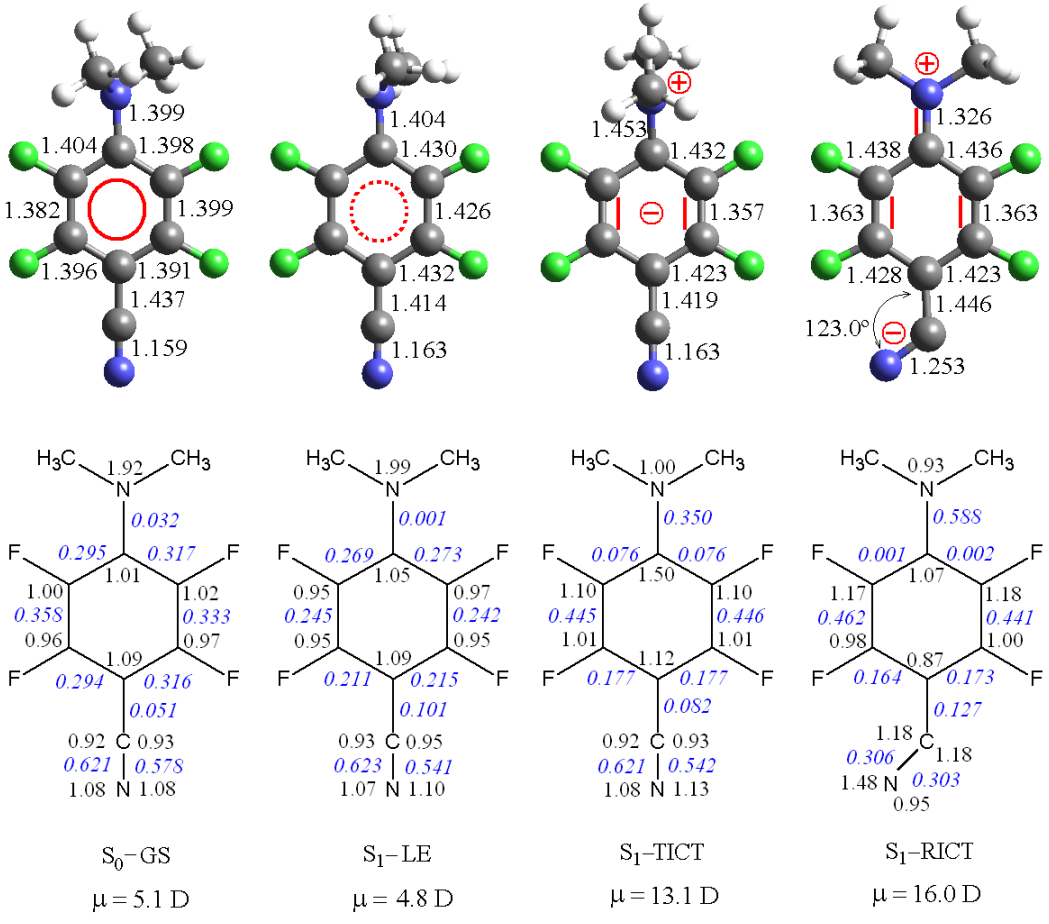

Let us first analyze the CASSCF results. At this level, the CT (L_a-like) state is located above the LE (L_b-like) state in both molecules and is characterized by a high dipole moment and large oscillator strength. This indicates that this is the initially promoted state as it will carry most of the energy after absorption because of the allowed character of the transition. Nevertheless, the energy gap between the two

Table 5.6: Absorption energies (kcal·mol^{-1}), dipole moments (μ, in Debyes) and oscillator strengths (f) obtained for DMABN and DMABN-4F at the CASSCF/6-31G(d) and CASPT2/cc-pVDZ level in the gas phase.

Molecule	State	ΔE CASSCF	ΔE CASPT2	ΔE Exp.[a]	μ	f
DMABN	LE	111.0	93.3	92.2	6.0	0.006
	CT	140.7	102.7	101.9	13.8	0.608
DMABN-4F	LE	121.0	97.9	Not visible	5.0	0.009
	CT	125.6	95.7	95.5	14.2	0.318

[a] Maxima of the low-energy absorption band measured in n-hexane. See reference [42].

excited states, $\Delta E(S_1,S_2)$, is much smaller in DMABN-4F than in DMABN. These results agree again with Zachariasse's generalization that relates the efficiency of the ICT process to the energy gap between the S_1 and S_2 states in the Franck-Condon region [37]. Interestingly, the inclusion of dynamic electron correlation in the calculations introduces some qualitative changes relative to the CASSCF results. For DMABN, the CASPT2 energies show the same ordering of the LE and ICT excited states (at the FC region as well as along the ICT path). For DMABN-4F, though, the situation is different: at the ground state geometry the CT (L_a-like) and LE (L_b-like) excited states appear almost degenerate but the CT (L_a-type) state is S_1, 2.2 kcal·mol^{-1} below the LE (L_b-like) state (Table 5.6). This result is in strong agreement with the fact that the weak shoulder ascribed to absorption to the LE (L_b-like) state in DMABN spectra is not visible in the spectra of DMABN-4F in n-hexane [43]. Furthermore, the CASPT2 energetics is in good agreement with the absorption energy experimental data. This effect will be enhanced in a polar solvent, which will comparatively stabilize the CT state even further.

Let's analyse the stable species located in the first excited PES. S_1-LE has an anti-Kekulé benzene moiety, twisted structure, with a torsional angle of 88°, and the C of the ring bonded to the amino group is pyramidalized, so the nitrogen and the carbon atoms of the dimethylamino group are slightly out of the plane, like in S_0-GS. S_1-TICT and S_1-RICT have similar zwitterionic characters (VB structures shown in Figure 5.20) that give rise to a large dipole moment. Both ICT species display a quinoidal structure in the benzene ring, that is, the two CC central bonds of the benzene ring are much shorter than the other four CC bonds. The computed dipole moment of 13.1 D for S_1-TICT is in a good agreement with the value of (13.8 ± 0.4) D estimated by Zachariasse for the emitting ICT species [42]. At this level of theory, the S_1-LE → S_1-TICT in DMABN-4F is an exoergic process, by 10.7 kcal·mol^{-1}, in contrast to DMABN where

it is an endoergic process, by 2.4 kcal·mol^{-1}. The S_1-RICT minimum, though, is located 50.1 kcal·mol^{-1} above S_1-LE, so it is too high in energy to be mechanistically interesting (see Table 5.7). An antiquinoidal twisted ICT structure, with the two CC central bonds of the benzene ring much longer than the other four CC bonds, has also been localized lying on the S_2 potential energy surface in DMABN and DMABN-4F (Figure 5.21), S_2-TICT, in agreement with previous calculations performed by Haas and co-workers [45, 46]. Given that the fluorescence emission will never take place from the second excited state potential energy surface, the antiquinoidal TICT species cannot be an emitting one. No S_1-PICT minimum could be located.

Figure 5.21: Geometry and electronic structure (in red), of the antiquinoid TICT structure localized in the S_2 PES in DMABN and DMABN-4F. All bond lengths are given in Å.

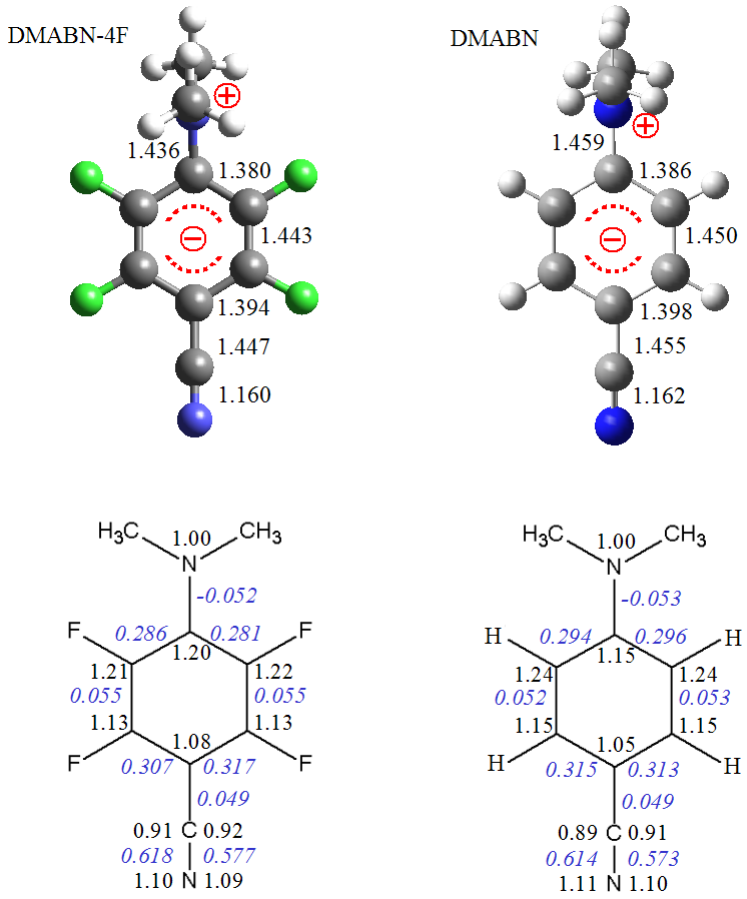

Because the CT state is S_2 in the Franck-Condon region but S_1 at the TICT structure at the CASSCF level, the first part of the reaction path after light absorption must be nonadiabatic. That is, at this level of theory the LE and CT surfaces must cross. The characteristics of the conical intersection (CI) found for DMABN-4F are the same as those reported for DMABN [9]: there is an extended seam that runs parallel to the $CN(Me)_2$ torsion coordinate. Nevertheless, the structure of the lowest

point of this S_1/S_2 conical intersection seam located in DMABN-4F has different twist and pyramidalization angles. Figure 5.22 shows this structure together with the two degeneracy-lifting coordinates defining the branching space (the derivative coupling vector and the gradient difference vector).

Table 5.7: Relative energies (in kcal·mol^{-1}) and dipole moments (μ, in Debyes) of the structures located in DMABN and DMABN-4F at the CASPT2/cc-pVDZ level in the gas phase.

	DMABN		DMABN-4F	
Structure	ΔE[a]	μ	ΔE	μ
S_1-LE	0.0	6.1	0.0	4.8
S_1-Q-TICT	0.1	13.5	-17.1	13.1
S_2-AQ-TICT	14.6	14.1	15.7	14.4
S_2-PICT	8.4	13.8		
S_1-RICT	22.8	16.8	22.9	16.0
S_1-$TS_{LE/TICT}$[b]	5.2	10.5		
S_1/S_2-CI	[7.3,21.4]	7.7	[-9.3,3.5]	9.8
S_0/S_1-CI	[-2.4,-13.5]	7.5	[-13.5,-18.8]	9.3
S_1-$TS_{LE/CI}$	8.2	5.5	-7.0	6.9

[a] Calculations performed at the CASSCF(12,11)/6-31G(d) optimized geometries. [b] See Figure 5.27 for DMABN-4F.

Figure 5.22: S_1/S_2 conical intersection located at CASSCF level for DMABN-4F. Degeneracy-lifting coordinates: (a) gradient difference vector and (b) derivative coupling vector. All bond lengths are in Å.

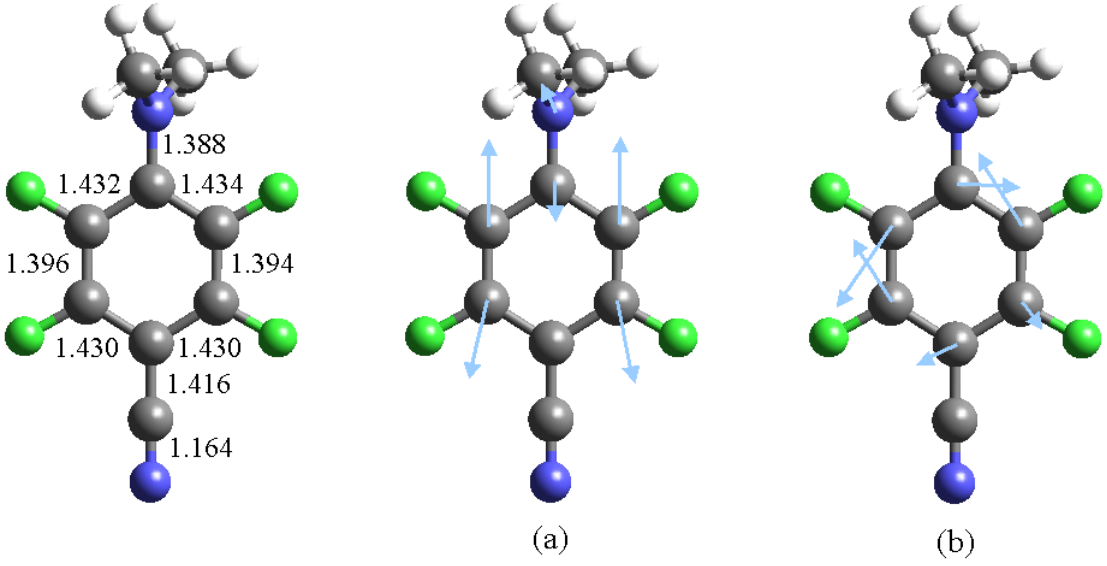

5.5.2 Mechanistic overview

Figure 5.23 shows a scheme of the mechanism of the ICT process in DMABN and BMABN-4F obtained on the basis our CASPT2 results that will be explained in detail in this section.

Figure 5.23: Schematic potential energy profiles of the ICT reaction for DMABN and DMABN-4F obtained at the CASSCF(12,11)/CASPT2/cc-pVDZ level. Energies are in kcal·mol^{-1}.

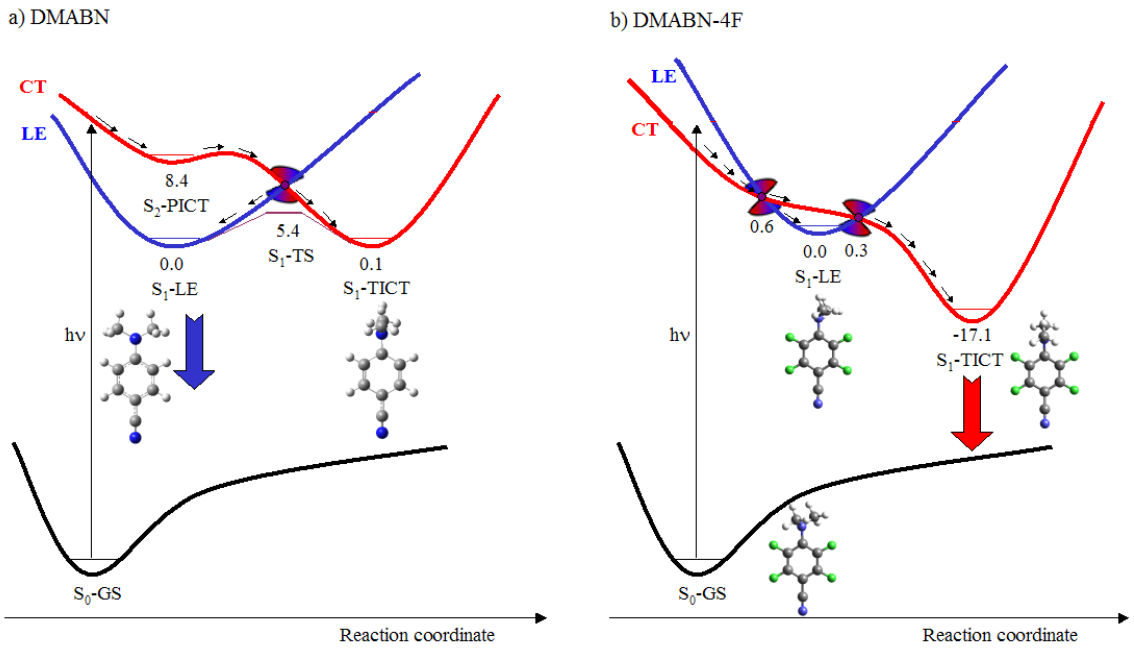

Figure 5.24: Forces in the potential energy surface of the S_2 (CT) state calculated at CASSCF level in the Franck-Condon region of DMABN-4F.

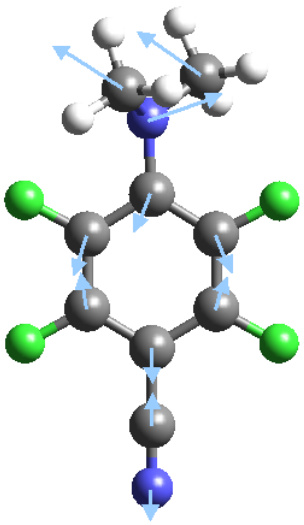

The results of the previous sections show that the initial excitation populates the

CT state. To determine how the system evolves immediately afterwards, the forces on the S_1-CT energy surface in the Franck-Condon region were calculated at the CASSCF level (Figure 5.24). They show that DMABN-4F tends to relax directly towards the TICT minimum. This feature was confirmed by an interpolated energy path calculation at the CASPT2 level on the S_1-CT (L_a-like) PES between the Franck-Condon geometry and the S_1-TICT minimum (Figure 5.25). No activation barrier was found, so it is expected that after the initial photoexcitation the ICT reaction proceeded adiabatically smoothly downhill towards the TICT minimum. These results are consistent with the ultrafast formation of an emitting ICT species in the excited singlet state of DMABN-4F in contrast to DMABN [42, 43].

Figure 5.25: CASPT2/cc-pVDZ energy profiles of the LE (blue) and CT (red) states from the Franck-Condon region to the S_1-TICT minimum for DMABN-4F obtained by a LIIC path. Energies are in kcal·mol^{-1}.

	Point in the path	ΔE CASPT2 (LE)	ΔE CASPT2 (CT)
S_0– GS	1	98.6	97.2
	2	101.3	95.0
	3	101.7	92.8
	4	100.8	90.5
	5	102.4	88.5
	6	103.5	86.5
	7	104.7	84.7
	8	105.9	83.0
	9	107.1	81.6
	10	108.4	80.4
	11	109.7	79.5
S_1– TICT	12	112.8	78.5

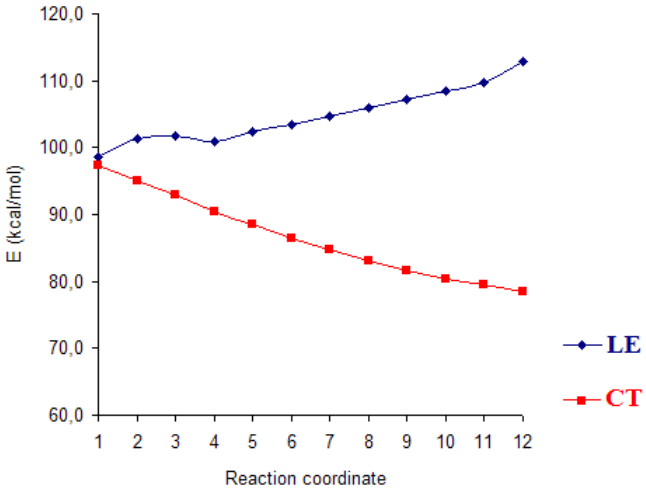

The emission from the S_1-LE species could not be detected in the fluorescence spectrum of DMABN-4F, but the excited-state absorption (ESA) spectra of DMABN-4F in n-hexane show a decay of the LE and a corresponding rise of the ICT absorption [42]. This indicates that the S_1-LE minimum must be populated and that it must be directly connected with the ICT one. To check it, we calculated the energy profile of the LE and CT states by linear interpolation between the Franck-Condon geometry and the S_1-LE minimum. The results are shown in Figure 5.26. They show that the LE and CT states are almost degenerated all along this pathway. Moreover, at the S_1-LE minimum, the LE state is lower in energy than the CT one. The crossing point between the two surfaces lies only 0.6 kcal mol^{-1} above the S_1-LE minimum, thus this minimum will be populated quickly and effectively.

Figure 5.26: CASPT2/cc-pVDZ energy profiles of the LE (blue) and CT (red) states from the Franck-Condon region to the S_1-LE minimum for the DMABN-4F obtained by a LIIC path. Energies are in kcal·mol^{-1}.

	Point in the path	ΔE CASPT2 (LE)	ΔE CASPT2 (CT)
S_0– GS	1	97.9	95.7
	2	97.4	95.3
	3	97.1	95.1
	4	96.7	95.0
	5	96.5	95.1
	6	96.2	95.2
	7	96.0	95.4
	8	95.8	95.7
	9	95.6	96.1
	10	95.4	96.5
	11	95.2	97.0
S_1– LE	12	95.1	97.6

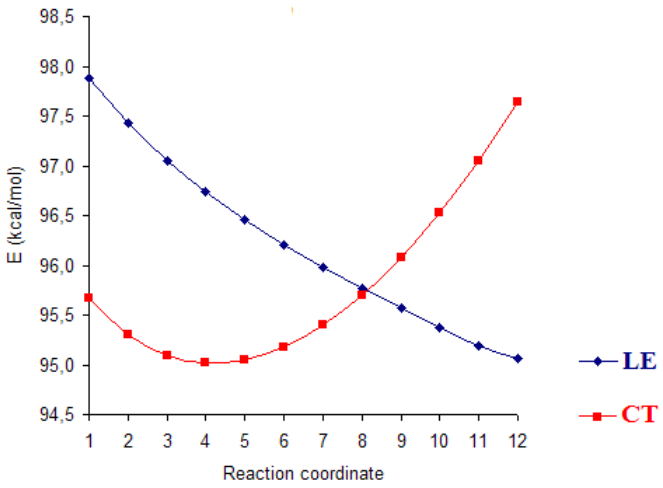

No transition state connecting adiabatically the LE and TICT minima could be located because of the flatness of the surface. In order to evaluate the LE→TICT energy barrier, we computed the energy profile of the LE and CT state by linear interpolation between the S_1-LE and the S_1-TICT minima. The results are depicted in Figure 5.27. They show that the activation barrier for the LE→TICT process is only 0.3 kcal·mol^{-1}, whereas the activation barrier for the backward process is 17.4 kcal·mol^{-1}. Therefore, the equilibrium is strongly displaced towards the S_1-TICT, explaining the presence of the ICT emission for DMABN-4F even in nonpolar solvents. The computed energy of this emission, of 58.4 kcal·mol^{-1} agrees satisfactorily with the 59.6 kcal·mol^{-1} obtained in n-hexane [42].

F-substitution in the phenyl ring of aminobenzontriles leads to smaller fluorescence quantum yields and shorter decay times than in the parent compounds. The number of fluorine substituents seems to be an important factor in the opening of the internal conversion channel, enhancing the accessibility to a conical intersection that leads to the electronic ground state.

The yield of internal conversion, Φ_{IC}, in n-hexane at 25°C is considerable larger for 2,3,5,6-tetrafluoro-4-aminobenzonitrile (ABN-4F) (1.00) and DMABN-4F (0.92) than for 3-fluoro-4-(1-azetidinyl)benzonitrile (P4CF3) (0.35), and for ABN and DMABN where it is of minor importance (0.10 in both cases) [42, 47]. Therefore, it seems interesting to discuss the possible nonradiative decay channels by internal conversion from S_1 as a competing photochemical reaction to the LE→ICT reaction, and show

Figure 5.27: CASPT2/cc-pVDZ energy profiles of the LE (blue) and CT (red) states from the S_1-LE to the S_1-TICT minima for DMABN-4F obtained by a LIIC path. Energies are in kcal·mol^{-1}.

	Point in the path	ΔE CASPT2 (LE)	ΔE CASPT2 (CT)
S_1– LE	1	95.1	97.6
	2	95.4	94.5
	3	95.6	91.7
	4	96.6	88.6
	5	97.6	84.8
	6	98.1	84.0
	7	101.1	82.6
	8	103.5	81.2
	9	105.8	80.0
	10	108.1	79.0
	11	110.6	78.3
S_1– TICT	12	113.3	78.0

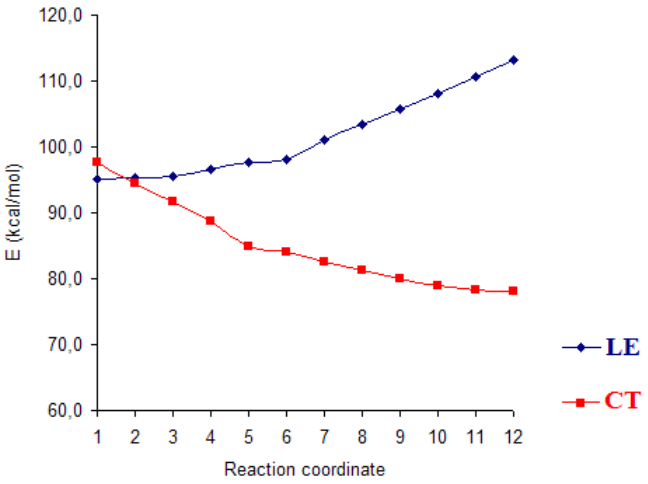

up the differences on this deactivation reaction for DMABN and DMABN-4F.

Figure 5.28: S_0/S_1 conical intersection located at CASSCF level in DMABN-4F. Degeneracy-lifting coordinates: (a) derivative coupling vector and (b) gradient difference vector. All bond lengths are in Å.

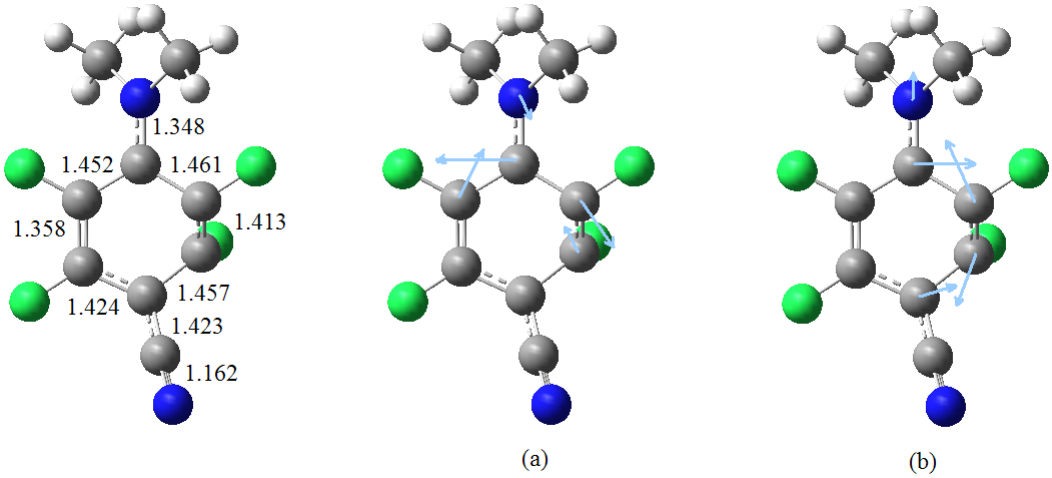

To characterize this radiationless decay channel on DMABN-4F, we located first the minimum energy point of the S_0/S_1 CI that would correspond to the funnel for the $S_1 \rightarrow S_0$ internal conversion. To check if this IC is accessible, we located the transition state (TS) of the path connecting the S_1-LE minimum with the CI. The energy of this TS corresponds to the measured activation energy of the IC [47]. The geometries of these critical points for DMABN-4F are shown in Figures 5.28 and 5.29, and the

Figure 5.29: Transition state connecting the S_0/S_1 conical intersection with the S_1-LE minimum, located at CASSCF level in DMABN-4F. All bond lengths are in Å.

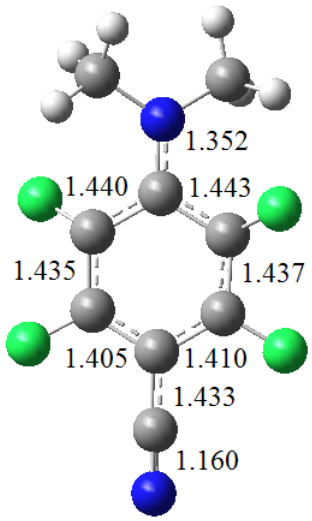

energetics for DMABN and DMABN-4F are collected in Table 5.7.

The structure of the S_0/S_1 CI shows a strong pyramidalization of C3, in such a way that the benzene ring looses the planarity and the H (or F) atom bonded to C_3 is well out of the plane of the molecule. This distortion is strongly unfavourable energetically for the ground state, so the energy gap between S_1 and S_0 is rapidly reduced along this coordinate. The fluorine atoms enhances the tendency of sp^3 hybridation on C atoms, facilitating the folding of the ring and lowering the energy of this path on DMABN-4F relative to DMABN. Accordingly to this fact, the CASSCF results give a CI on DMABN 2.8 kcal·mol^{-1} above the S_1-LE minimum, while for DMABN-4F the CI is 3.9 kcal·mol^{-1} below the same minimum. The same tendency is found for the TS: it is 19.9 kcal·mol^{-1} for DMABN, but only 2.6 kcal·mol^{-1} for DMABN-4F. It is worth pointing out that the geometry optimization of these critical points is only carried out at the CASSCF level, so when the energies are recalculated at the CASPT2 level, these do not necessarily correspond to critical points of the PES at the CASPT2 level. This is the case for the S_0/S_1-CI: when the energies are recalculated at the CASPT2 level, it is found that the S_0 and S_1 states are no longer degenerated. For the same reason, the energy of the transition state denoted as S_1-$TS_{LE/CI}$ in DMABN-4F is lower than the supposed initial point of the path. Nevertheless, comparison of the CASPT2 energies of DMABN and DMABN-4F lead to the same conclusion than CASSCF results: the nonradiative decay from S_1 to the ground-state is almost a barrierless process in DMABN-4F while for DMABN the barrier is non negligible. It is noticeable that the CASPT2 activation barrier obtained for this system (8.2 kcal·mol^{-1}) is in very good

agreement with the 8.3 kcal·mol^{-1} estimated experimentally in n-hexane [47]. In view of these results, it can be concluded that internal conversion becomes the dominating process from the S_1-LE minimum in DMABN-4F in such a way that, if this minimum is reached, it will be quickly depopulated through the S_0/S_1-CI precluding the normal fluorescence emission. These results explain the fact that normal fluorescence could not be detected for DMABN-4F and its ICT fluorescence quantum yield in n-hexane is only $\Phi_f = 2.6\ 10^{-3}$ [42]. On the other hand, the activation barrier found in DMABN explains that internal conversion in this molecule only becomes an important decay channel above room temperature.

5.5.3 Conclusion

The stabilization of the ICT state is further enhanced by the fluoro substituents of DMABN-4F relative to the effect of the methyl substituents added to the ABN to give DMABN. Consequently, the anomalous fluorescence band, non-existent in ABN, appears in polar solvents in the DMABN spectrum and is eventually the only band shown in the DMABN-4F spectrum. Moreover, in DMABN-4F, the steric repulsion precludes the existence of planar low-energy structures, so the GS and LE minima are pretwisted, which supports the hypothesis of a TICT structure for the CT fluorescent species. The agreement of our results with the available experimental data supports the conclusions of our study.

5.6 Conclusion

Our different studies on DMABN and derivatives give informations on the role that the substituents and their position play on the fluorescence behaviour of potential ICT systems. Both geometrical constrains, through a series of alyciclic derivatives and DTABN isomers, and electronical effects, with the fluoro substitution, have been studied. Globally, our results show that the fluorescence patterns of the ICT systems are given in most cases by the energy differences between the LE and TICT excited states, both at the Franck-Condon region and at the minima. These last ones are generally located on the S_1 PES. The geometrical constrains that preclude rotation or planarity of the molecule will destabilized the TICT or the LE minimum preferentially, favouring the normal or the anomalous fluorescence. Nevertheless, although in all cases studied up to now PICT minimum is located on S_2 PES and therefore can not be a luminescent species, we could not rule out the stabilization of these species in other systems and the consequent involvement on the fluorescence emission. The small

energy differences between the minima of the species involved in the ICT process make that a small quantitative change could produce important qualitative changes. For this reason, these results prove that it is not possible to make *a priori* prediction of the fluorescent behaviour of a new system, based on the results for similar systems. Unfortunately, the experience accumulated up to now make advisable to carry out specific studies for any new system of interest.

The agreement of our predictions with the experimental observations support the suitability of the computational method used for the study of this kind of photochemical problems. The good agreement of compared absorption and emission energies shows that CASSCF/CASPT2 methodology can be used not only for qualitative but also for quantitative predictions.

Bibliography

[1] Platt, J. *J. Chem. Phys.* **17**, 484 (1949).

[2] Lippert, E., Lüder, W., Moll, F., Nägele, W., Boos, H., Prigge, H., and Seybold-Blankestein, I. *Angew. Chem.* **73**, 695 (1961).

[3] Lippert, E., Lüder, W., and Boos, H. *Advances in Molecular Spectroscopy*, Mangini, A, (1962).

[4] Al-Hassan, K. and Khanfer, M. *J. Fluoresc.* **8**, 139 (1998).

[5] Rettig, W. and Lapouyade, R. *Topics in Fluorescence Spectroscopy; Lakowitz, J.R., Ed; Plenum Press: New York* **4** (1994).

[6] Suresh, M., Kar, P., and Das, A. *Inorg. Chim. Acta* **363**, 2881 (2010).

[7] Grabowski, Z. R., Rotkiewicz, K., and Rettig, W. *Chem. Rev.* **103**, 3899–4032 (2003).

[8] Serrano-Andrés, L., Merchan, M., Roos, B. O., and Lindh, R. *J. Am. Chem. Soc.* **117**(11), 3189–3204 (1995).

[9] Gómez, I., Reguero, M., Boggio-Pasqua, M., and Robb, M. A. *J. Am. Chem. Soc.* **127**, 7119 (2005).

[10] Zachariasse, K. a., Druzhinin, S. I., Kovalenko, S. a., and Senyushkina, T. *J. Chem. Phys.* **131**(22), 224313 (2009).

[11] Fujiwara, T., Lee, J.-K., Zgierski, M. Z., and Lim, E. C. *Chem. Phys. Lett.* **481**(1-3), 78–82 (2009).

[12] Zgierski, M. Z., Fujiwara, T., and Lim, E. C. *Acc. Chem. Res* **43**(4), 506–17 (2010).

[13] Gustavsson, T., Coto, P. B., Serrano-Andrés, L., Fujiwara, T., and Lim, E. C. *J. Chem. Phys.* **131**(3), 031101 (2009).

[14] Grabowski, Z. R., Rotkiewicz, K., and Grellmann, K. H. *Chem. Phys. Lett.* **19**, 315 (1973).

[15] Schuddeboom, W., Jonker, S. A., Warman, J. H., Leinhos, U., Künhle, W., and Zachariasse, K. A. *J. Phys. Chem.* **96**, 10809 (1992).

[16] Zachariasse, K. A., Von Der Haar, T., Hebecker, A., Leinhos, U., and Künhle, W. *Pure Appl. Chem.* **65**, 1745 (1993).

[17] Zachariasse, K. a., Grobys, M., Von Der Haar, T., Hebecker, A., Ilichev, Y., Jiang, Y., Morawski, O., and Kunhle, W. *J. Photochem. Photobiol. A: Chem.* **102**(1), 59–70 (1996).

[18] Zachariasse, K. A. *J. Photochem. Photobiol. A: Chem.* **105**(2-3), 373–383 (1997).

[19] Sobolewski, A. *Chem. Phys. Lett.* **259**(1-2), 119–127 (1996).

[20] Sobolewski, A. *Chem. Phys. Lett.* **250**(3-4), 428–436 (1996).

[21] Hättig, C., Hellweg, A., and Köhn, A. *J. Am. Chem. Soc.* **128**, 15672 (2006).

[22] Okada, T., Uesugi, G., Kohler, K., Rechtaler, K., Rotkiewicz, K., Rettig, W., and Grabner, G. *Chem. Phys.* **241**, 327 (1999).

[23] Kwok, W. M., Ma, C., George, M. W., Grills, D. C., Matousek, P., Parker, a. W., Phillips, D., Toner, W. T., and Towrie, M. *Phys. Chem. Chem. Phys.* **5**(6), 1043–1050 (2003).

[24] Druzhinin, S. I., Kovalenko, S. a., Senyushkina, T., and Zachariasse, K. a. *J. Phys. Chem. A* **111**(50), 12878–90 (2007).

[25] Druzhinin, S. I., Jiang, Y. B., Demeter, A., and Zachariasse, K. A. *Phys. Chem. Chem. Phys.* **3**, 5213 (2001).

[26] Bearpark, M. J., Robb, M. A., and Schlegel, H. B. *Chem. Phys. Lett.* **223**, 269 (1994).

[27] Roos, B. O. and Andersson, K. *Chem. Phys. Lett.* **245**, 215 (1995).

[28] Roos, B. O., Andersson, K., Fülscher, M. P., Serrano-Andrés, L., Pierloot, K., Merchán, M., and Molina, V. *J. Mol. Struct. Theochem* **388**, 257 (1996).

[29] Malmqvist, P.-A. and Roos, B. O. *Chem. Phys. Lett.* **155**, 189 (1989).

[30] Malmqvist, P.-A. *Int. J. Quantum Chem.* **30**, 479 (1986).

[31] Blancafort, L., Celani, P., Bearpark, M. J., and Robb, M. A. *Theor. Chem. Acc.* **110**, 92 (2003).

[32] Rotkiewicz, K., Grabowski, Z. R., Krówczyñski, A., and Künhle, W. *J. Lumin.* **12/13**, 877 (1976).

[33] Leinhos, U., Künhle, W., and Zachariasse, K. A. *J. Phys. Chem.* **95**, 2013 (1991).

[34] Zachariasse, K. A., Grobys, M., Von Der Haar, T., Hebecker, A., Leinhos, U., and Künhle, W. *J. Photochem. Photobiol., A: Chem.* **102**, 59 (1996).

[35] Jamorski Jödicke, C. and Lüthl, H. P. *J. Am. Chem. Soc.* **125**, 252 (2003).

[36] Jamorski Jödicke, C. and Lüthl, H. P. *J. Chem. Phys.* **24**, 12852 (2003).

[37] Zachariasse, K. a., Druzhinin, S. I., Bosch, W., and Machinek, R. *J. Am. Chem. Soc.* **126**, 1705–15 (2004).

[38] Hättig, C. and Köhn, A. *J. Am. Chem. Soc.* **126**, 7399 (2004).

[39] Bulliard, C., Alan, M., Wirt, G., Haselbach, E., Zachariasse, K. A., Detzer, N., and Grimme, S. *J. Phys. Chem. A* **103**, 7766 (1999).

[40] Druzhinin, S. I., Dubbaka, S. R., Knochel, P., Kovalenko, S. a., Mayer, P., Senyushkina, T., and Zachariasse, K. a. *J. Phys. Chem. A* **112**(13), 2749–61 (2008).

[41] Kasha, M. *Discussions of the Faraday Society* **9**, 14 (1950).

[42] Galievsky, V. A., Druzhinin, S. I., Demeter, A., Jiang, Y. B., Kovalenko, S. A., Lustres, L. P., Venugopal, K., Ernsting, N. P., Allonas, X., Noltemeyer, M., Machinek, R., and Zachariasse, K. A. *Chem. Phys. Chem.* **6**, 2307 (2005).

[43] Murali, S., Kharlanov, V., Rettig, W., Tolmachev, A. I., and Kropachev, A. V. *J. Phys. Chem A* **109**, 6420 (2005).

[44] Nakagaki, R., Kohtani, S., and Nakamura, Y. *Anal. Sci.* **19** (2003).

[45] Cogan, S., Zilberg, S., and Haas, Y. *J. Am. Chem. Soc.* **128**, 3335–45 (2006).

[46] Zilberg, S. and Haas, Y. *J. Phys. Chem. A* **106**, 1 (2002).

[47] Druzhinin, S. I., Demeter, A., Galievsky, V. A., Yoshihara, T., and Zachariasse, K. A. *J. Phys. Chem. A* **107**, 8075 (2003).

UNIVERSITAT ROVIRA I VIRGILI
AB-INITIO INSIGHT INTO THE ORGANIC PHOTOCHEMICAL DIVERSITY: NON-RADIATIVE DECAY IN URACIL AND DERIVATIVES AND INTRAMOLECULAR CHARGE TRANSFER MECHANISMS IN THE BENZONITRILE FAMILY
Yannick Mercier
DL:T. 1371-2011

La utopía está en el horizonte. Camino dos pasos, ella se aleja dos pasos y el horizonte se corre diez pasos más allá. ¿Entonces para que sirve la utopía? Para eso, sirve para caminar.

Eduardo GALEANO

UNIVERSITAT ROVIRA I VIRGILI
AB-INITIO INSIGHT INTO THE ORGANIC PHOTOCHEMICAL DIVERSITY: NON-RADIATIVE DECAY IN URACIL AND DERIVATIVES AND INTRAMOLECULAR CHARGE TRANSFER MECHANISMS IN THE BENZONITRILE FAMILY
Yannick Mercier
DL:T. 1371-2011

Chapter 6

Conclusion

Two photochemical processes have been studied in this work: the non-radiative decay in uracil and some of its derivatives and the intramolecular charge transfer mechanism in DMABN derivatives.

In the first part, about uracil and its derivatives, the 5-fluorouracil and the 5- and 6-aminouracil, we confirmed the ultrafast decay mechanism. Uracil, which has the shortest excited lifetime of this family of compounds, shows a direct pathway from the FC region to the ground state without any barrier along the axis coordinate that breaks the planarity of the benzene ring that explains this ultrafast decay. After the initial excitation, the wave packet decay quickly to the ground state surface trough CIs without passing by any of the minimum on the upper excited states surface. Part of the wave packet might go to the $S_1(n\text{-}\pi^*)$ minimum, which is connected with the ground state by a CI energetically innaccesible. The part of the wave packet temporally trapped in the $S_1(n\text{-}\pi^*)$ minimum might then cross back to the $(\pi\text{-}\pi^*)$ surface accounting for the largest excited state lifetime, as the other potential path, trough the $(n\text{-}\pi^*)$/GS CI shows a huge barrier. This late structure has been found for the first time in this work, allowing to discard definitively this option as a probable mechanism of nonradiative decay of Uracil. We have then explained the longer lifetime of the derivatives. In the case of 5-FU, a small barrier on the relaxation path explains why the decay, even being still quick, is not as fast as in uracil. Differences between the two amino derivatives have been related to the presence or not of a minimum on the $(\pi\text{-}\pi^*)$ surface: while this minimum is not present for 6-AU, which shows a direct decay pathway, it exists in 5-AU so the decay is slower, waht accounts for the larger lifetime of excited 5-AU. Our results are in very good agreement with the experimental measurements, in particular the absorption and emission energies predicted in this work. As these are biological systems, which are usually found surrounded by solvents,

modelizing the solvent will become a more and more important issue in their studies. Our first results confirmed the influence of the solvent, for example on the order of the lower excited states.

On the other hand, the results on systems derived from the DMABN molecule are in good agreement with experimental results as well. We confirmed the TICT hypothesis that support this structure as the emitting species, even in more rigid systems: the bicycle derivatives showing anomalous fluorescence all present a stable and energetically accessible TICT minimum. The pathway to reach these emitting species when dual or anomalous fluorescence appears has been explained in terms of equilibrium between the LE and TICT-states. Influence of different substitutions, depending on their characteristics (electronic effects in the case of the fluor substitutions, or steric effects for the DTABN isomers), and of the substitution position have been studied with nice agreements with the experimental observations too.

In both cases, the choice of a multiconfiguration *ab-initio* method has been proven to be reliable as computational results fit the experimental data available. The importance of the dynamic correlation in the accuracy of the calculations is clearly demonstrated. This point is of great interest as the recent developments in methodology and computational facilities now allow to do full optimizations at this level. If these calculations are still expensive and time-comsuming, it brings great expectatives for the future of the computational science in the field of photochemistry. Moreover, methods mixing different levels of calculations as used in the study of bulky derivatives of DMABN seems to give interesting results as well, even if they have to be handle with care and their validity checked in any case.

Publications

"The decay from the dark npi* excited state in uracil: an integrated CASPT2/CASSCF and PCM/TD-DFT study in the gas phase and in water." Mercier, Y.; Santoro, F.; Reguero, M.; Improta, R. The journal of physical chemistry. B., 2008, 112, 10769-72.

"Theoretical investigation of luminescence behavior as a function of alkyl chain size in 4-aminobenzonitrile alicyclic derivatives." Gómez, I.; Mercier, Y.; Reguero, M. The journal of physical chemistry. A., 2006, 110, 11455-61.

"The Peculiar Spectral Properties of Amino-Substituted Uracils: A Combined Theoretical and Experimental Study." Bányász, A.; Karpati, S.; Mercier, Y.; Reguero, M.; Gustavsson, T.; Markovitsi, D.; Improta, R. The journal of physical chemistry. B., 2010, 114, 12708-19

"Comparison of the deactivation mechanism of 5-fluorouracil with that of its parent system, uracil. The need of the use of the MS-CASPT2 method." Reguero, M.; Mercier, Y. International Journal of Quantum Chemistry, to be published.

UNIVERSITAT ROVIRA I VIRGILI
AB-INITIO INSIGHT INTO THE ORGANIC PHOTOCHEMICAL DIVERSITY: NON-RADIATIVE DECAY IN URACIL AND DERIVATIVES AND INTRAMOLECULAR CHARGE TRANSFER MECHANISMS IN THE BENZONITRILE FAMILY
Yannick Mercier
DL:T. 1371-2011